AD-A258 084

JMENTATION PAGE

Form Approved
OMB No. 0704-0188

1. AGENCY USE ONLY (Leave blank)	2. REPORT DATE	3. REPORT TYPE AND DATES COVERED
	1992	DISSERTATION

4. TITLE AND SUBTITLE
CFD-Based Approximation Concepts for Aerodynamic Design Optimization with Application to a 2-D Scramjet Vehicle

5. FUNDING NUMBERS

6. AUTHOR(S)
Peter D. McQuade, Major

7. PERFORMING ORGANIZATION NAME(S) AND ADDRESS(ES)
AFIT Student Attending: University of Washington

8. PERFORMING ORGANIZATION REPORT NUMBER
AFIT/CI/CIA-92-019D

9. SPONSORING/MONITORING AGENCY NAME(S) AND ADDRESS(ES)
AFIT/CI
Wright-Patterson AFB OH 45433-6583

10. SPONSORING/MONITORING AGENCY REPORT NUMBER

11. SUPPLEMENTARY NOTES

12a. DISTRIBUTION/AVAILABILITY STATEMENT
Approved for Public Release IAW 190-1
Distributed Unlimited
ERNEST A. HAYGOOD, Captain, USAF
Executive Officer

12b. DISTRIBUTION CODE

13. ABSTRACT *(Maximum 200 words)*

012200
92-31046
102pf

14. SUBJECT TERMS	15. NUMBER OF PAGES
	90
	16. PRICE CODE

17. SECURITY CLASSIFICATION OF REPORT	18. SECURITY CLASSIFICATION OF THIS PAGE	19. SECURITY CLASSIFICATION OF ABSTRACT	20. LIMITATION OF ABSTRACT

CFD-Based Approximation Concepts for Aerodynamic Design Optimization With Application to a 2-D Scramjet Vehicle

by

Peter D. Mc Quade

A dissertation submitted in partial fulfillment
of the requirements for the degree of

Doctor of Philosophy

University of Washington

1992

Approved by _____
(Chairperson of Supervisory Committee)

Program Authorized
to Offer Degree Aeronautics and Astronautics

Date August 21, 1992

In presenting this dissertation in partial fulfillment of the requirements for the Doctoral degree at the University of Washington, I agree that the Library shall make its copies freely available for inspection. I further agree that extensive copying of this dissertation is allowed only for scholarly purposes, consistent with "fair use" as prescribed in the U.S. Copyright Law. Requests for copying or reproduction of this dissertation may be referred to University Microfilms, 300 North Zeeb Road, Ann Arbor, Michigan 48106, to whom the author has granted "the right to reproduce and sell (a) copies of the manuscript in microfilm and/or (b) printed copies of the manuscript made from microfilm."

Signature Peter D. McQuade

Date 20 August 1992

University of Washington

Abstract

CFD-Based Approximation Concepts for Aerodynamic Design Optimization, With Application to a 2-D Scramjet Vehicle

by Peter D. Mc Quade

Chairperson of the Supervisory Committee: Professor D. Scott Eberhardt
Department of Aeronautics and Astronautics

This dissertation investigates the application of approximation concepts to aerodynamic optimization. Such techniques, which are gaining popularity in structural optimization, offer the potential of providing the accuracy of a high-fidelity "detailed" analysis model at greatly reduced computational cost. This is because the detailed model is used only to "fine-tune" an approximate model which is then used in the optimizer. The test problem treated is the design optimization of a 2-D scramjet vehicle flying at Mach 6.0 at 30 km altitude. The objective function is net thrust. The following approximation concepts are used: the Taylor series approximation to wall pressures and inlet plane flow properties; and Haftka's Global-Local Approximation applied to the same variables. The performance of these techniques is compared to that for optimization using CFD alone. Cost reductions are quantified.

It is shown that modifications must be made to the formulation of the approximation concepts as they are used in structural optimization, due to the changing grid geometries required by the CFD solver. All correction factors for the approximation concept are applied not to the CFD grid points, but to a constant, dense, nondimensionalized "correction point grid", which does not change as the CFD grid changes. It is also shown that, in areas where discontinuous phenomena are not important (such as in the scramjet nozzle), the approximation concepts can be successfully used, after this modification is made. Optimizations of the nozzle region show that all the

approximation concepts result in a 68% reduction in the number of calls to the CFD solver.

In regions dominated by shock impingements (such as the forebody/inlet), it is found that approximation concepts applied to point properties cannot be used as they currently are in structural optimization, due to the effects of shock movement during correction factor calculations, and due to artifacts of the CFD solver, such as shock smearing. In fact, even though the CFD and the (uncorrected) approximate models optimize to very nearly the same design, the Taylor series and GLA fail to do so. However, application of the GLA to the integrated objective function (net thrust) with zeroth-order correction factors, is successful.

To lay the groundwork for future investigation, a method of improving the behavior of the point-property GLA in the presence of shock impingements is developed and tested. This involves using "floating" pre- and post-shock coordinate systems for each wall surface. The result is a dramatic reduction in the erratic behavior of the GLA. This technique may form the basis of a generally-applicable GLA technique for aerodynamic optimization.

Table of Contents

List of Figures

List of Tables

ACKNOWLEDGMENTS

The author wishes to express his sincere appreciation and gratitude to Professor Scott Eberhardt and Professor Eli Livne, who together provided the greatest portion of the guidance, advice, and often-needed encouragement for this project. In addition, I wish to give special thanks to Professors David Russell, Mitsuru Kurosaka, and David Pratt, without whose help I would have been lost. I also wish to thank Dr. Gerald C. Paynter for serving as a special member of my PhD committee, and Professor Reiner Decher for all his cheerful help with combustion issues.

Many thanks are also due to my friends in the University of Washington CFD Lab, from whom I learned so much. I am also especially indebted to Linda Sigalla Hedges, Perry Meyer and Ken Barker for their help and counsel.

Finally, I wish to thank Mr. Brian Leverson for all his help with the computers and his late-night company over the months.

Dedication

This work is respectfully dedicated to my family:

To my mother, father, brothers, sisters, and in-laws, who deluged heaven with prayers for my success.

To our beautiful children, Rebecca, David, and Linda, who payed such a high price because their daddy decided to get a PhD.

To my beloved wife Marilyn, who made it all possible and worthwhile, and who is a much better choice for a doctoral candidate.

And to the memory of our darling daughter, Carrie.

Chapter 1

Introduction

1.1 Background

The dramatic improvements in computing power and computational techniques in recent years have made computational fluid dynamics (CFD) a valuable tool for analyzing complicated internal and external flows. CFD has begun to see use in aircraft design, including the wing designs of the next generation of commercial transport aircraft, and the preliminary design of the National Aerospace Plane (NASP). Indeed, for this latter program, CFD provides the *only* means of gathering detailed flow data for the high-speed portion of the flight envelope.

As CFD continues to mature and to become more reliable and cheaper to use, it is natural that designers will seek to incorporate CFD with automated design synthesis (optimization) methods. Such techniques have been used successfully in structural design in recent years. (Ref's. 7, 11 and 14.) They have also been applied to aerodynamic design problems, but using only relatively simple flow analysis techniques. (Ref's. 6, 10 and 11.) The high cost of using CFD as an analysis model has generally precluded its direct use in vehicle design optimization, which requires repeated analyses of the objective function and constraints.

Recent developments in structural optimization techniques have focused on ways to reduce the cost of using "detailed" analysis models in optimization. One such promising area of research is "approximation concepts". (See Ref. 7.) These concepts are based upon replacing the original problem with a simpler (and much cheaper), "approximate" problem which is used in the actual optimization process. The fidelity of such an approximate problem can be enhanced by using information from a limited number of analyses from the detailed model to "fine tune" the approximate model before it is used by the optimizer.

A simple, and now commonly-used example of approximation concepts involves forming a first-order Taylor series approximation to the physical properties of interest (point stresses, for example), in terms of the design variables. The coefficients in the Taylor series come from applying the detailed analysis model at a baseline design.

Naturally, such an approximation is only guaranteed to be valid in the vicinity of the baseline design. For this reason, Taylor series approximations are referred to as "local approximations." These approximations are implemented in a design optimization by performing a complete optimization within certain "move limits" about the baseline, and then forming a new Taylor series approximation about the optimum design, establishing new move limits, and repeating the process. The detailed model is never actually used in the optimizer.

An approximation concept which is potentially less limited than the Taylor series approach is Haftka's "Global-Local Approximation" (GLA), in which a simple, but globally-applicable analysis model is "fine-tuned" by data from a few analyses from the detailed model. (Ref. 8.) The fine-tuned approximate model is then submitted to the optimizer. The GLA is implemented by forming correction factors which relate the detailed model's results to the approximate model's results at a baseline design. Such a correction factor may itself take the form of a first-order Taylor series approximation to the ratio of detailed/approximate model results. Thus, the GLA would be expected to provide very accurate results near the baseline design, but retain much better accuracy than the Taylor series approach as the design leaves the vicinity of the baseline.

Although GLA's have been applied to some structural problems (Ref's. 7 through 9), they have only very recently been applied to aerodynamic optimization. Ref. 10, which is perhaps the first published example, was published in January, 1992. GLA's have not heretofore been applied using CFD as the detailed model.

The cost savings resulting from the successful application of approximation concepts can be great. This is increasingly true as the number of design variables increases. For instance, a problem with 100 design variables and which is solved using a detailed model for all analyses would require more than 100 calls to the detailed model. A successful approximation concept might reduce this to 10 calls or less (and hundreds of calls to the much faster approximate analysis model).

However, there are potentially serious problems inherent in applying approximation concepts, as they have been formulated for structural problems, to aerodynamic optimization. For example, the presence of shock waves, transition to turbulence, and flow separation/reattachment are discontinuous phenomena which could interfere with the linear extrapolations used in the fine-tuning process, particularly if these phenomena move as the design is changed. In addition, artifacts of the CFD solution

process (such as shock smearing and pre-shock oscillation) may influence the fine tuning and introduce errors in calculating search directions. This is complicated by the fact that the detailed and approximate models may not capture shocks or other phenomena equally "crisply", which can lead to erroneous correction factors. Also, the structural applications of approximation concepts have so far only dealt with fixed-grid geometries. For CFD to be used, however, the grid must be allowed to vary as the geometry and/or flow phenomena change, even to the point of adding or subtracting grid points. This precludes a straightforward assignment of correction factors to grid points as was used in previous structural optimizations.

There are other problems, not related to the approximation concepts, but which are unique to applying nonlinear optimization to aerodynamic design. First, it is not yet clear if the sudden appearance of shock waves, separation, or other phenomena on the aircraft surface might introduce more discontinuity in such measures as lift, thrust, and drag than can be handled by a gradient-based optimizer. Also, as has been shown in structural optimization, the choice of design variables can have a great impact on whether the optimization leads to the proper design. But in aerodynamic vehicle design, additional complexity is introduced by the fact that certain defining geometries of a design are, in practice, not changed independently, but are changed in concert. For example, a transonic swept wing might use twist to maintain a desirable lift distribution. As the sweep is increased, the twist should also be increased. One could devise one or more sets of design variables which would make this connection automatically. However, it is not always clear at the outset which set of design variables will work best in an optimizer.

1.2 Problem Statement

It is the purpose of this research effort to investigate the application of CFD-based approximation concepts to aerodynamic design optimization. The test case selected is the design of a 2-dimensional scramjet-powered vehicle in an inviscid, perfect gas flow. (See Fig. 1.1.) The flight conditions are: $M_\infty = 6.0$, h = 30 km. Only the lower surface of the vehicle is treated, since this is where all the dominant phenomena occur. This test case is illustrative of all the problems mentioned above. Specifically, it has regions dominated by relatively isentropic flow, and regions dominated

by shock waves which impinge upon vehicle walls. It requires grid clustering which must change as the design is changed. And the design is complicated enough that the best selection of design variables is not obvious in advance. Finally, the design problem is significant and timely in its own right, since scramjet vehicle design is currently being vigorously pursued in support of the NASP program.

Both CFD-based Taylor series and GLA's were formulated, and the unique problems inherent in applying these approximation concepts to aerodynamic optimization were investigated. New techniques, not required in structural optimization, needed to be developed for this application. The approximation concepts were then applied to the optimization process, and their behavior and cost savings relative to straightforward optimizations using CFD alone were observed. The optimization package used was "Design Optimization Tools" (DOT). See Ref. 12 and Appendix A.

Because of the inherently different natures of the flows in the forebody/inlet region (which is dominated by oblique shock waves) and in the nozzle/afterbody region (which is primarily an isentropic expansion process), these optimization techniques were applied to each of these regions separately. Thus, problems arising from the various flow phenomena were observed. It was found that such effects have a great impact on the ease with which the approximation concepts can be applied.

In order to provide a challenging test of approximation concepts in the presence of shocks which move as the design changes, the forebody/inlet optimizations were performed allowing arbitrary shock configurations there. That is, the problem was not limited to one with "perfectly-placed" shocks, with the nose and ramp shocks impinging on the cowl lip, and the resulting cowl lip shock hitting the inlet corner. This formulation of the problem highlighted the difficulties one would encounter in applying GLA's to more general problems with moving shocks, such as in transonic wing design.

1.3 Original Contributions

This research effort is the first application of the GLA technique in which CFD is the detailed analysis model. As such, this research identifies general procedures for using CFD with GLA's. It also identifies problems which will be encountered, not only with the design problem at hand, but in all aerodynamic design problems where

discontinuous phenomena (such as shock waves or transition to turbulence) exist and move as the design is changed. Indeed, it is shown that the GLA, as currently employed in structural optimization, cannot be straightforwardly employed when such phenomena are present. Proposed solutions to these problems are investigated, and areas of further work are recommended.

This work identifies the general problem that changing grids cause in any approximation concept. Although this problem had been observed in a different type of optimization approach (Ref. 3), it was not explicitly solved there, but was "worked around" by changing the objective function. In this research effort a direct, general solution to this problem has been found and successfully applied.

This is also the first application of GLA's to the aerodynamic optimization of a scramjet vehicle design. It provides new insights into the selection of approximate models and design variables for vehicle design optimization.

Approximation concepts hold great promise for dramatically reducing the cost of aerodynamic design optimization using CFD. Research such as this work is an important part in the effort to make CFD-based optimization techniques a part of the aircraft designer's repertoire.

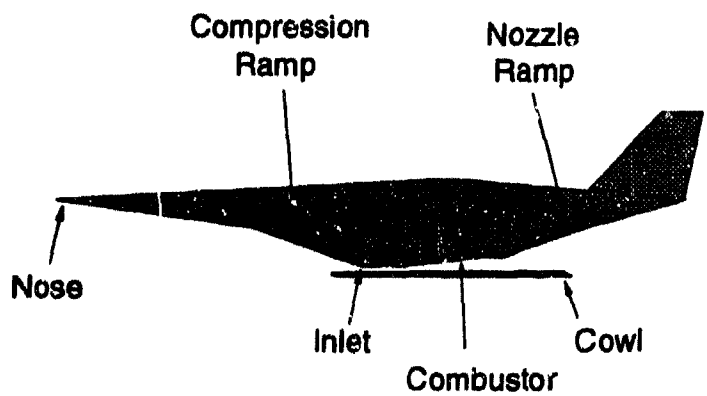

Fig. 1.1 2-D scramjet vehicle geometry.

Chapter 2

Approximation Concepts

2.1 Introduction

The field of approximation concepts, as currently used in structural optimization, has produced techniques which can be used to substantially reduce the number of costly function evaluations in an optimization process. The basic principle of approximation concepts is to replace the original problem with an approximate problem, which is simpler and less costly to solve. An approximate problem solver is then implemented for function evaluations. It is this approximate model which is then submitted to the optimizer: the original, "detailed" model is never used directly by the optimizer. It is possible to improve the fidelity of the approximate model by using information from a limited number of analyses from the detailed model to "fine tune" the approximate model. The focus of this research is on this type of approximation concept.

For the purposes of this research, the detailed model is the CFD solver. Several approximate models were used with the CFD solver to form the bases of the various approximation concepts.

Approximation concepts can be applied to "point" properties, such as wall pressures, or to "integral" properties, such as thrust, drag, or net thrust. If the objective function is itself an integral property, the use of point properties for the approximation concept may capture nonlinearities in the objective function that the use of integral properties might not. Thus, for most cases in this research, the approximation concepts were applied to point properties (wall pressures and inlet plane flow properties).

This chapter describes the two approximation concepts used in this project: the Taylor series "local approximation" and the Global-Local Approximation (GLA). It also presents details of how these concepts are implemented in the 2-D scramjet aerodynamic optimization problem. There are special difficulties encountered in applying them to aerodynamic, versus structural, optimization problems. These difficulties, and insight into their solutions, are presented as well.

2.2 Local Approximations

One often-used method of reducing the number of costly calls to the detailed analysis program in an optimization, while still retaining some of the accuracy of that detail is to use "local approximations" (using Haftka's nomenclature, Ref. 8.). Such approximations extrapolate the results of a detailed analysis done at a baseline design point, and are therefore valid only in the immediate vicinity of that design point. The most common type of local approximation is a Taylor series expansion of the relevant properties about the latest baseline design.

A first-order Taylor series approximation for a point property can be formed as follows. Let $\mathbf{X}$ be the vector of design variables (such as nose angle, compression ramp angle, etc), and let $f(\mathbf{X})$ be the property of interest (say the pressure at a particular point on a wall). Define $\mathbf{X}^0$ to be the latest "baseline" design; that is, the latest design for which we have results from the detailed model. We then have

$$f(\mathbf{X}) \approx f_d(\mathbf{X}^0) + \nabla f_d \Delta \mathbf{X}, \tag{2.1}$$

where: f_d is the value of the property found using the detailed model; ∇f_d is a row vector containing the elements of the gradient of f_d with respect to the design variables; and $\Delta \mathbf{X} = \mathbf{X} - \mathbf{X}^0$. Note that every point at which wall pressures are to be evaluated has its own Taylor series approximation to $f(\mathbf{X})$.

Optimization using local approximations proceeds as follows. (See Fig. 2.1.) The detailed model is used to find the baseline values of f_d and and ∇f_d. A complete optimization (or "iteration") is then performed, following a technique such as that outlined in the Appendix. Since the approximation is only valid in the vicinity of $\mathbf{X}^0$, we apply "move limits", which restrict $\Delta\mathbf{X}$ so that no design variable changes by more than a given percentage during the iteration. When the iteration is completed, a new detailed analysis is performed, and new coefficients for the approximation are calculated. The process continues until convergence is reached.

Local approximations have proven useful in structural optimization problems (Ref's. 8 and 9), but have only recently been used in aerodynamic optimization prolems. (Ref. 4.) First-order Taylor series were employed in several of the optimizations done in this research, as explained in Chapters 4-6.

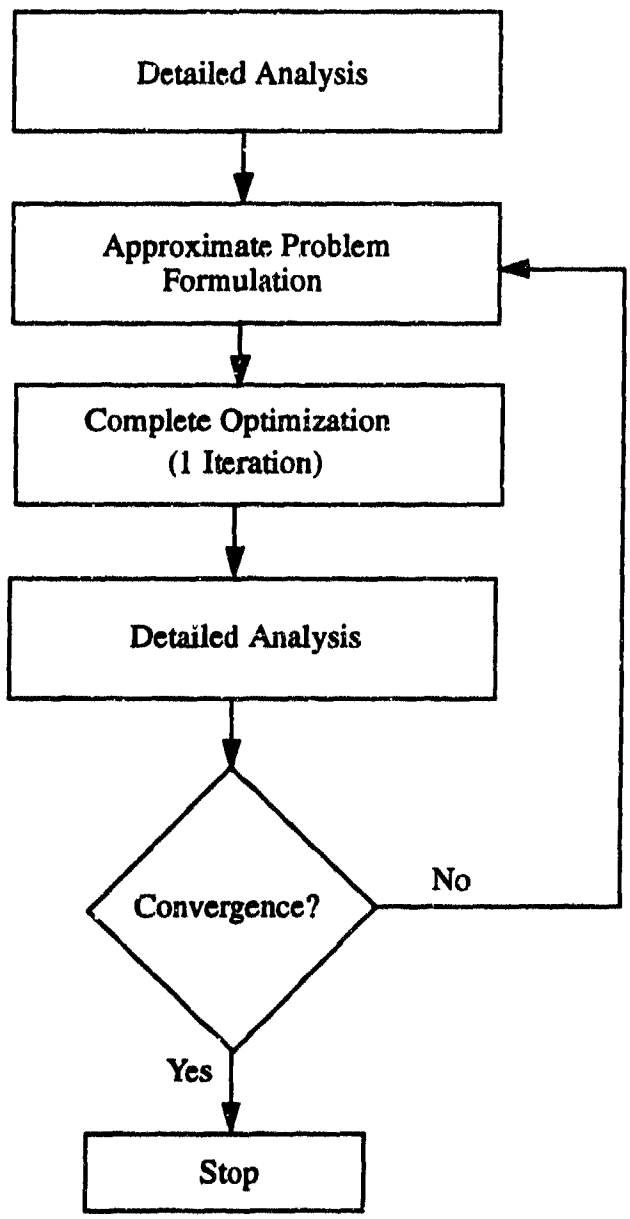

Fig. 2.1 General application of an approximation concept.

2.3 Global-Local Approximations

A method of adding some degree of global accuracy to a local approximation is to use a "Global-Local Approximation" (GLA). See Ref's 8 and 9. In this technique, we use $f_a(\mathbf{X})$, the result from a (globally-applicable) approximate model of f(X), and apply a linearly-varying correction factor $\beta(\mathbf{X})$, which "corrects" f_a to more closely resemble the results of the detailed model, f_d.

$$f(\mathbf{X}) \approx \beta(\mathbf{X}) f_a(\mathbf{X}) \tag{2.2}$$

where

$$\beta(\mathbf{X}) = \frac{f_d(\mathbf{X})}{f_a(\mathbf{X})} \approx \beta(\mathbf{X}^0) + (\nabla \beta(\mathbf{X}^0))\Delta\mathbf{X} \tag{2.3}$$

and, by chain rule differentiation,

$$\nabla \beta(\mathbf{X}^0) = \nabla \frac{f_d(\mathbf{X})}{f_a(\mathbf{X})}\bigg|_0 = \beta(\mathbf{X}^0)\left[\frac{1}{f_d}\nabla f_d - \frac{1}{f_a}\nabla f_a\right]\bigg|_0 \tag{2.4}$$

Eq. (2.3) shows that $\beta(\mathbf{X})$ is represented by a first-order Taylor series about the latest design point for which detailed model data is available. At the conditions of the latest design point, the GLA representation of f(X) is equal to the detailed model results. This is the local nature of the GLA. Note that the calculation of $\nabla \beta(\mathbf{X}^0)$ requires calculation of the various elements of both $\nabla f_d(\mathbf{X}^0)$, which can be costly, and $\nabla f_a(\mathbf{X}^0)$, which is much less so.

The GLA method is applied in the same general fashion as the local approximation was. (Fig. 2.1.) For the point-property GLA applied to the 2-D scramjet vehicle, β's are determined for all surface pressures, and for the inlet-plane flow properties, based on the initial design. A complete optimization (or "iteration") is conducted, using only the approximate model with corrections applied as per Eq. (2.2). Since the GLA is only valid in the vicinity of $\mathbf{X}^0$, we apply "move limits", which restrict $\Delta\mathbf{X}$ so that no design variable changes by more than a given percentage during the iteration. Upon completion of the iteration, new β's are determined, new move limits are established, and a new iteration is conducted. The process continues until convergence is reached. GLA's were used for several of the optimizations used in this research project, as explained in Chapters 4-6.

2.4 Applying Approximation Concepts to Aerodynamic Optimization

A special problem is posed when applying these approximation concepts to CFD-based aerodynamics problems, which necessarily involve using CFD grids which add or delete grid points as the design variables change (to accommodate a lengthened cowl, or a change in clustering, for example). The variation of the grid excludes the possibility of simply calculating the Taylor series coefficients or the GLA coefficients in the baseline design's grid, and applying them to all steps in an iteration in the optimization process. This problem had been previously identified (Ref. 3), but was solved by "working around" the problem, by changing the objective function. This research has identified a general solution to this problem, by creating a set of "correction point" grids, which are independent of the size of the CFD grid.

A system of correction points was defined for each wall surface (the inlet compression ramp, for instance), in non-dimensionalized coordinates, x/L, where L is the length of that surface. (See Fig. 2.2.) 100 to 3500 correction points were used for each surface, depending on the length of the surface. At the beginning of each iteration, the approximation concept coefficients (e.g. $\beta(\mathbf{X}^0)$ and $\nabla\beta(\mathbf{X}^0)$) were interpolated from the baseline results, in the CFD grid system, into the non-dimensionalized coordinates. As the search progressed and the grid changed, Eq. (2.3) was applied at the correction points to find the correction factors. Wall surface pressures were then calculated at these points, which were then scaled to the proper physical positions. No conversion back into the CFD grid system was done. In fact, to do so introduces interpolation and roundoff errors which were found to yield incorrect search directions.

Another important consideration when using approximation concepts in aerodynamic optimizations is that the nature of the flow in a given region may strongly affect the behavior of the correction factors. For example, the presence of shock impingement points which move as the design is changed would introduce severe nonlinearities into the problem which such relatively simple approximation concepts could not handle. This problem was encountered in optimizing the forebody/inlet region. (See Chapter 5.)

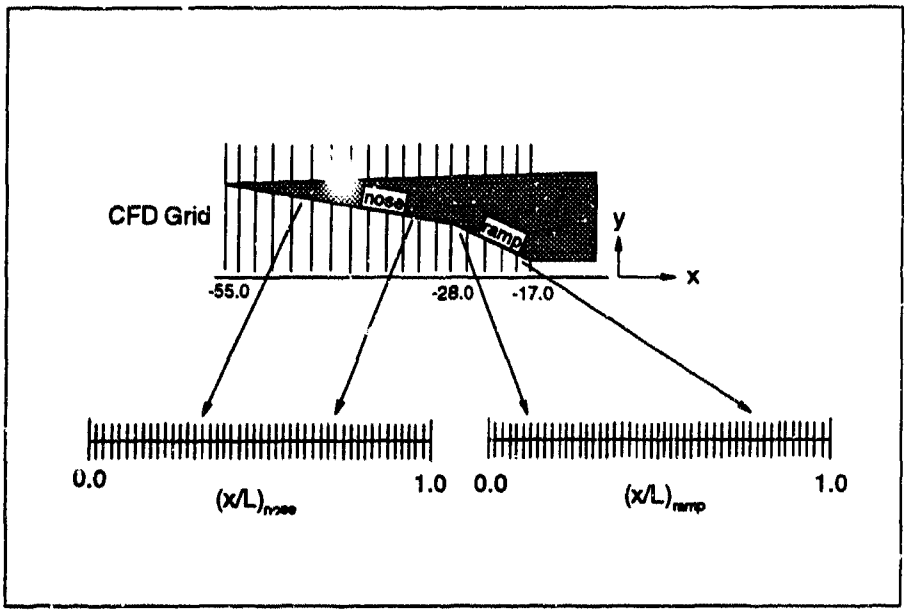

(a) Constructing the correction point grid system for the forebody.

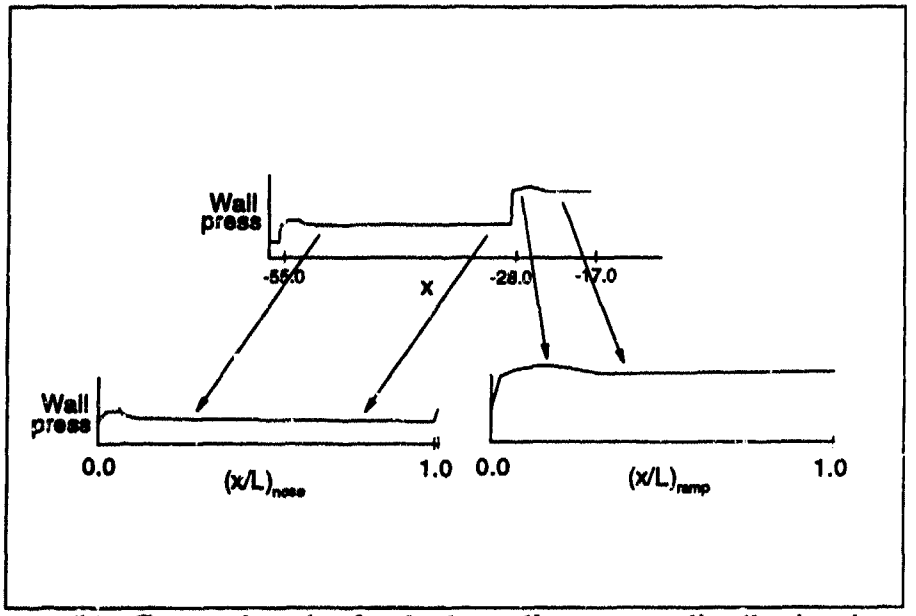

(b) Converting the forebody wall pressure distribution into correction point grid system.

Fig. 2.2 Example of correction point grid system.
(Only forebody shown.)

2.5 Summary

Local approximation concepts (based on Taylor series expansions of point properties) and GLA's (which combine results from detailed and approximate models) were investigated in this research. Both methods seek to reduce the number of detailed analyses required in an optimization. But there are special problems inherent in applying these approximation concepts to aerodynamic problems. This research has yielded a general solution to the problem of applying correction factors to grids which change size and/or clustering as the design is changed.

Chapter 3

Details of Flow Solvers

3.1 Introduction

The analysis programs provided objective function and constraint data to the optimizer. Two different levels of sophistication were used for these programs: a "detailed" level and an "approximate" level. These levels of modeling can be used individually in the optimizer, or in concert, to form "Global-Local Approximations", as detailed in Section 2.3. The detailed analysis program, which is herein considered the most accurate, consisted of a CFD flow solver for the scramjet vehicle, incorporating a 1-D, constant Mach number combustor model. Separate approximate analysis programs were used for the nose/forebody region and for the nozzle/afterbody region. These used the same combustor model as the CFD program. The forebody/inlet approximate flow solver was based on oblique shock theory, and allowed for arbitrary placement of the shocks there. A simple Method of Characteristics (MOC) model of the nozzle/afterbody was used as the approximate model of that region. In addition, a relatively crude nozzle/afterbody model, using 1-dimensional isentropic flow theory, was used as an alternative model, to examine the effects of various levels of fidelity in the approximate modeling.

This chapter outlines the details of each of these flow solvers, and examines its fidelity.

3.2 CFD Solver

The detailed analysis program consisted of a 2-D inviscid CFD solver for the nose, forebody and inlet, a 1-D constant Mach number combustor model, and a 2-D inviscid CFD solver for the nozzle/afterbody region. All flow in the forebody/inlet, and nozzle/afterbody regions was treated as being ideal-gas frozen flow, with $\gamma = 1.4$.

The solver used the Steger-Warming implicit time marching algorithm for solving the unsteady Euler equations to a steady state. (Ref. 26) This algorithm is an

upwind-differenced flux-splitting technique, using exact flux Jacobians. As implemented in this research effort, the scheme is second-order accurate spatially everywhere except in the vicinity of large pressure gradients (such as near shocks), where a "switch" lowers the spatial differencing to first-order. Generalized curvilinear coordinates were used to allow various types of geometries to be analyzed with the same flow solver.

This well-proven scheme has one major drawback, in that it is inherently more dissipative than some other schemes, such as Harten's Scheme. One result of this is that it does not capture shocks as crisply as those other schemes. This fact can have an impact on the optimization process, if a Global-Local Approximation (GLA) is used. In such a case, the detailed and approximate models may not represent shocks equally crisply, which can lead to problems in calculating the correction factors in the GLA as shocks move. (See Section 5.5.1.) Shock diffusion caused no noticeable problems with optimizations not involving GLA's.

The flow solution process involved solving for the flow in the forebody/inlet region, without regard to the combustor or nozzle flows, since supersonic flow was assumed throughout. Then the combustor flow was calculated, using the 1-D constant Mach number model described in Section 3.3. Finally, the nozzle region solution was found, using the combustor exit flow and the free-stream flow from the forebody solution as upstream boundary conditions.

A special grid generation package was written for the scramjet-powered vehicle problem. A sample grid made by this package is shown in Fig. 3.1. A simplified zonal-type grid was used, with one zone being defined by the grid lines which enter the engine and the other by those which do not. Details of the grid are shown in Fig. 3.2. This figure shows the generalized coordinate system, (ξ, η). Note that there is elliptically-generated η-clustering about the walls. This peculiarity for an inviscid problem is brought about by the need to insure that the grid lines near the wall are very nearly tangent to the wall, when calculating the wall boundary conditions. For the large flow contraction from the nose to the inlet, an elliptic grid-generation scheme for the η coordinates was found to be an effective way of insuring the grid lines near the wall were parallel to the wall, while keeping the changes of slope smooth. This smoothness was found to prevent pressure "spikes" near the wall corners, such as at the nose and compression ramp corners. Such spikes caused problems with the optimization process, since they often introduced spurious changes in

the objective function and constraints. Indeed, for high Mach numbers, sharp changes in grid line slope made the CFD solution unstable.

Note the clustering of horizontal grid lines in the freestream ahead of the inlet in Fig. 3.1. This is an artifact of the simple zonal nature of the grid: the grid lines which have not yet entered the inlet are clustered in the same way as those which have entered the inlet.

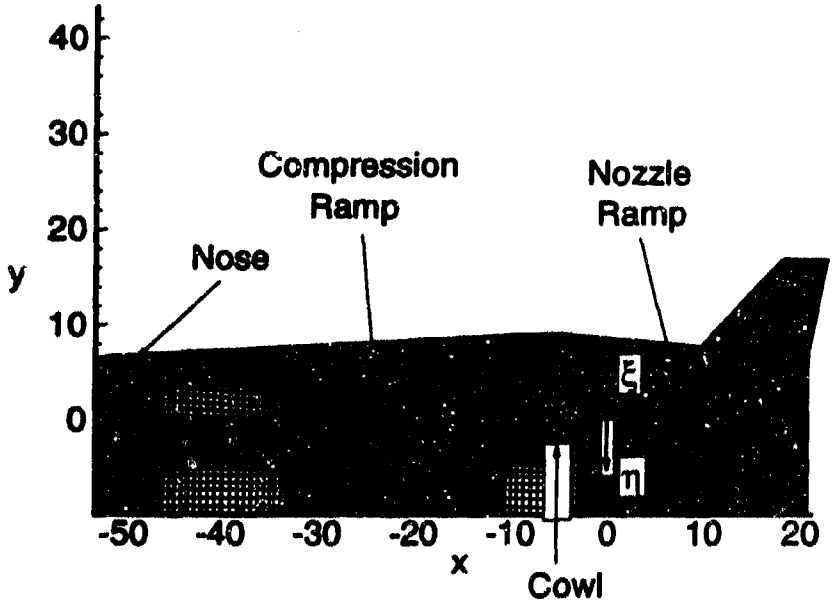

Fig. 3.1 Typical CFD grid for the 2-D scramjet vehicle.

The lines of constant ξ (i.e. vertical lines) were generated algebraically, using cosine-type clustering near the nose, inlet compression ramp, inlet, nozzle throat and nozzle cowl lip.

A maximum grid size of 400x50 was found to give a reasonable compromise between accuracy of the CFD solution and computational time. Actual grid sizes were somewhat smaller in the ξ direction, depending on the values of the design variables. The grid size in the η direction was kept constant at 50 grid points. Run times on an IBM RS-6000/320 Powerstation were about 2.5 hours.

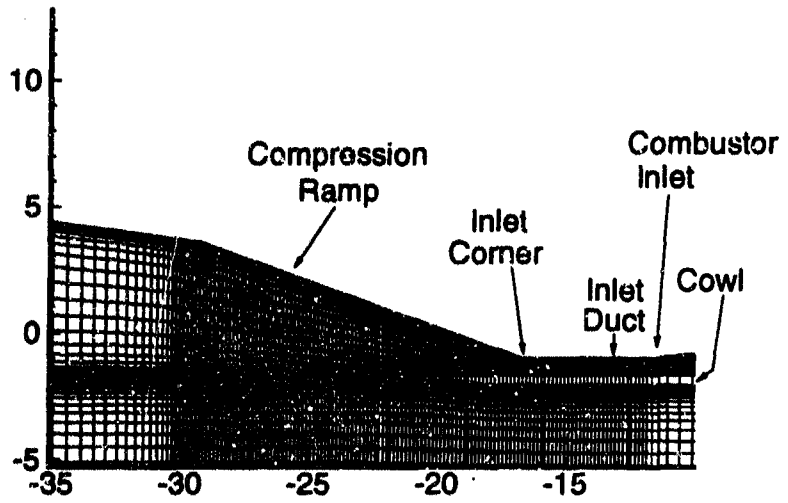

(a) Forebody/inlet region.

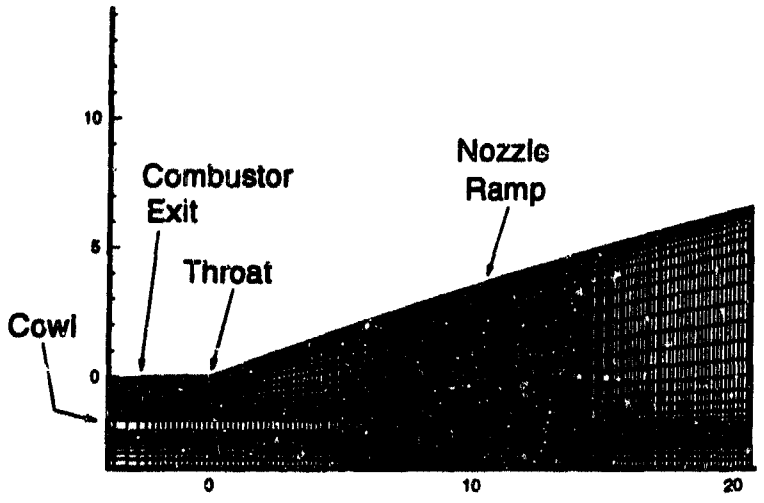

(b) Nozzle/afterbody region.

Fig. 3.2 Details of a typical CFD grid for the 2-D scramjet vehicle.

As the CFD solution developed, the nose and ramp shocks formed near the walls, and then rotated to their correct angles after further iteration. This progression is shown in Fig. 3.3. During the period when the shocks impinged upon the cowl, and continued their progress (if the design warranted further shock rotation), the algorithm was often found to be unstable. This problem was circumvented by using the switch which controlled the spatial accuracy of the scheme to impose first-order accuracy throughout the domain until the shocks had moved approximately to their final positions. Then the switch was changed so that the scheme was second-order accurate everywhere except very near the shocks.

A representative CFD solution is shown in Fig. 3.4. Note the diffusion of the shocks at the nose, inlet compression ramp corner, and off the inlet cowl lip. Recall that the combustor is modeled as a 1-D constant Mach number process, as described in Section 3.3. Convergence histories of the forebody/inlet and nozzle/afterbody solutions are shown in Fig. 3.5 and Fig. 3.6, respectively.

Two measures of convergence were used: the sum of the L-2 norms of the changes in flow variables from one iteration to the next; and the variation of thrust or drag, as appropriate for the forebody or nozzle, from one iteration to the next. There is substantial pre-shock oscillation in the solutions, which keeps the L-2 norms from decreasing more than about 1.5 orders-of- magnitude for the forebody/inlet solution. (See Fig. 3.5a.) However, the effect of this on the drag results is small, as shown in Fig. 3.5b. For the design shown, after 700 iterations, the peak-to-peak variation in drag is less than 0.05% of the mean value. This level of "noise" can be important, though, when using the CFD solver to calculate gradients by a "brute force" finite difference method. In such calculations, we perturb the design variables by a small amount, and difference the CFD results. To keep the resulting differences above the noise level, it was found that the design variables had to be perturbed by at least 1%.

On the other hand, the nozzle solution converged to well over 6 orders-of-magnitude decrease in the L-2 norms; after 800 iterations, the variation of thrust was negligible. See Fig. 3.6a and b.

Based upon such observations, all CFD runs were limited to a maximum of 850 iterations for the nose/forebody region, and 1100 iterations (or 5 orders-of-magnitude decrease in L-2 norms) for the nozzle/afterbody region. It is possible to achieve better convergence with this algorithm, at the expense of lowering the scheme to first-order accurate over more of the flow domain. However, it was found that doing this intro-

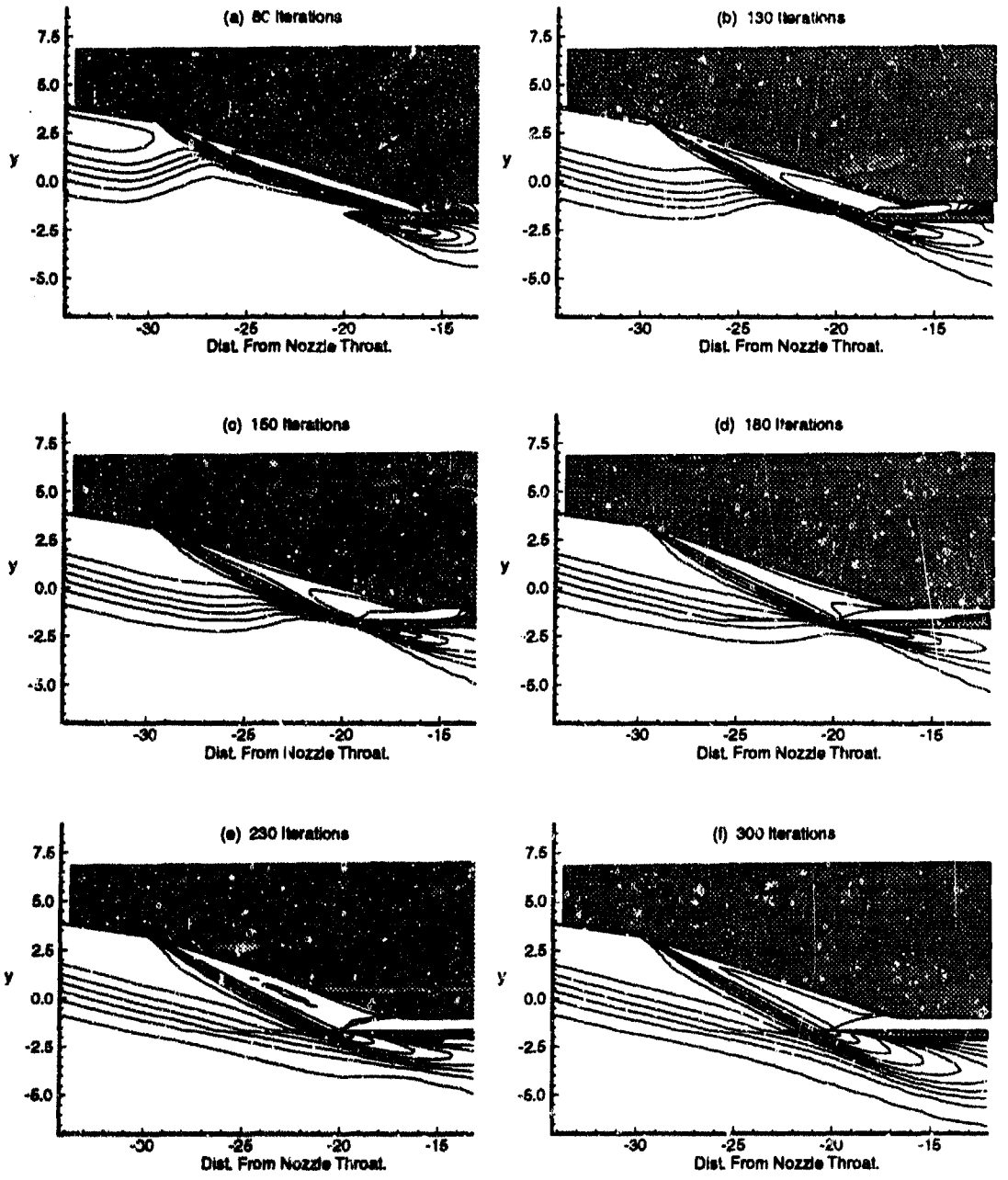

Fig. 3.3 Shock progression during CFD solution of nose/ forebody flow.

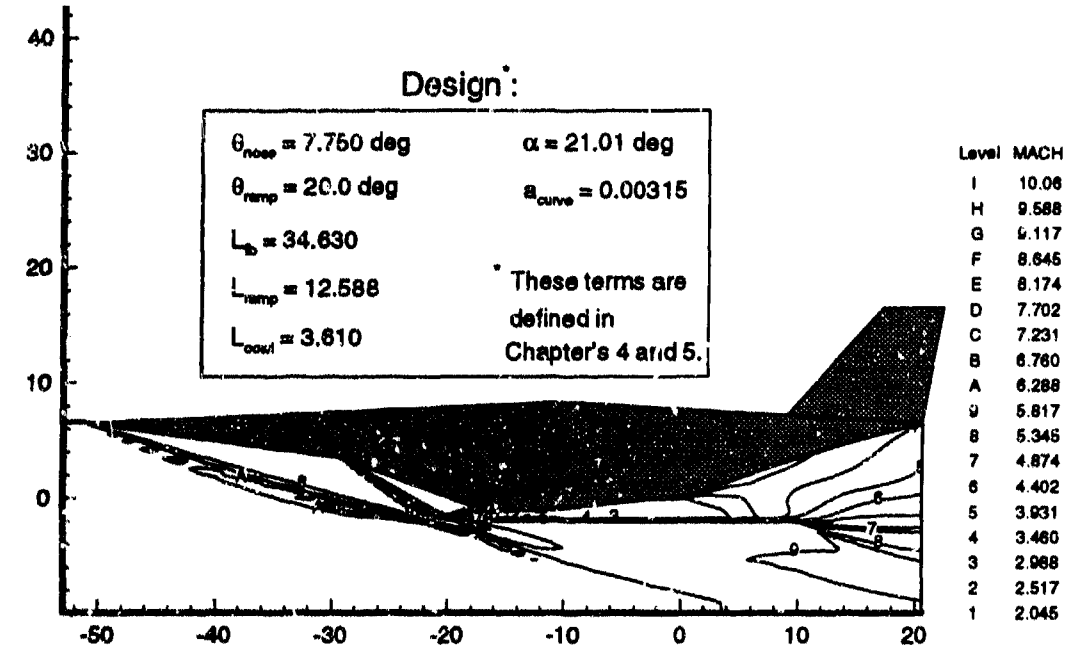

(a) Entire vehicle

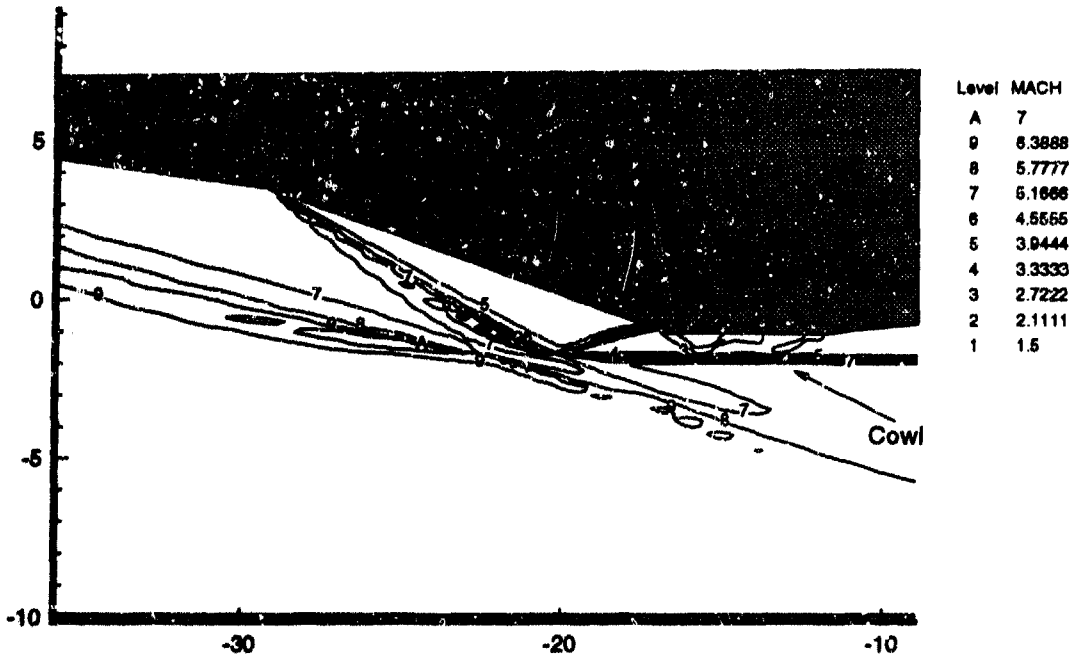

(b) Inlet region

Fig. 3.4 Mach number contours from a representative CFD solution: (a) entire vehicle, (b) inlet region, and (c) nozzle region.

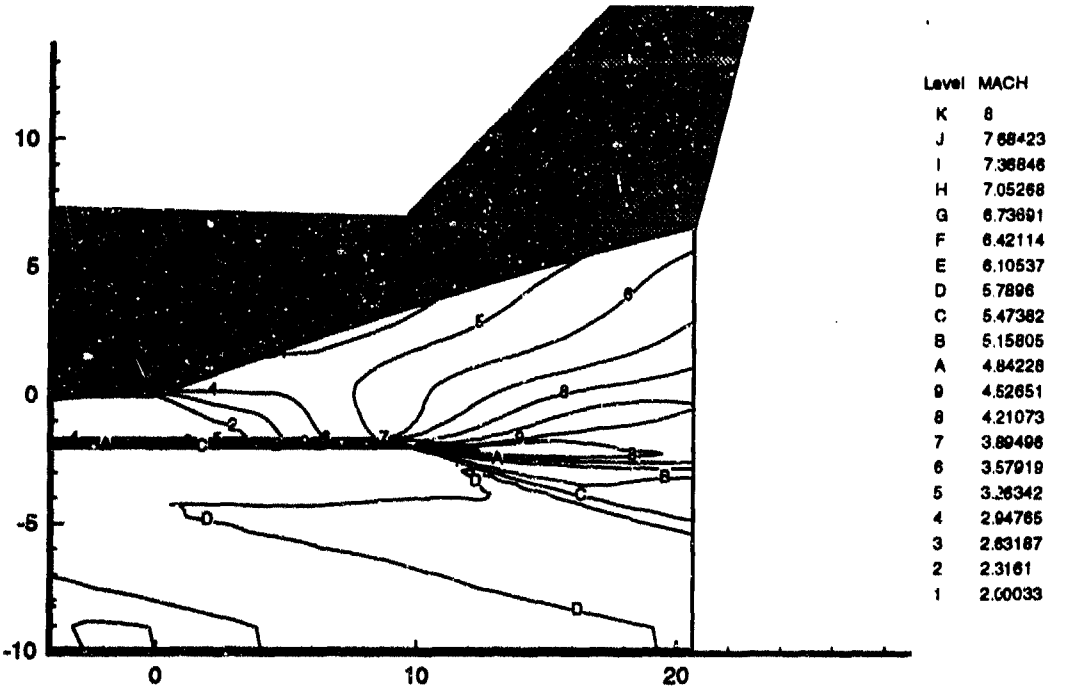

Fig. 3.4 (cont'd) CFD solution for optimum configuration, nozzle region.

duces errors in the shock angles, which can have a dramatic effect on the thrust and drag calculations, due to the sensitivity of the results to shock reflections near the inlet.

To validate the CFD solver, the nozzle/afterbody configuration of Ref. 4 (p. 723, Fig. 4.) was modeled, and the results were compared to the experimental results quoted in that reference. A comparison of the pressure distributions along the nozzle ramp, for the Steger-Warming CFD code, and for the experimental results, is shown in Fig. 3.7. The results are generally quite good, especially bearing in mind that the CFD code is for inviscid flow.

Validation of the CFD solver for the nose and forebody was done by comparing the results to those from oblique shock theory. An example of such a comparison is shown in Fig. 3.8. Again, the agreement is quite good. But note the diffusion of the shocks, due both to the discretization of the CFD method and to the dissipative nature of the Steger-Warming algorithm.

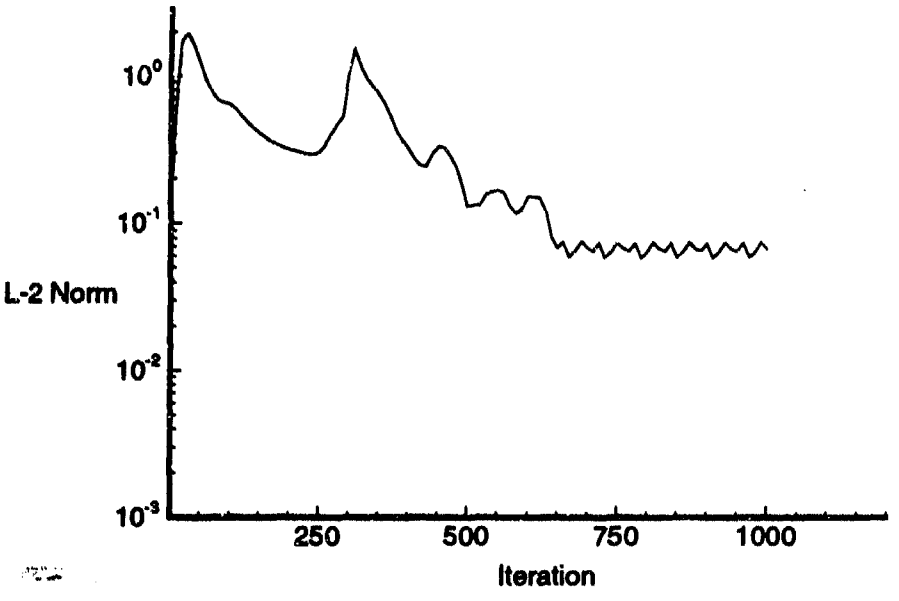

(a) History of nose/forebody L-2 norms.

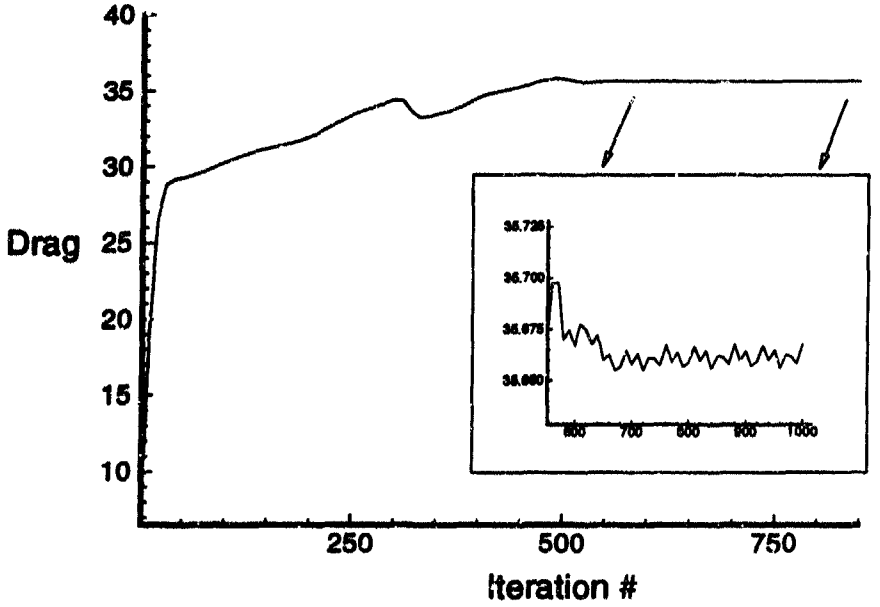

(b) History of nose/forebody drag.

Fig. 3.5 CFD convergence histories for forebody/inlet region for a typical design: (a) sum of L-2 norms, and (b) drag.

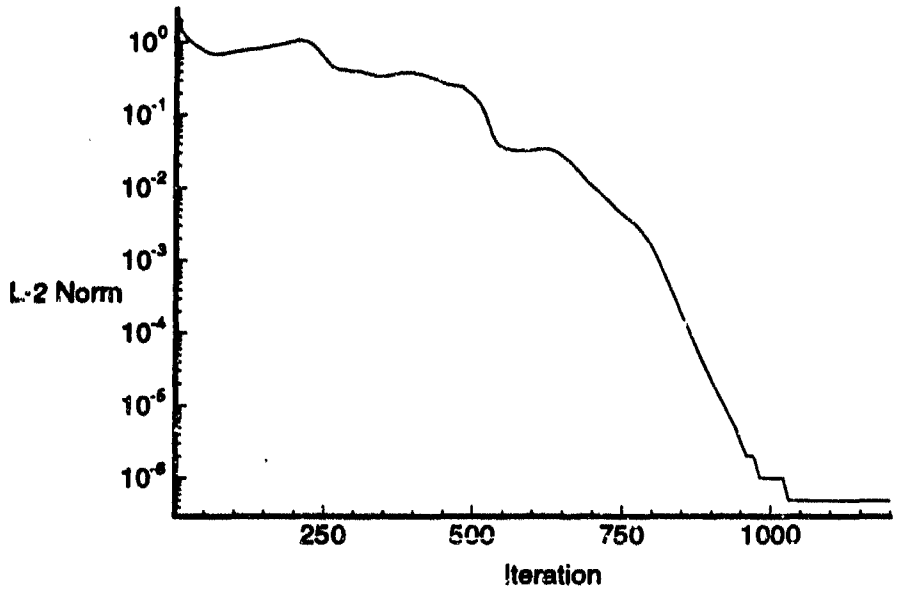

(a) History of nozzle/afterbody L-2 norms.

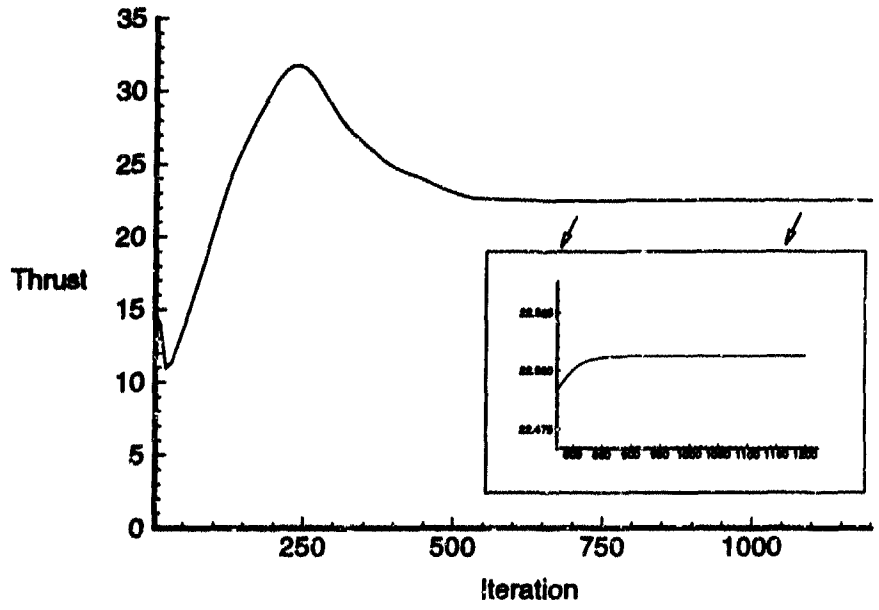

(b) History of thrust.

Fig. 3.6 CFD convergence histories for nozzle/afterbody region for a typical design: (a) Sum of L-2 norms, and (b) thrust.

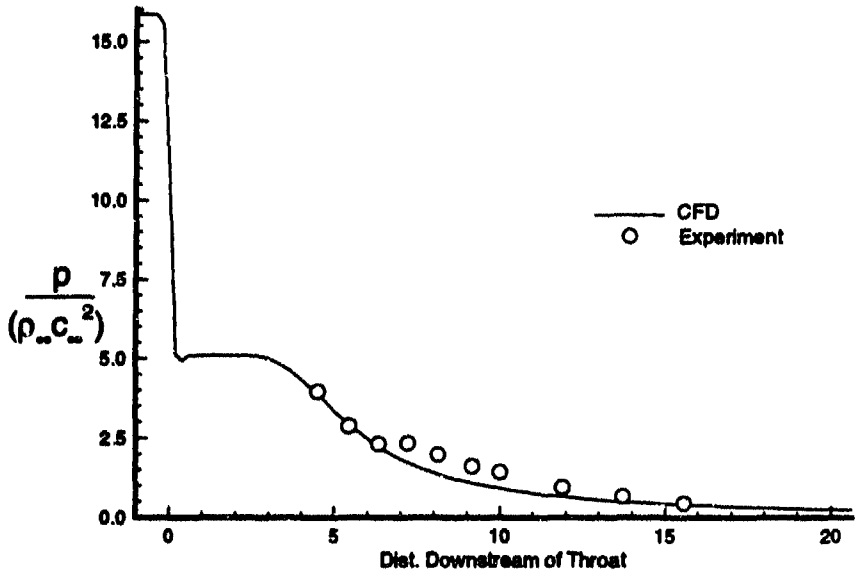

Fig. 3.7 Comparison of CFD nozzle ramp pressure distribution with experiment.

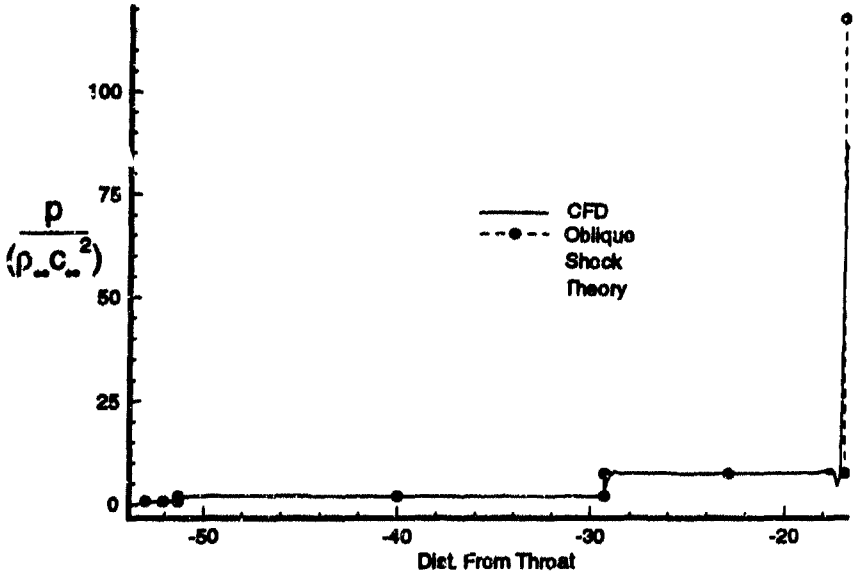

Fig. 3.8 Comparison of CFD nose/forebody wall pressure distribution with oblique shock theory.

3.3 Combustor Model

The combustor was modeled as a 1-dimensional, constant-Mach number process. The fuel-air mixture was assumed to be a perfect gas with $\gamma = 1.4$. The addition of mass due to fuel injection was neglected. It would be more customary to employ a constant-pressure combustor, but as Ref. 22 points out, the constant-Mach number combustor offers two advantages from an analysis standpoint: it explicitly avoids choking in the combustor, and it greatly simplifies the analysis. In fact, the differential equations for generalized steady 1-dimensional flow with heat addition, as given in Ref. 32, can be reduced to algebraic equations for constant-Mach number flow. Note that, to maintain a constant Mach number while heat is being added to the flow, the combustor cross-sectional area must expand from inlet to exit. Such a combustor would be difficult to employ in practice, as it would require that the heat addition be specifically tailored along the length of the combustor. However, for the purposes of demonstrating different optimization strategies, the constant-Mach number combustor provides a useful, simple tool which captures the salient features of total temperature increase and total pressure decrease.

The combustor process is governed by the following relations, in which the subscripts "i" and "e" refer to conditions at the combustor inlet and exit, respectively.

$$\frac{T_{t_e}}{T_{t_i}} = \left(\frac{A_e}{A_i}\right)^{2/(1+\gamma M_c^2)} \tag{3.1}$$

$$\frac{p_e}{p_i} = \frac{A_i}{A_e}\left(\frac{T_e}{T_i}\right)^{1/2} \tag{3.2}$$

where T_t and p_t are the total temperature and total pressure, A is the combustor cross-sectional area, and M_c is the (constant) combustor Mach number.

The area ratio was set by determining a baseline value of total temperature ratio for given freestream and combustor conditions, and applying (3.1) along with the following relations for T_{t_e}.

$$T_{t_e} = T_{t_i} + \frac{Q}{C_{P_{air}}} \tag{3.3}$$

where

$$Q = \Delta H_{fuel} \varphi (FAR)_{stoich} \eta_{mix} \tag{3.4}$$

in which Q is the heat added by combustion, ΔH_{fuel} is the heating value of the fuel, ϕ is the equivalence ratio, $(FAR)_{stoich}$ is the stoichiometric fuel/air mass ratio, and η_{mix} is the mixing efficiency. The freestream conditions were set equal to those for M_∞ = 6.0 at 30 km altitude, and the combustor Mach number was set at 1.20. The fuel was gaseous hydrogen, and η_{mix} was set at 0.90. The resulting area ratio was about 2.693; for simplicity, and because the choice is actually somewhat arbitrary, it was set to 2.5 for all optimizations.

Note that the area expansion in the combustor results in a large portion of the thrust coming from the combustor; for most designs evaluated in the optimizations, "combustor thrust" accounted for about 50% of the total thrust.

Although the combustor length is not critical to the design optimization for the problem at hand, it was felt that a reasonable length should be used. The combustor length was chosen by specifying that, for all designs used in the optimizations, the combustor should be at least long enough to guarantee that mixing and complete combustion take place within the combustor. Using H_2-air reaction rate data from Ref. 35, mixing efficiency data from Ref. 19, and results from the initial design used in the optimizations, the minimum combustor length was found to be about 4 meters. To guarantee that all designs that would be evaluated in the optimizations would have complete combustion, a combustor length of 10 meters was used. The combustor performance is characterized in Fig. 3.9. Shown in Fig. 3.9a are curves of total temperature ratio and total pressure ratio across the combustor, as a function of combustor Mach number. Fig. 3.9b is a parameterization of combustor Mach number for a range of ramp angles, assuming a constant 8.0 degree nose angle. Perfectly-placed forebody/inlet shocks were assumed here. (This restriction was removed for the actual optimizations.) Fig. 3.9c is a similar parameterization, for the thrust produced by the

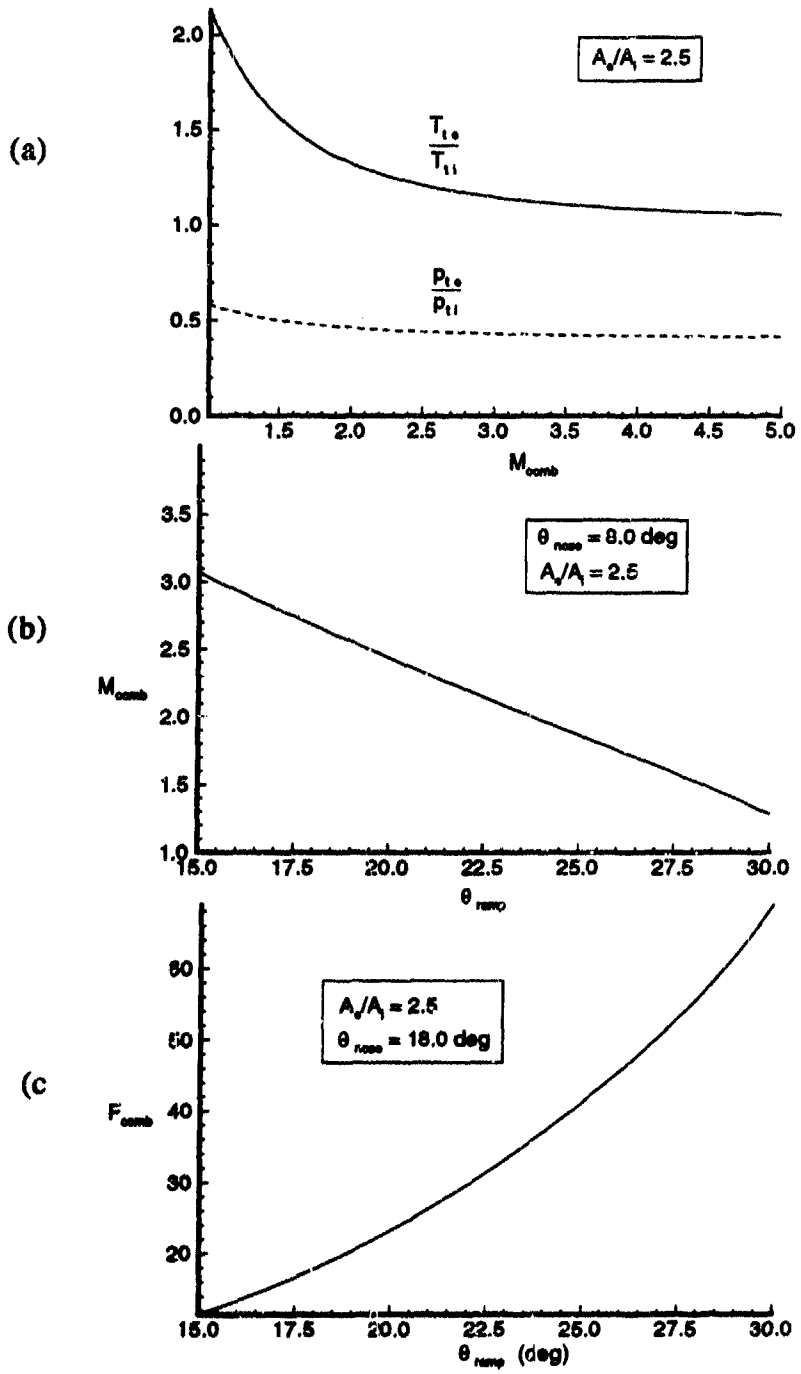

Fig. 3.9 Combustor performance: (a) combustor total temperature and total pressure ratios vs combustor Mach number; (b) combustor Mach number vs ramp angle, for constant nose angle; and (c) combustor force vs ramp angle for constant nose angle.

combustor walls. It is obvious that there is a great deal to be gained (as far as combustor performance is concerned) by using a large degree of flow turning in the forebody. For the nose/forebody optimizations the nose angle was limited to a maximum of 11.0 deg, and the ramp angle was limited to 20.0 deg, since improper placement of the cowl shock (which is allowed by the optimization strategy chosen for this research) could result in engine unstart for angles much greater than these. As can be seen from Fig. 3.9, this greatly limits the combustor performance that can be achieved by the optimizations. However, allowing for arbitrary shock placement helps us examine more thoroughly the performance of the optimization techniques in various flow regimes. The limitation in combustor performance is thus justified.

3.4 Approximate Forebody/Inlet Model

The "approximate" method used to model the nose, compression ramp and inlet was based on oblique shock theory. The conventional design process for such a configuration would limit the possible designs to those with perfect shock placement, with the nose and compression ramp shocks hitting the cowl lip, and the cowl shock impinging on the inlet corner. But in this demonstration of advanced optimization techniques, the optimization process proceeds without explicit regard to the shock locations. Therefore, this approximate model had to be given the capability to treat designs which did not perfectly place the shocks.

This approximate model begins by calculating the shock strengths and angles for the nose and compression ramp shocks (see Fig. 3.10.), using oblique shock theory. It then determines into which of four general categories the shock structure will fall:

Case 1. Nose shock and ramp shock do not intersect each other before reaching the cowl lip, and neither shock impinges anywhere on the cowl. See Fig. 3.10a.

Case 2. Nose shock and ramp shock do not intersect before reaching the cowl lip, and both hit the cowl surface either at or downstream of the lip. See Fig. 3.10b.

Case 3. Nose shock and ramp shock do not intersect before reaching the cowl lip, and the nose shock does not intersect the cowl, while the ramp shock hits the cowl either at or downstream of the lip. See Fig. 3.10c.

Case 4. Nose shock and ramp shock intersect before reaching the cowl lip. See Fig. 3.10d.

For Case 1, the model then calculates the strength and angle of the cowl shock. It finds the intersection of this shock with the fuselage surface, and determines if the shock will reflect from the fuselage surface before passing into the inlet plane. If so, the reflection properties are calculated, and the intersection of the reflected shock with the inlet plane is found. If not, the intersection of the cowl shock with the inlet plane is found. The model then calculates surface pressures along the fuselage forebody and cowl lip, and finds the flow properties along the inlet plane. This information is used to calculate forebody and cowl drag and the average inlet plane flow properties, which are passed to the combustor model.

For Case 2, no shock emanates from the top of the cowl lip, since the flow there is already parallel to that surface. Thus the intersection of the nose shock with the cowl surface is found, and the reflection is found. This reflection then intersects the ramp shock. The method outlined in Ref. 29 for finding the intersection of two shocks of opposite families is used to find the resulting two shocks and slip line. The model then determines if these shocks and slip line intersect the inlet plane directly, or reflect off the inlet surfaces first. It calculates such reflections, if necessary, and so finds the average inlet plane flow properties and surface pressure distributions.

In Case 3, there is a shock off the cowl lip. The model finds the intersection of this shock with the ramp shock, and finds any subsequent intersections of shocks with the inlet surfaces and then with the inlet plane. It then determines the surface pressures and inlet plane flow properties.

Note that, in Cases 1-3, the model treats the intersection of slip lines with shocks very crudely. It simply terminates a slip line when it reaches a shock. Also, the effect of the slip line on the strength, shape and direction of downstream shocks is neglected. The only real accounting of a slip line occurs when it intersects the inlet plane. In such a case, the difference in flow properties on either side of the slip line affect the average inlet plane flow properties that are passed to the combustor model.

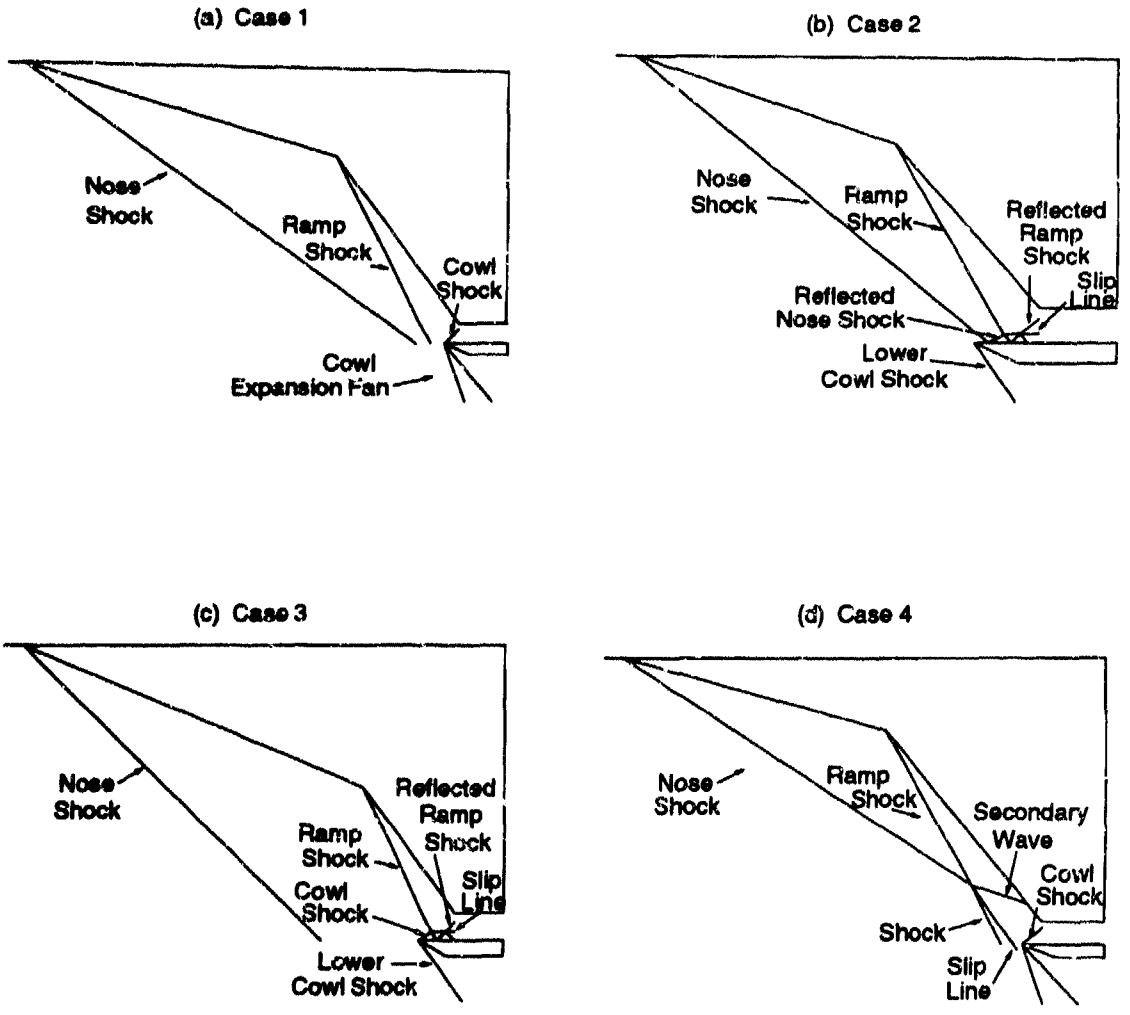

Fig. 3.10 Forebody/inlet shock configurations used by the approximate model.

Case 4 invokes the calculation of the intersection of two shocks of the same family, as explained in Ref. 29. It determines the resulting "transmitted" and "reflected" waves and slip line. Then it checks to see if the transmitted shock hits the cowl. From this point, it proceeds in much the same manner as Cases 1-3. Note that the slip line from the intersection of the nose and compression ramp shocks is tracked all the way to the inlet plane. Furthermore, the treatment of the intersection of this slip line with a shock is rather better than similar intersections in Cases 1-3, in that, upon crossing the slip line, the shock is deflected. This additional fidelity (and complexity) was warranted by the influence this slip line has on the location of the intersection of the cowl shock with the wall surface. This intersection has a great effect on the drag and thrust results, since the presence of a shock reflection near the inlet corner can greatly increase forebody drag, as well as the average pressure and density in the inlet plane.

Note also that the "reflected" or "secondary" wave from the shock intersection in Case 4 is tracked no further than its intersection with the wall. This was done to simplify the analysis.

Since this approximate model uses oblique shock theory for its shock calculations, the shock-jump values and shock angles for the nose, compression ramp and cowl shocks may actually be slightly more accurate than their CFD counterparts. However, the approximations concerning the treatment of slip lines in Cases 1-3 and the treatment of the reflected wave in Case 4 introduce errors in the results of the approximate model.

The greatest source of error in the approximate forebody model is that it does not model the interaction of the inlet shock system with the expansion at the inlet corner. It simply assumes that the effect of the expansion is to "freeze" and to average the inlet plane flow conditions. This assumption greatly simplifies the model. Comparisons of the approximate model's results with those of the CFD solver (which models the flow through the entire inlet length) show that this assumption is reasonable, if somewhat in error. In the optimizations, the largest difference between drag values observed for the two different models was less than 12%, and the largest difference between thrust values was less than 23%. Most often, the differences were less than 7%. The values of *net* thrust, however, were in error by as much as 80%. But for the purposes of optimization, this model does quite well, as will be shown in Section 5.5. It correctly captures the trends in net thrust that changes in the design variables cause.

This was demonstrated by the similar results obtained from optimizations using CFD alone and using the approximate model alone.

3.5 Approximate Models for the Nozzle

For the purpose of comparing models of differing accuracy, two different approximate models of the nozzle/afterbody were made. The first was a straightforward application of the steady, 2-dimensional Method of Characteristics (MOC), as detailed in Ref. 33. The second was a simple application of 1-dimensional isentropic flow, assuming that no shock waves impinge upon the nozzle ramp.

3.5.1 MOC Model

A typical MOC mesh for the scramjet nozzle/afterbody is shown in Fig. 3.12a. In this model, all characteristics emanate from the expansion corners. That is, half of the characteristics have their origins at the ramp corner, and the other half have their origins at the cowl corner. Each expansion fan is divided into 50 characteristic lines. (For clarity in Fig. 3.12a , only 25 characteristic lines are shown emanating from each corner.)

Depending on how much the flow at the cowl lip is under- or over-expanded, there will be either an oblique shock or an expansion wave there to adjust the freestream flow pressure and direction, and possibly also one to adjust the nozzle flow. See Fig. 3.11. It is assumed in the MOC analysis that no such shock intersects the nozzle ramp. This is justified because, for all the optimiztions performed, the flow was only slightly over-expanded or under-expanded. Also in the MOC analysis, the interactions between the characteristics and these waves emanating from the cowl lip are neglected. This is justified on the assumption that the resulting reflection of the characteristic is unlikely to intersect the ramp, given our geometry. (See Fig. 3.12a.) Also, as pointed out in Ref. 29, Article 16.8, the result of an intersection between an expansion wave and a shock of the same family is a weak reflected expansion wave and a curving of the shock. The weak expansion wave is not likely to have much of an impact on the ramp surface pressure distribution, even if it is felt there.

Fig. 3.12a also shows that, since the characteristics emanate only from the corners, no characteristics intersect the ramp between the ramp corner and the intersec-

tion of the first reflected characteristic with the ramp. The correct wall pressure will be found at the first intersection with the ramp, but the variation of pressure between the ramp corner and this point will be unknown. In this model, the wall pressure is assumed to vary linearly between these two points.

Fig. 3.12b compares wall pressure distributions for the MOC model with those from the CFD solver, for a representative configuration. Note the linear distribution of pressure immediately downstream of the ramp corner, as mentioned in the previous paragraph. This is due to the lack of characteristics modeled in this region. Note, also that the general character of the CFD wall pressure distribution is reasonably well replicated by the MOC.

Although the values of net thrust found by the MOC model differ from the CFD values, the general trends of behavior, as the design variables are allowed to vary, do follow those of the CFD quite well, as shown in Fig. 4.2 and Fig. 4.3.

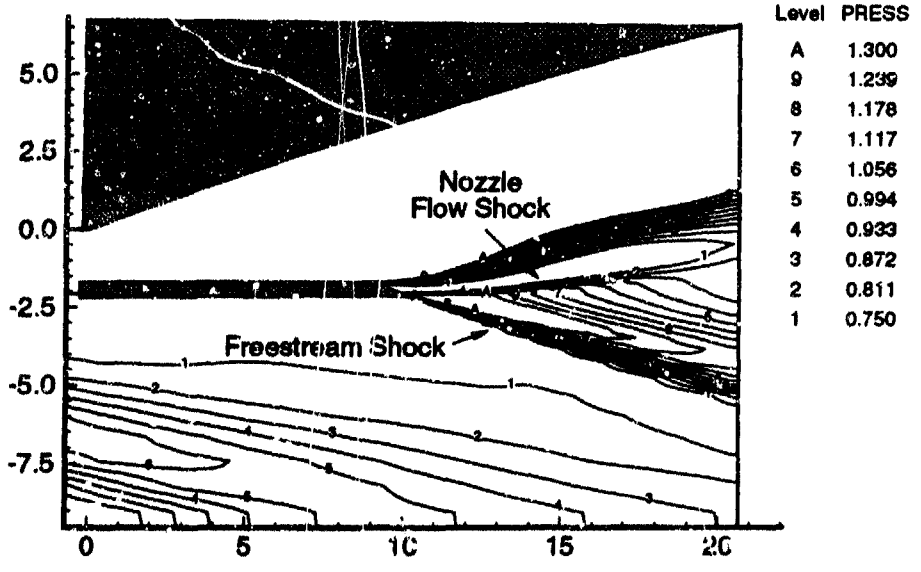

Fig. 3.11 Example of waves emanating from cowl lip.

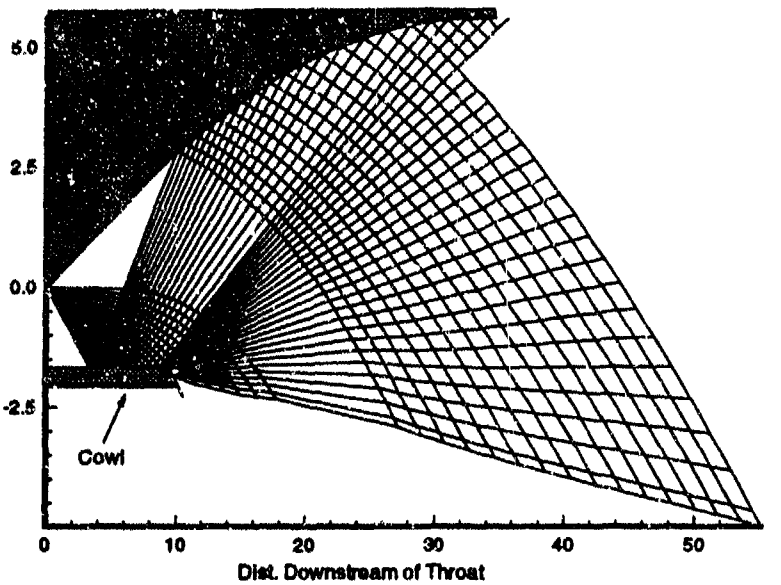

(a) MOC Nozzle Mesh.

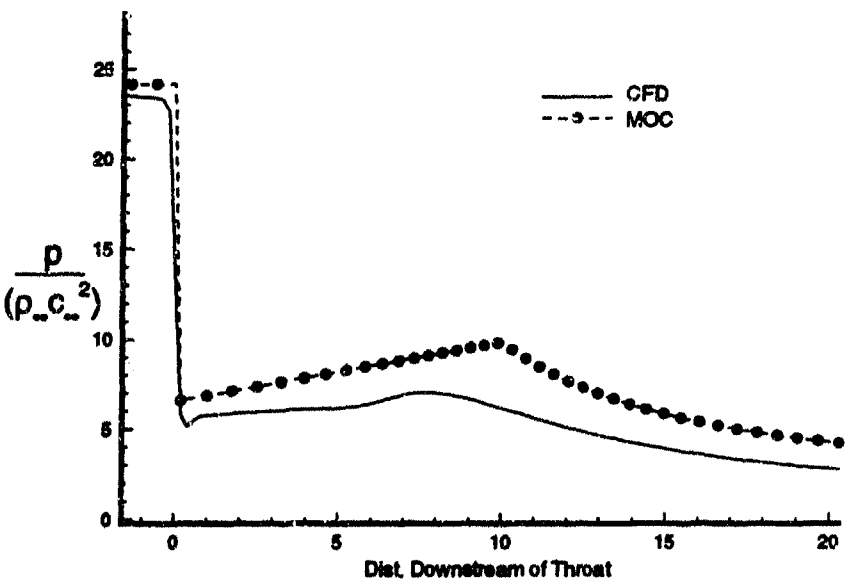

(b) Ramp Pressure Distribution.

Fig. 3.12 Method of Characteristics nozzle mesh and ramp wall pressure distribution, with comparison to CFD results. (Same configuration as in Fig. 3.4.)

3.5.2 1-D Isentropic Flow Model

The 1-D flow model assumes the flow in the nozzle/afterbody region behaves one-dimensionally, with flow cross-sectional areas defined by the area between the ramp surface and either the cowl inner surface (if appropriate), or the "contact surface" bounding the nozzle plume. See Fig. 3.13a.

This contact surface is found by examining the CFD solution for a baseline design configuration. To identify the location of the contact surface at some station downstream of the cowl lip, we draw a vertical line segment at that station and search along this line, between the lowest point in the freestream and the point which is on a level with the cowl lip. See Fig. 3.11. We identify the point of maximum fluid density as the point on the contact surface. This definition of contact surface is motivated by the observation that, for the configurations used in the optimizations, the two waves emanating from the cowl lip are usually both weak shocks. We know that the contact surface must lie somewhere between these two waves, and that the point of maximum density will also lie between them. Since this point is readily identifiable from the CFD solution, the point of maximum density is attractive for identifying the contact surface.

When the contact surface is found by this method, it has a "staircase" quality, as shown in Fig. 3.13a. This is due to the discrete nature of the CFD solution. For the 1-D model, this surface is smoothed by connecting the midpoints of the vertical legs of the steps as shown.

A typical nozzle ramp pressure distribution found by the 1-D isentropic flow model is shown in Fig. 3.13b. The CFD solution is also shown. Note that over the first half of the length, the 1-D model does not provide a good representation of the flow at the wall, as would be expected from its inherent limitations. However, over the downstream half it becomes much more accurate.

Reference to Fig. 4.3 and Fig. 4.4 show that, as expected, the net thrust predictions from the 1-D model do not follow the CFD values as well as the MOC predictions do.

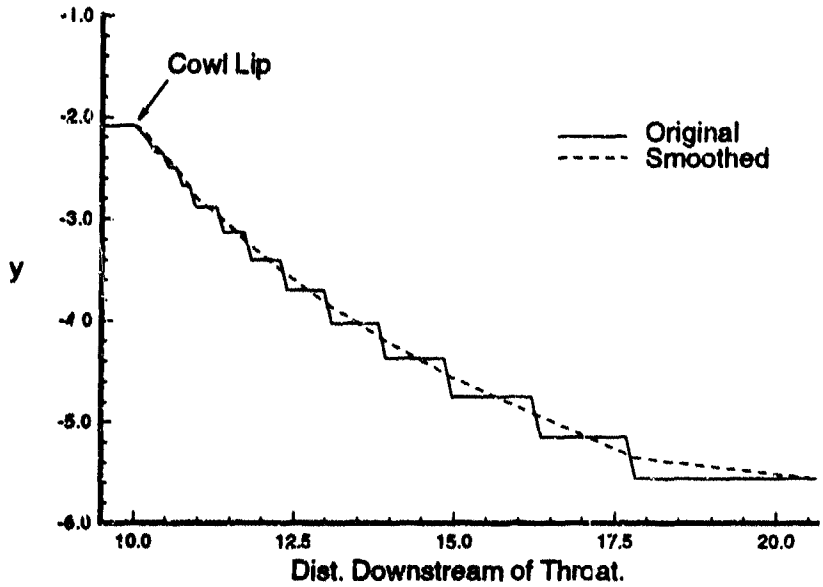

(a) Contact surface.

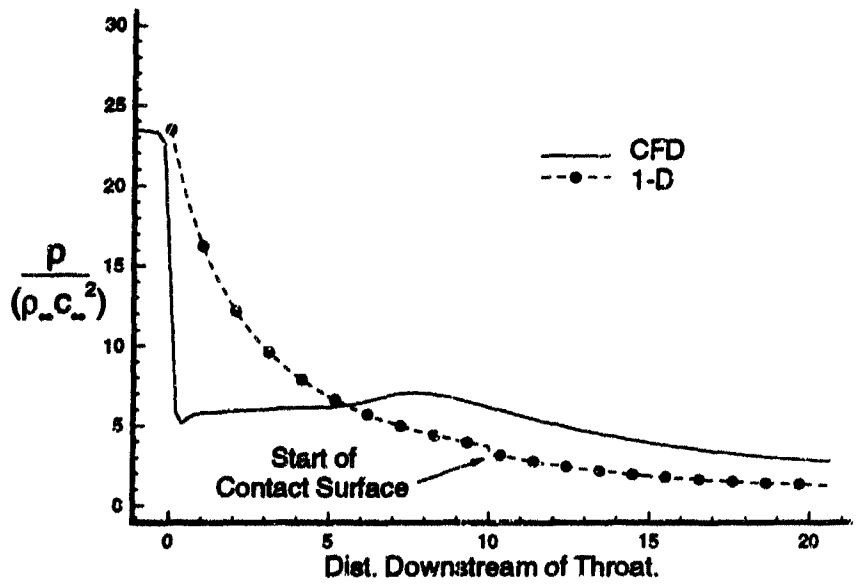

(b) 1-D ramp pressure distribution.

Fig. 3.13 Typical results from 1-D isentropic flow model: (a) contact surface, and (b) ramp surface pressure distribution, compared to CFD.

3.6 Summary

A 2-D Euler-solver CFD program provided the "detailed" analysis capability for the optimizations. The "approximate" model of the nose/forebody consisted of an oblique shock theory model which allowed for simplified treatment of arbitrary shock configurations. Two approximate models of the nozzle/afterbody region were made, for purposes of comparison: one based on the steady 2-D Method of Characteristics, and a more crude one based on 1-D isentropic flow theory. The approximate models were all shown to provide generally reasonable fidelity in relation to the CFD program.

The detailed and approximate models were intended to be used individually in the optimizations, as well as in concert, to form the bases of the "Global-Local Approximations" (GLA's).

Chapter 4

Nozzle/Afterbody Optimizations

4.1 Introduction

The approximation concepts were first applied to optimizations of the nozzle/afterbody region. This region is characterized by wall flow that is essentially isentropic, and thus is a rather benign environment for the approximation concepts. Nozzle optimizations are also cheaper to perform than forebody/inlet optimizations, since the nozzle inlet conditions can be specified, and only the nozzle portion of each of the flow solvers has to be run. Thus, it is particularly attractive to begin the optimizations with the nozzle.

This chapter describes the nozzle optimization setup. Then it investigates the fidelity of each of the approximation concepts by performing a series of single-variable design parameterizations. Finally, it discusses the actual optimizations that were performed on the nozzle using each of the approximation concepts, as well as CFD-alone and each of the uncorrected approximate methods. Forebody/inlet optimizations will be treated in Chapter 5.

4.2 General Problem Considerations

Fig. 4.1 shows the setup for this design problem. Note that the ramp surface is defined by a quadratic equation in x, where x is the horizontal distance from the throat. (This follows from the observation in Ref. 4 that skewed parabolic contours have been considered for 2-D NASP nozzles. Other families of surface descriptions may be just as easily used in the optimization process.)

The following design parameters were considered to have predominant influences on the thrust: initial angle of the ramp (α); curvature of the ramp, a_{curve}, as defined by the quadratic coefficient in the equation for the ramp surface; cowl angle (β). Note that these parameters can be expressed by combinations of other parameters, and that using such alternative parameters for the design variables may actually

result in better optimizer behavior. (See Section 4.4.1) Other potentially important design parameters, such as cowl length and cowl curvature were not treated, in the interest of limiting the size of the problem.

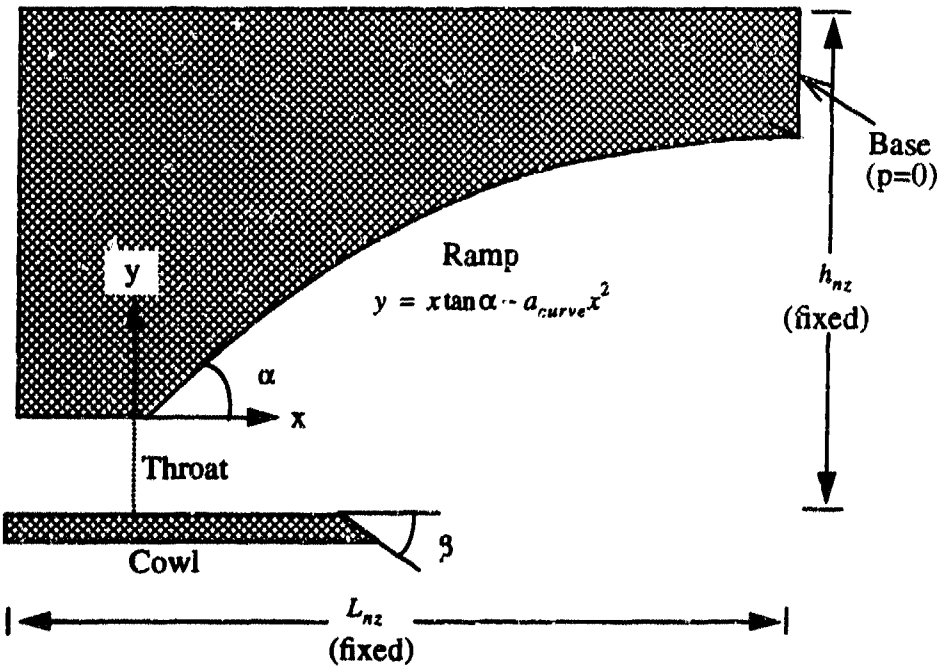

Fig. 4.1 Nozzle optimization geometry.

The approximate analysis models used were the 1-D isentropic flow model, and the Method of Characteristics (MOC) model. Local (Taylor series), and Global-Local Approximations (GLA's) were used. (See Sections 2.2 and 2.3.) The CFD method is herein deemed to be the most accurate of the methods, since it most accurately treats the effects of the nozzle plume, and since it is much more finely discretized than the next most accurate method, the MOC. (The CFD model's accuracy is somewhat lessened by its numerical damping, which is absent in the MOC.) Thus, the CFD results will be the baseline against which all other methods will be compared.

Throat flow conditions were fixed, and corresponded to those resulting from the design shown in Fig. 3.4. (The forebody/inlet design in that figure is close to the optimum design, as will be seen in Chapter 5.) The throat flow was assumed to be uniform, 1-D flow. All flow in the nozzle was assumed to be frozen, perfect gas flow, with $\gamma = 1.4$. The inflow conditions for the external flow were set equal to the freestream values.

4.3 Single-Variable Parameterizations

In order to gain insight into the relative accuracies of the different analysis models and approximation concepts, a set of nozzle performance curves were generated, in which the normalized net thrust is presented as a function of each design variable, with the other design variables held constant. Each of the analysis models and approximation concepts was used and the results were plotted on the same plot. These "parameterizations" are shown in Fig. 4.2 through Fig. 4.4.

In those figures, the darkened square data points are from the CFD solutions. The Global-Local Approximations (GLA's) using the MOC and 1-D models are labeled MOC GLA and 1-D GLA. Both of these GLA's and the Taylor series model were based upon baseline designs at $\alpha = 18.0°$, $\beta = 18.0°$, and ramp curvature coefficient of 0.005. In the plots the minor vertical displacements of the Taylor series and GLA curves relative to the CFD baseline design solution are due to the different grids and integration schemes used by these methods. These "DC shifts" have no effect on the trends of the results, and thus do not affect the optimization process. The shifts in F_{nst} at the design point are less than 0.15.

Figs. 4.2--4.4 highlight the advantage of the GLA approach over the uncorrected approximate methods and, to a lesser degree, over the Taylor series method. Near the baseline design point, the trends of the GLA results agree quite well with those from the CFD, even when the uncorrected approximate methods do not. Indeed, in Fig. 4.2, for α between 17.5 and 18.5 deg, the Taylor series, 1-D GLA and MOC GLA results follow the CFD results so well that they are indistinguishable from the CFD curve. As the design is shifted further away from the baseline, the GLA and Taylor results still follow the general trends of the CFD far better than the uncorrected approximate results do. Note in Fig. 4.3 that the 1-D GLA and MOC GLA overlay

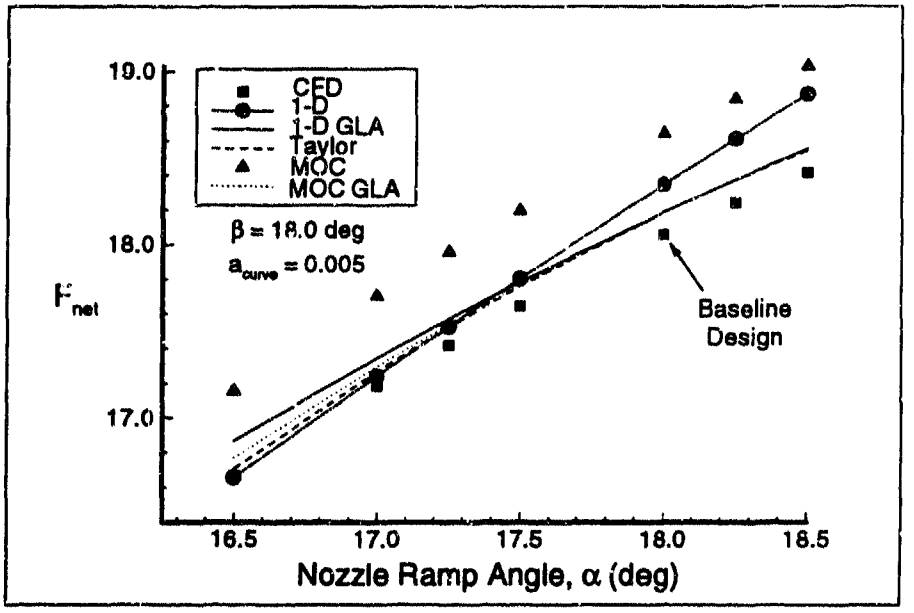

Fig. 4.2 Parameterization of F_{net} vs nozzle ramp angle, α, for various models.

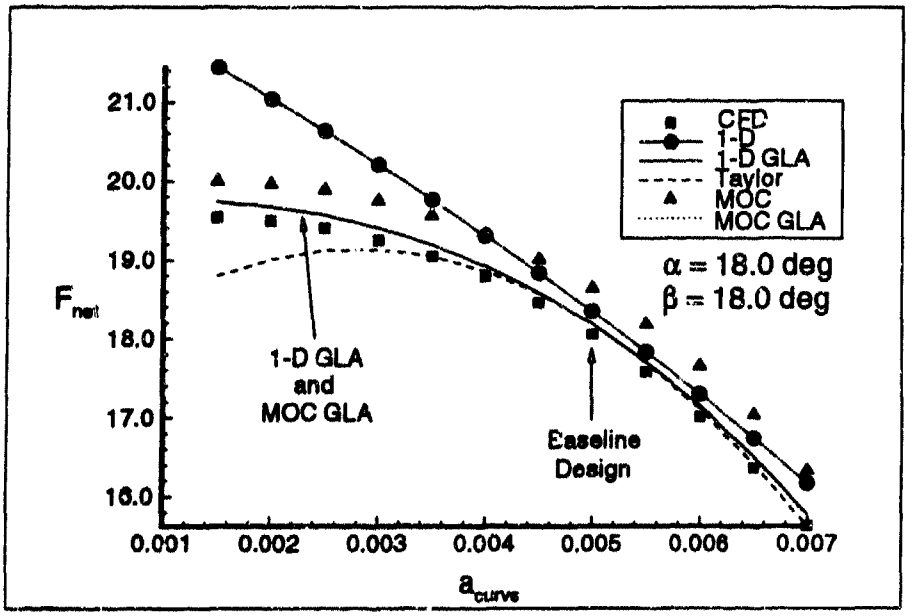

Fig. 4.3 Parameterization of F_{net} vs nozzle ramp curvature coefficient, a_{curve}, for various models.

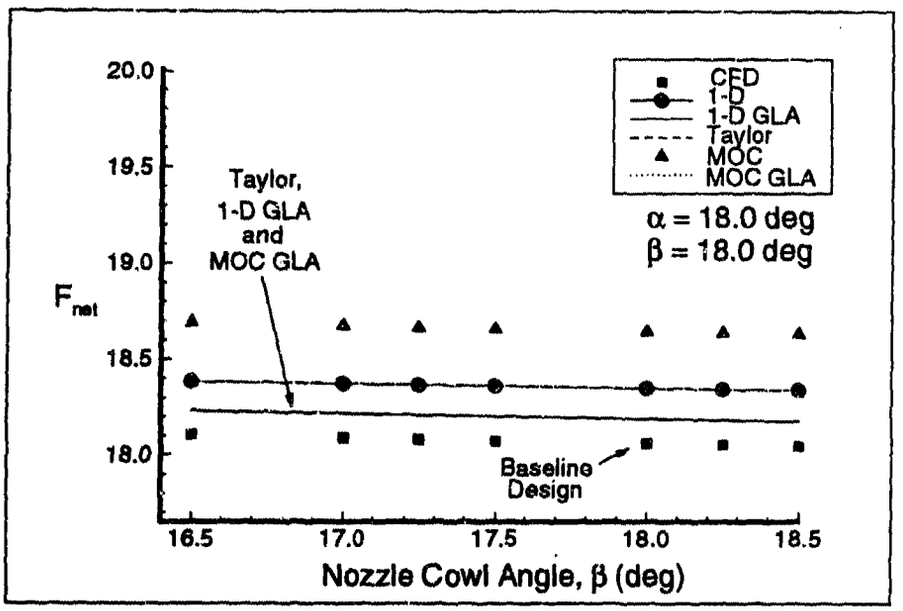

Fig. 4.4 Parameterization of F_{net} vs nozzle cowl angle for various analysis models.

each other perfectly over the entire range of shown.

The parameterization curves show that, for the parameterizations in this particular problem, the GLA's are better at mimicking the CFD solver than the uncorrected approximate models are. There is really very little to choose between these two GLA's. The Taylor series also does better than the approximate methods, except in the a_{curve} parameterization, where the uncorrected MOC conforms better to the shape of the CFD curve, for values of a_{curve} far from the baseline design.

Note, especially in Fig. 4.3, that the first-order Taylor series approximation applied to point properties (wall pressures) does not produce a linear F_{net} behavior. Had we applied the Taylor series directly to the *integral* property (F_{net}), the curve would have been linear. This is a clear example of how nonlinearities in a problem can be better handled by some formulations of approximation concepts than by others.

4.4 2-Variable Nozzle Optimizations

Having established the general behavior of the various modeling levels and approximation concepts, the nozzle design was optimized, using each of them. Because the effect of cowl angle on thrust was seen to be much smaller than that of ramp angle and curvature, only the nozzle ramp geometry was considered for determining the design variables.

Each optimization was performed by combining the well-proven optimization software package "Design Optimization Tools", or DOT (See Ref. 12.), with one or more 2-D flow solvers (or "analysis programs"). DOT uses the "Modified Method of Feasible Directions" to solve constrained nonlinear optimization problems. In this case, DOT was instructed to find the vehicle design which maximized net thrust (Thrust - Drag).

4.4.1 Choice of Design Variables

It has long been known that the choice of design variables can have an impact on the optimization process. Although α and a_{curve} seem to be the most obvious choices for ramp design variables, another set of design variables was considered. This set comprised α and h_{nz}, the height of the nozzle exit plane, with a_{curve} being determined from these two.

To investigate the appropriateness of each of these 2 choices of design variables, a set of optimizations was run with each, using the MOC only and the conditions listed in Section 4.4.2. The results are shown in TABLE 4.1.

As can be seen in TABLE 4.1, there was virtually no difference in the optimum designs. However, it was decided to use α and h_{nz} for all subsequent optimizations, for the following reasons.

First, in order to minimize axial momentum loss in the nozzle, we would like to keep the nozzle exit wall angle as close to horizontal as possible, while still meeting the other requirements of the optimization, such as the fixed nozzle length and maximum nozzle exit height. This tendency can be incorporated into the optimization process if, for a reasonable initial design, an increase in α is accompanied by an

TABLE 4.1

Effects of using different design variable sets on the nozzle optimization, using uncorrected MOC.

	α and a_{curve}	α and h_{nz}
Initial α	18.000	18.000
Initial a_{curve}	0.0050	0.0050
Optimum α	18.051	18.084
Optimum a_{curve}	0.00033	0.00036

increase in a_{curve}. That is, if the effect of an increased initial wall angle is tempered by an increase in the curvature. (See Fig. 4.1.)

To make this design philosophy a part of the optimization process, this tendency should be reflected in the gradient calculations, to insure that a proper search direction is always chosen. This is the case for the design variable pair α and h_{nz}. That is, if we increase α while keeping h_{nz} constant (as is done when calculating the partial derivative of F_{net} with respect to α) then a_{curve} will necessarily increase. We could consider this to be a "smart" design variable set. If, on the other hand, α and a_{curve} are used as design variables, the two can change independently, and this design philosophy would be lost.

Secondly, choosing a length instead of an angle can help to reduce the non-linearity in the problem. As a greatly simplified example of this effect, consider a straight ramp with a constant pressure distribution as shown in Fig. 4.5. The axial force exerted on the ramp is

$$F_x = pL\tan\alpha \tag{4.2}$$

which is clearly nonlinear in the design variable, α. However, if we use h_{nz} as the design variable, we have

$$F_x = ph \tag{4.3}$$

which is linear in the design variable. Although the actual nozzle design problem is much more nonlinear than this example, we might expect some improvement in the optimization process due to choosing the right design variables.

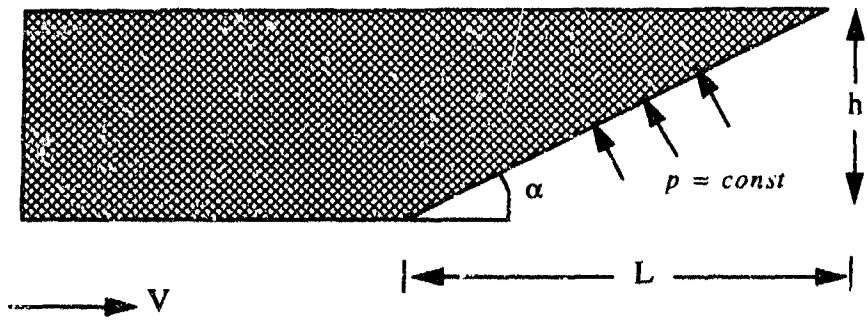

$$F_x = pL\tan\theta = ph$$

Fig. 4.5 Example of the linearizing effect of choosing h_{nz} as a design variable.

4.4.2 Optimization Setup

For each of the nozzle-only optimizations, the design was optimized using the initial ramp angle, α, and the nozzle exit height, h_{nz}, as design variables. Optimizations were run for all analysis models and approximation concepts: CFD alone; 1-D isentropic flow alone; MOC alone; Taylor series; GLA using 1-D isentropic flow; GLA using MOC. The resulting designs were compared, and the savings in computer resources for each method were then found. The figure of merit for these savings was the number of required calls to the CFD solver, exclusive of the calls used to calculate the gradients of the objective function and constraints. The number of CFD calls is used as the figure of merit since the CFD solutions are by far the costliest part of the analysis, and since this measure is independent of the type of computer used. The CFD calls for gradient calculations are excluded because there are methods of finding the gradients analytically or semi-analytically, without relying on finite-differencing the results of CFD solutions, as was done in this research. (See Ref's. 4, 13, and 14.)

For all these optimizations, the initial values of α and h_{ij} were 18.0 deg. and 3.74 times the combustor exit height, respectively. (This corresponds to a ramp curvature coefficient, a_{curve}, of 0.005.) The forebody, compression ramp, and inlet configurations were held constant at the design shown in Fig. 3.4. The forebody and cowl drag and the combustor inlet properties were held constant. However, the contribution of drag due to base pressure was allowed to vary as the nozzle geometry changed. (If the height of the nozzle exit plane was less than the height of the forebody, then the pressure on the bluff base was set to zero. (See Fig. 4.1.) The nozzle height was not allowed to be greater than the forebody height for the nozzle optimizations, and the nozzle length was fixed. The only constraint placed on the solution was that the pressure at the tip of the ramp should be at least 0.41 times the freestream pressure. This constraint was chosen to prevent reverse flow into the nozzle from the freestream, and the limiting value of 0.41 was rather arbitrarily chosen by examining the data from Ref. 4.

The following side constraints were imposed on the optimizations: the initial ramp angle, α, was to be between 10 and 26 degrees; the nozzle exit plane height was to be between 4.0 and 6.5815 (which was the forebody height). No direct constraints were placed on a_{curve}.

For the Taylor series and the GLA's, move limits of 10% were arbitrarily imposed on the design variables. That is, for each iteration, the design variables were limited to be within 10% of the baseline design for that iteration.

4.4.3 Optimization Results

The results for all the nozzle optimizations are shown in TABLE 4.2. Shown in the table are the final values of α and a_{curve}, net thrust (normalized by $\rho_\infty c_\infty^2 L_{ref}$, where L_{ref} = 1.0 meters.), and the required number of calls to the CFD solver. For consistency, the optimized net thrust values shown were all were evaluated by applying the CFD solver to the optimum design found by each method. Also shown, for each approximation concept, is the cost in computer time for 1 step in an iteration, normalized by the cost for 1 step using CFD only. Fig. 4.6 shows the nozzle contours for the initial and all optimized designs.

Fig. 4.6 shows that all the optimized designs led to relatively sharp afterbody trailing edges, in order to eliminate base drag. Thus the differences in the various

TABLE 4.2 Results of nozzle/afterbody optimizations. (All net thrust values are as found by CFD solver.)

	α	a_{curve}		CFD Calls	Relative Cost/Step
	18.000	0.0050		----	----
	26.000	0.0082		----	----
	26.000	0.0082		----	----
	20.362	0.0031		7	.0098
	20.850	0.0035		7	.0083
	20.563	0.0033		7	.0109

* As calculated by the CFD solver.

optimized designs have to do with how the optimizer varied the ramp contour between the fixed throat location and the essentially fixed trailing edge.

TABLE 4.2 shows that the CFD-only optimization required 22 calls to the CFD solver (exclusive of calls for calculating gradients). Each of these calls required 66 minutes of CPU time on an IBM RS 6000 workstation.

The uncorrected 1-D and MOC optimum designs were very different from the CFD optimization. They both optimized to the same design, because each hit the maximum allowable α, and then set the base area nearly to zero by adjusting h_{nz}. (See Fig. 4.6c.) In addition, their optimum values of F_{net} were 6% lower than for the CFD, Taylor series and GLA methods.

The Taylor series and the MOC GLA optimized to designs very close to that which the CFD-only optimization selected, but did so with only 7 calls to the CFD solver respectively. This represents a savings in computer time of 68%. Although 10% move limits were imposed on the design variables for these optimizations, it is possible that greater move limits could be imposed, perhaps resulting in some further savings. Although the 1-D GLA optimum design is not quite as close to the CFD opti-

mum design, the optimum net thrust is almost identical, and the savings in CFD calls are the same as for the Taylor series and MOC GLA.

The relative cost of one step within a given iteration was about 23% cheaper for the 1-D GLA than for the MOC GLA. It was about 15% cheaper for the 1-D GLA than for the Taylor series. Each of these methods required about the same number of steps within each iteration (about 14). Thus, if the minor error in the 1-D GLA solution is acceptable, it is the most cost-effective of the approximation concepts tested in the nozzle region.

Optimization histories for the CFD-only, Taylor series and the GLA's are shown in Fig. 4.7 through Fig. 4.9. The effectiveness of the Taylor series and the GLA's are highlighted by Fig. 4.7, which portrays F_{net} versus CFD calls. Fig. 4.8 and Fig. 4.9 depict the histories of α and a_{curve}, respectively. Note that the Taylor series and 1-D GLA curves are relatively smooth up to the final design, whereas the MOC GLA histories are rather jagged. But all these methods find nearly the same optimum design.

4.3 Summary

The Taylor series local approximation and the 1-D GLA and MOC GLA were seen to provide suitable substitutes for the CFD solver in optimizing the nozzle. They all found nearly the same optimum design as the CFD-only optimization did, but with a savings in computer resources of 68%. Their performance was presaged by the single-variable parameterizations, in which they all followed the trends of the CFD solver, even when far from the design point upon which the approximations were based. Note that the neither the uncorrected 1-D nor the uncorrected MOC finds the same optimum design as the CFD does.

Thus, in regions in which the flow is basically isentropic, the approximation concepts, as currently used in structural optimization, only require modest modifications to be applied to this aerodynamic optimization problem. The savings in computer resources would be much greater if a larger number of design variables were used.

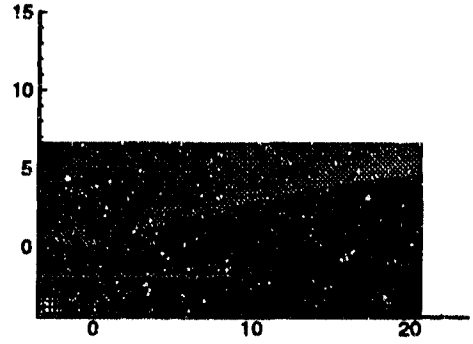

(a) Initial design contour.

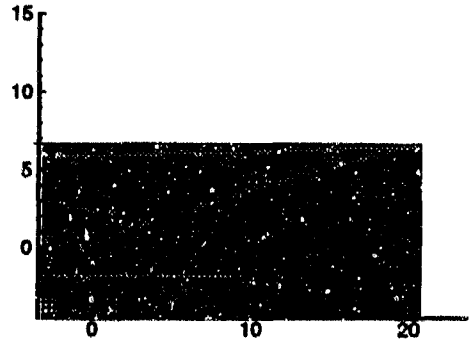

(b) Optimum design found by CFD, Taylor and GLA's.

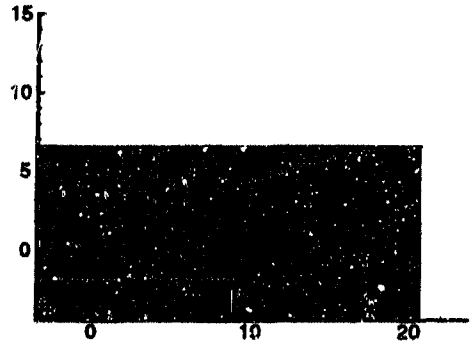

(c) Optimum design found by uncorrected 1-D and MOC.

Fig. 4.6 Nozzle contours for the initial configuration and for the optimum designs found by various methods.

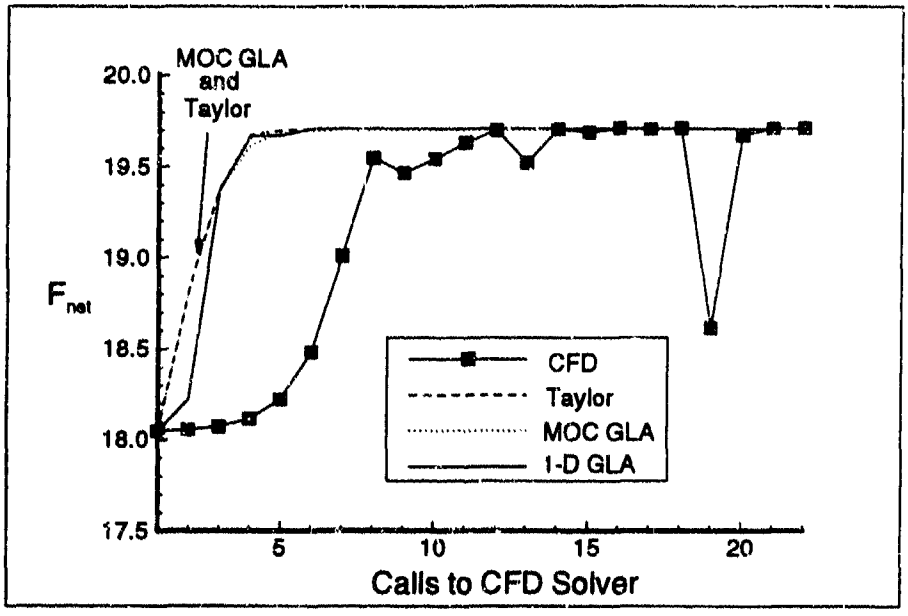

Fig. 4.7 Optimization history of F_{net} for CFD-only, Taylor series, and GLA's.

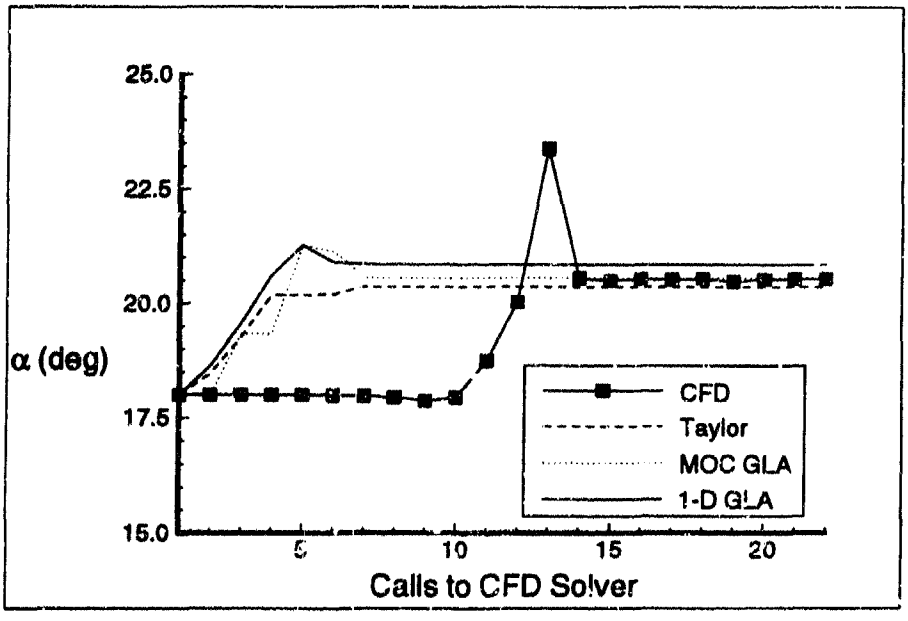

Fig. 4.8 Optimization history of α for CFD-only, Taylor series, and GLA's.

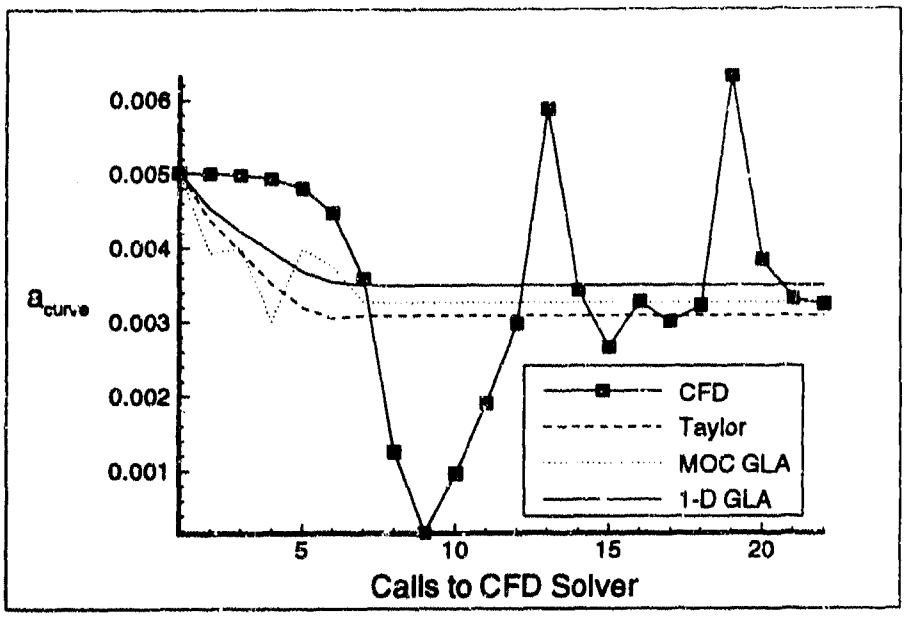

Fig. 4.9 Optimization history of a_{curve} for CFD-only, Taylor series, and GLA's.

Chapter 5

Forebody/Inlet Optimizations

5.1 Introduction

Having found the approximation concepts to be successful in the nozzle region, where the flow near the walls is essentially shock-free, these techniques were next applied to the optimization of the forebody/inlet region. The flow there is very different from the nozzle flow, as it is characterized by the presence of oblique shock waves. It is not clear beforehand how these shock waves might affect the approximation concept techniques. Thus there is a great deal more risk involved in trying to apply these techniques there.

This chapter describes the formulation of the design problem, in which the optimizer is allowed to choose designs without explicit regard to the resulting shock structures. (This is in contrast to actual design practice, which only uses "properly" placed shocks.) It then describes the special considerations required because of the presence of imperfectly-placed shocks. Next it outlines the selection of suitable design variables. Then the results of the optimizations are presented.

5.2 General Design Considerations

The 2-D scramjet vehicle uses a mixed-compression inlet. Such an inlet can be constructed by combining a nose/ forebody, compression ramp and cowl, as shown in Fig. 5.1. The nose/forebody region is a straight wedge, whose oblique shock provides the initial compression for the scramjet engine. The compression ramp generates a second shock to provide further compression. Ideally, these two oblique shocks would impinge on the cowl lip. A third (internal-compression) shock is formed at the cowl lip and ideally would impinge upon the corner of the compression ramp, as shown in Fig. 5.1. This shock would then interact with and, ideally, would exactly cancel the expansion fan created at the ramp corner. In such an ideal design, the combustor is provided with uniform, 1-D flow at high static pressure. The pressure rises

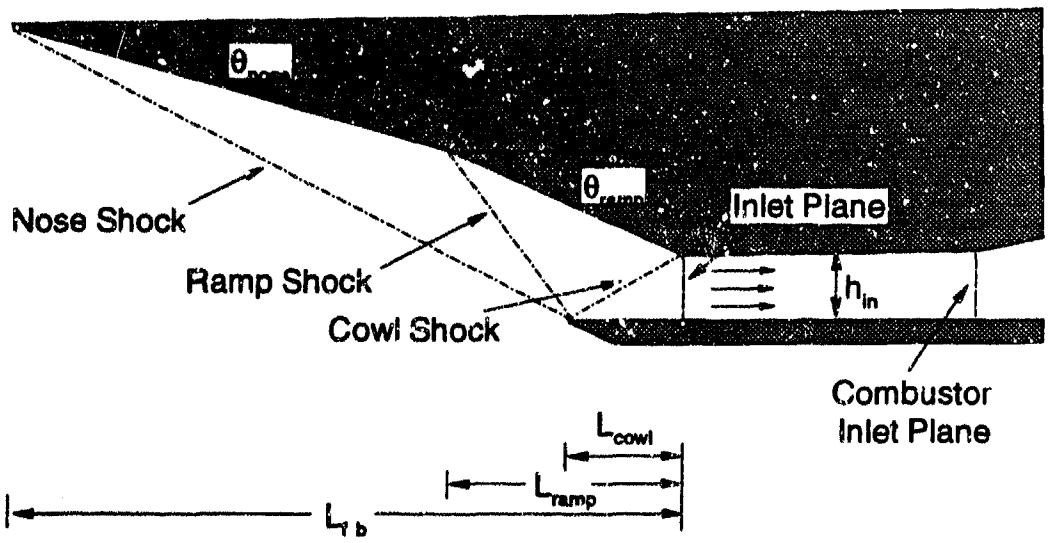

Fig. 5.1 Forebody/Inlet geometry.

across the nose and compression ramp shocks also create a "forebody drag". The cowl shock can also contribute to forebody drag if it is not properly placed at the ramp corner. There is also a small contribution to drag from the oblique shock on the lower surface of the cowl lip.

For ideally-placed shocks and given freestream conditions, the design problem then becomes one of determining the nose and compression ramp angles, Θ_{nose} and Θ_{ramp} which strike the best balance between high combustor performance and low forebody drag. For given Θ_{nose} and Θ_{ramp}, the parameters which determine whether the shocks are ideally-placed are: the forebody length, L_{fb}; the compression ramp length, L_{ramp}; the inlet cowl length, L_{cowl}; and the inlet height h_{in}.

In this research, to demonstrate the use of approximation techniques for use in design optimization, the following problem was chosen. Given an initial design with non-ideally placed shocks and arbitrary Θ_{nose} and Θ_{ramp}, optimize to the design which

maximizes F_{net}. Thus, we expect the optimizer to find the best Θ_{nose} and Θ_{ramp}, and to place the shocks to best advantage. (As explained in Section 5.3, this will not necessarily correspond to perfectly-placed shocks, if the effects of flow nonuniformity in the inlet duct are not taken into account.)

The general utility of this approach is that, for a more complicated and realistic design problem (such as for a 3-D vehicle with viscous, reacting flows) it may be difficult to specify, a priori, a configuration which will perfectly place the shocks. Thus, a method which would, as a natural consequence of the optimization process, place the shocks in the best way, would be a powerful design tool. The approximation techniques, such as Taylor series and the Global-Local Approximations may hold this promise, and the problem as stated in the previous paragraph is one way of assessing their validity. More specifically, if an approximation technique can be made to optimize to the same configuration as the CFD, then that technique would become an attractive alternative to using the CFD alone in the optimization process.

The following sections describe how the various modeling levels and approximation techniques were applied to this problem.

5.3 Special Design Considerations

The presence of shocks which impinge upon the walls, and which may interact with each other and with expansions in the flow makes this problem essentially very different from the problem of optimizing the nozzle. Some discussion of the special problems encountered in this design problem will serve to make clear the approach that was used to perform the optimizations, and their results.

In practice, it is undisputed that the only desirable shock configuration for the mixed-compression inlet is perfect shock placement, as described in the introduction to this chapter. However, given that this research is limited to inviscid flows, without consideration of shock/boundary layer interactions, and without any details of the flow in the combustor, some of the impetus to place the shocks perfectly is missing. Thus, it is possible that the optimizer will select non-perfect shock placements. A discussion of why this might be so is warranted.

5.3.1 Effects of Non-Perfect Shock Placement

Neglecting viscous and unsteady effects, the consequences of imperfect placing of the shocks are as follows.

a.) If the cowl shock hits the compression ramp short of the corner, as shown in Fig. 5.2a, a reflection results. (This shock may be strong enough to become a normal shock, thus unstarting the engine.) The very high pressure jump downstream of this reflection causes an increase in forebody drag, which can be quite severe. In addition, the reflected shock interacts with, but does not cancel the expansion fan from the corner. The result is a complicated system of shocks and expansions in the inlet duct, with a resulting flow nonuniformity. This non-uniformity can be extremely detrimental to the combustion process. The only positive aspect of having the cowl shock fall short of the ramp corner (assuming it does not unstart the engine) is that it provides an additional compression, which may contribute to improved combustor performance, if the nonuniformity is not too great.

b.) If the cowl shock passes inside the inlet duct, as shown in Fig. 5.2b, there is again an non-cancelling interaction with the expansion fan, and a resulting flow nonuniformity in the combustor entrance. However, there is no additional forebody drag.

c.) If the nose shock falls short of the cowl lip, as shown in Fig. 5.2c, the nose section of the forebody is longer than it needs to be, with a consequent increase in forebody drag, and no more engine mass flow than if the shock were perfectly placed. In addition, the flow around the cowl lip is changed, since the angle of attack there is now nonzero. This will result in a reduction in cowl drag, since the effective wedge angle on the upper surface is decreased. Due to the small vertical area of the cowl, this reduction in cowl drag does not usually offset the forebody drag increase. So the net result of having the nose shock fall short of the cowl is usually a reduction in the net thrust. Similar changes occur if only the compression ramp shock or both the nose and compression ramp shocks fall short of the nose. Thus, there will be a natural tendency for the optimizer to avoid solutions which place these shocks short of the lip.

d.) If the nose shock, compression ramp shock, or both are too shallow, and hit inside the cowl (see Fig. 5.2d), they would interact with and cause changes in the strength and angle of the cowl shock. This, in turn, could cause improper placement of the cowl shock, with all of the problems shown in a.) and b.) above. But, it is possible to have the nose and/or ramp shock hit inside the cowl, and have the resulting

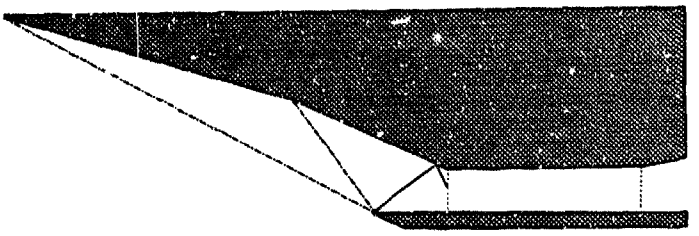

(a) Cowl shock hits short and reflects off ramp.

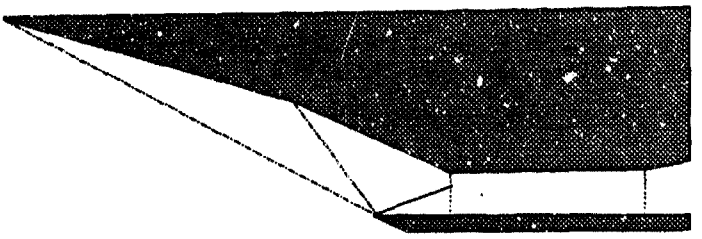

(b) Cowl shock enters inlet duct directly.

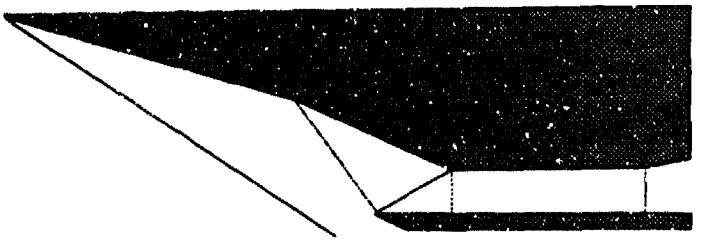

(c) Nose shock misses cowl.

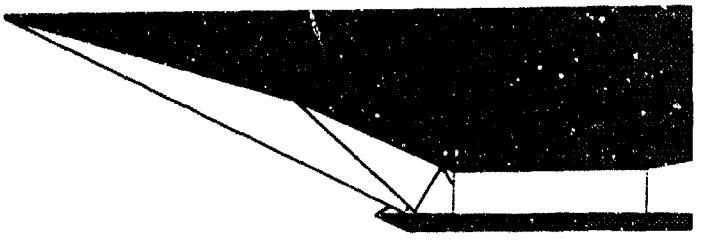

(d) Nose and cowl shocks hit inside cowl.

Fig. 5.2 Improperly-placed inlet shocks.

cowl shock be perfectly-placed, or nearly so. This indeed happened on some of the optimizations to be presented in Section 5.5. In fact, it was observed that, during the optimization process, once a shock has been placed so as to impinge inside the duct, it is almost impossible to get it back outside again.

5.3.2 Inlet Duct Flow Non-Uniformity

The CFD solver naturally accounts for all of the shock-shock and shock-expansion interactions in the inlet duct. It then averages the flow properties in the combustor inlet plane, and passes this information to the 1-D combustor model. On the other hand, the approximate flow model for the forebody/inlet region terminates at the corner of the compression ramp (i.e. in the inlet plane), and averages the properties there. (See Section 3.4.) Thus this model does not account for the shock-expansion interactions and reflections inside the duct. These effects influence both the flow non-uniformity at the combustor inlet, as well as the averaged properties being passed to the combustor model. This is a major reason that the CFD solver is herein considered to be more accurate than the approximate model.

In this research, no penalty was assessed to the combustor performance for such flow non-uniformity. It is not a simple matter to determine such a penalty. In addition, as the primary purpose of this work is to demonstrate approximation techniques which accurately mimic the CFD solutions in the optimization process, this additional complexity is not required, as long as the optimum designs do not posses unreasonably high non-uniformities.

An alternate procedure for handling flow non-uniformity is to impose a constraint in the optimization procedure. This was tried by using the approximate model and optimizing, imposing the constraint that the standard deviation of the pressures (at the CFD grid points) in the inlet plane be less than a certain value. Depending upon which set of design variables was used (See Section 5.4), the optimizer did one of the following: either froze Θ_{nose} and Θ_{ramp} (if not directly, then by whatever design variables control them) and adjusted the remaining design variables to place the cowl shock perfectly at the ramp corner, then stopped; or reduced Θ_{nose} and Θ_{ramp} as low as possible and then sought an optimum there. Both of these results are reflections of the fact that the optimizer places first priority on insuring that the design is feasible (i.e. not in violation of any constraints). It will do so to the exclusion of

improving the objective function, if necessary, until the design is feasible. And since the amount of non-uniformity increases very rapidly as we move away from perfect cowl shock placement, the optimizer finds a very steep local optimum, from which it is unlikely to extract itself.

For these reasons, no constraints on inlet duct flow non-uniformity were imposed in this research, nor were any penalties imposed on the combustor performance for having such non-uniformity. However, this is somewhat mitigated by the fact that certain influences will tend to keep the cowl shock from being grossly misplaced. First, if this shock hits short of the ramp corner (Fig. 5.2a), the reflection causes an increase in forebody drag, which can offset any increase in thrust. Secondly, if the shock passes inside the duct, as in Fig. 5.2b, the average pressure in the inlet plane is lowered, reducing combustor performance. Together, these two influences act to keep any misplacement of the cowl shock (and the resulting flow non-uniformities) from becoming wildly excessive.

5.3.3 Summary of Design Considerations

No satisfactory way was found to explicitly prevent the imperfect placing of the shocks, or of penalizing the combustor performance for flow non-uniformity in the inlet duct. However, certain influences were seen to dictate against gross non-uniformities and against having the nose and cowl shocks fall short of the cowl lip. There is no such influence to keep the nose and/or ramp shock from entering the duct, as long as this does not cause the cowl shock to be grossly misplaced.

5.4 Choice of Design Variables

As in the nozzle optimizations of Chapter 4, an investigation was made to find the best set of design variables to use in optimizing the forebody/inlet. To do this, the approximate model (based on oblique shock theory for the forebody/inlet, and the Method of Characteristics, or MOC, for the nozzle) was used in the optimizer, and optimizations were run for various sets of design variables. The resulting optimizer behavior was observed. The design variable set which led to the best behavior was then selected as the best set.

The following design variable sets were considered. Their meanings are explained in Fig. 5.3.

a.) θ_{nose}, θ_{ramp}, L_{fb}, L_{ramp}, and L_{cowl}
b.) h_{nose}, s_{nose}, h_{fb}, s_{ramp}, and L_{cowl}
c.) h_{nose}, s_{nose}, h_{ramp}, s_{ramp}, and L_{cowl}
d.) h_{nose}, s_{nose}, Δh_{ramp}, Δs_{ramp}, and L_{cowl}

Design variable set a.) is the most intuitive one, because it is these variables which directly control the shock strengths and angles, and the placement of the shocks. However, there is a disadvantage to using this set in the optimization. Let us examine the behavior of the gradient calculations (for finding the search direction) using set a.). Assume an initial design that has nearly perfect shock placement. We calculate the gradient element $\frac{\partial F_{net}}{\partial \theta_{ramp}}$ by incrementally increasing θ_{ramp} while leaving all other design variables constant. In so doing, we might expect to see an increase in combustor performance due to the increased ramp compression. We would also expect an increase in forebody drag, both due to the increase in pressure on the ramp (which is unavoidable), but also due to the increase in the ramp height. (See Fig. 5.4a.) In addition, since the origin of the ramp shock has not changed, the increase in oblique shock angle may cause the ramp shock to miss the cowl. The increased ramp height and improperly-placed shock may nullify the improvement in ramp compression. Accordingly, the gradient calculation would indicate that there is no benefit to be had by increasing θ_{ramp}.

The natural solution to this is to decrease L_{fb} as we increase θ_{ramp}. This would have the effects of reducing the ramp height, and moving the ramp shock closer to the cowl lip. Thus, we might increase inlet compression with a reduced increase in forebody drag, while simultaneously helping to maintain a favorable shock placement. We might then find that there is actually a great deal to be gained by increasing θ_{ramp}. However, this logic is missing in a gradient calculation performed with design variable set a.). Thus, a beneficial search direction may well be not be recognized by the optimizer. (Indeed, in the tests of the design variable sets, set a.) often caused the optimizer to fail to see beneficial search directions which would be obvious to an engineer.)

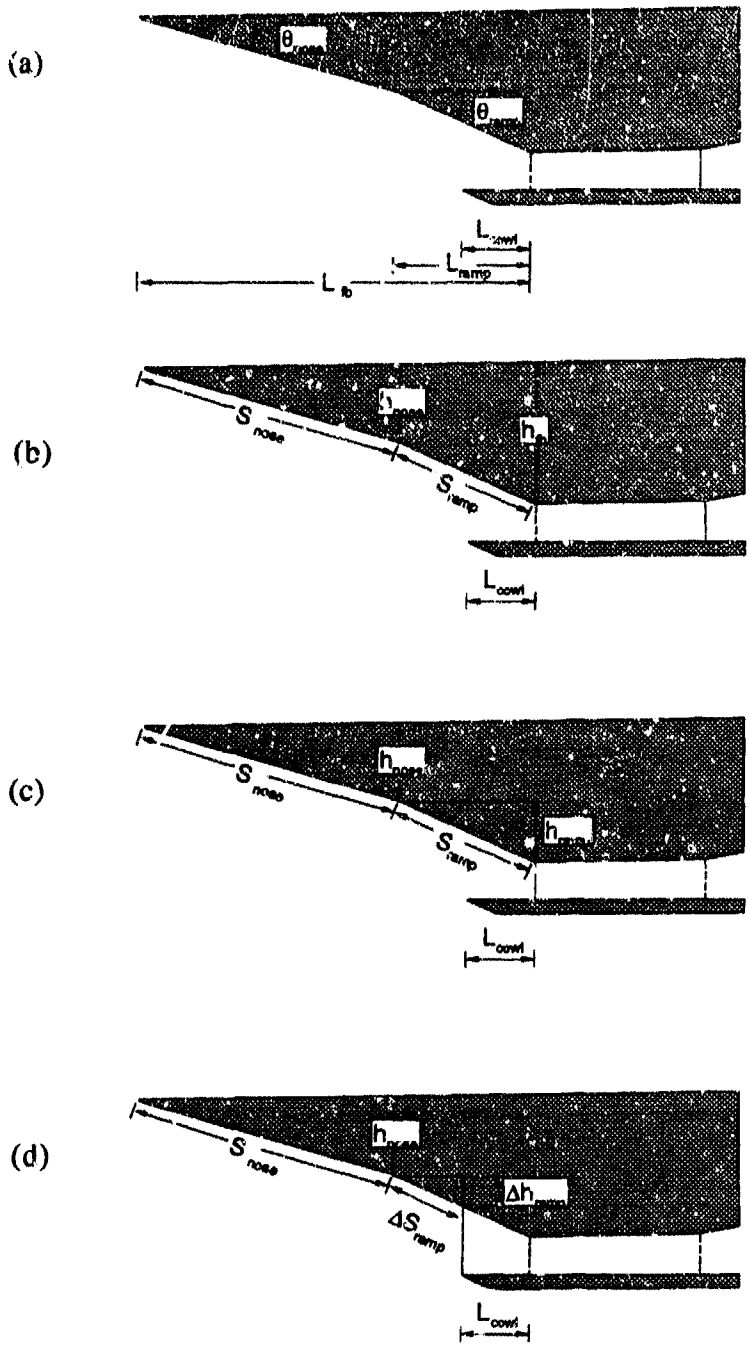

Fig. 5.3 Design variable sets considered for use in forebody/ inlet optimization. (Set b was eventually chosen.)

So, it seems sensible that we should build into the gradient calculations the fact that, in reality, we would often change some of the design parameters simultaneously.

Design variable sets b.) through d.) were selected because they build such multi-variable flavor into the gradient calculations. Thus, they may be considered "smart" design variable sets. Consider, for example, set b.). If we calculate $\frac{\partial F_{net}}{\partial h_{fb}}$, we will incrementally increase h_{fb}, while holding s_{ramp} (as well as the nose design variables) constant, which effectively requires shortening L_{ramp}. (See Fig. 5.4b.) For a given increase in the value of θ_{ramp}, L_{ramp} will be less than it would be when using design variable set a.). This also implies that h_{ramp} is shorter. And so the optimizer will, in one element of the gradient calculation, consider a search direction which simultaneously seeks the benefits of increased ramp compression and decreased forebody drag, while making an effort to maintain the proper shock placement.

TABLE 5.1 shows the results of the design variable tests. Note that the initial conditions for all of these tests (when converted into terms of θ_{nose}, θ_{ramp}, L_{fb}, L_{ramp}, and L_{cowl}) are as follows: θ_{nose} = 8.0 deg, θ_{ramp} = 18.0 deg, L_{fb} = 35.0, L_{ramp} = 13.0, and L_{cowl} = 2.0. Note also that the nozzle design was the same as the initial condition used in the nozzle tests of Chapter 4, with α = 18.0 deg, and a_{curve} = 0.005. The inlet height was fixed at 0.6667. The free stream flow conditions were those at M_∞ = 6.0 and 30 km altitude. The maximum allowable ramp angle was 20.0 deg.

In TABLE 5.1 the optimum design for each of the design variable sets is shown, as well as the resulting net thrust. (Note that these net thrust values are those found by the approximate model, and not by the CFD solver.) From these tests, it was clear that the design variable set b.), that is n_{nose}, s_{nose}, h_{fb}, s_{ramp}, and L_{cowl}, is the most attractive one. Set a.) did not allow the ramp angle to increase, for the reasons mentioned previously in this section. Set c.) made the nose and ramp angles decrease, counter to reason. Although set d.) found reasonable nose and ramp angles, the cowl shock was badly placed, passing directly inside the inlet duct, instead of impinging on the ramp. (Similar to the ramp shock configuration shown in Fig. 5.2b.) Based on its superior performance in these tests, design variable set b.) was used for all subsequent optimizations of the forebody/inlet region.

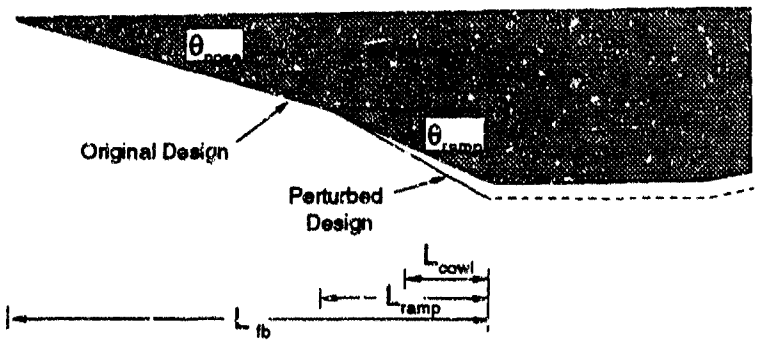

(a) Using design variable set a.).

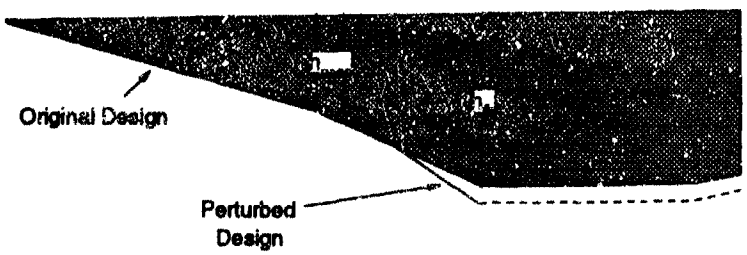

(b) Using design variable set b.).

Fig. 5.4 Effects on search direction calculation of choosing different design variable sets.

TABLE 5.1

Results of design variable tests: optimum configurations for each set of design variables. (All design variables are converted into angles and lengths.)

	θ_{nose}	θ_{ramp}	L_{fb}	L_{ramp}	L_{cowl}	F_{net}
	8.000	18.000	35.000	13.000	2.000	[illegible]
	6.986	17.640	34.802	12.340	4.304	[illegible]
	[illegible]	[illegible]	[illegible]	[illegible]	[illegible]	[illegible]
	3.129	13.646	35.422	13.646	3.887	[illegible]
	7.917	20.001	37.968	8.231	2.598	[illegible]

5.5 Optimization Results

Optimizations of the forebody/inlet design were performed using each of the following modeling levels and approximation techniques: CFD only; approximate model (based on oblique shock theory for the forebody/inlet, and MOC for the nozzle); Taylor series; GLA based on the approximate model. Just as for the nozzle optimizations, the objective function was the normalized net thrust, F_{net}, which has been normalized by $\rho_\infty c_\infty L_{ref}$. Side constraints were imposed to keep the design variables within reasonable limits, and inequality constraints were placed on θ_{nose} and θ_{ramp} to keep them within certain limits ($6.0 \le \theta_{nose} \le 11.0$ and $11.5 \le \theta_{ramp} \le 20.0$). The inlet height was fixed at 0.6667.

The initial conditions for these optimizations were (converted from the actual design variables into those which are more easily visualized):

$\theta_{nose} = 8.0$ deg
$\theta_{ramp} = 18.0$ deg
$L_{fb} = 35.0$
$L_{ramp} = 13.0$
$L_{cowl} = 3.20$

To gain insight into what the optimum solutions should generally look like, a preliminary optimization was run with a special program which always placed the shocks

perfectly, and which used only the approximate model. Since the shock placement in such cases is uniquely determined by θ_{nose} and θ_{ramp}, these were the only two design variables. The optimum design from this test selected the maximum value of θ_{ramp} (20.0 deg), and very nearly the maximum value of θ_{nose} (10.9 deg). This is because the inlet compression has not yet reached that which is most efficient for the combustor. (See Section 3.3 and Fig. 3.9.) It is likely that θ_{ramp}, would have been increased even further, had the inequality constraints not prevented that.

Thus, we should expect that the optimizations to be performed with non-ideal shock placement should generally follow the trend of seeking increased compression from both the nose and ramp angles.

5.5.1 Performance of the GLA

It was observed early on that the GLA method behaved very erratically within any given iteration. Fig. 5.5 shows the history of F_{net} (on a logarithmic scale) for the steps within the second iteration. (Recall that an iteration is a complete optimization performed using only the corrected approximate method, and based on a given baseline design. A step is a single function evaluation within that optimization.) The uncorrected approximate method history is shown for comparison, since it was found to be a reasonably good approximation to the CFD solver. (See TABLE 5.2) The figure shows the very erratic behavior of the GLA. The values of F_{net} shown are as found by the approximate method and by the GLA respectively, and have not been evaluated by the CFD solver.

The wild variations in the GLA history were found to be due in large part to difficulties that this method has in dealing with shifting shock impingement points on the ramp surface near the inlet. Basically, as a shock moves to a new position, the correction factors of the GLA do not account for this, and improperly magnify or reduce the pressures in the vicinity of the shock. In addition, the fact that the CFD solver and the approximate method do not capture shocks equally crisply causes further error.

The GLA and Taylor series methods, as heretofore implemented, share an inability to account for the effect of discrete phenomena such as shocks that shift position as design variables are changed. This effect is most crucial when it is manifested in the calculation of correction factors for the GLA, and somewhat less critical, although still important, if it occurs in the calculation of the search direction, for either method.

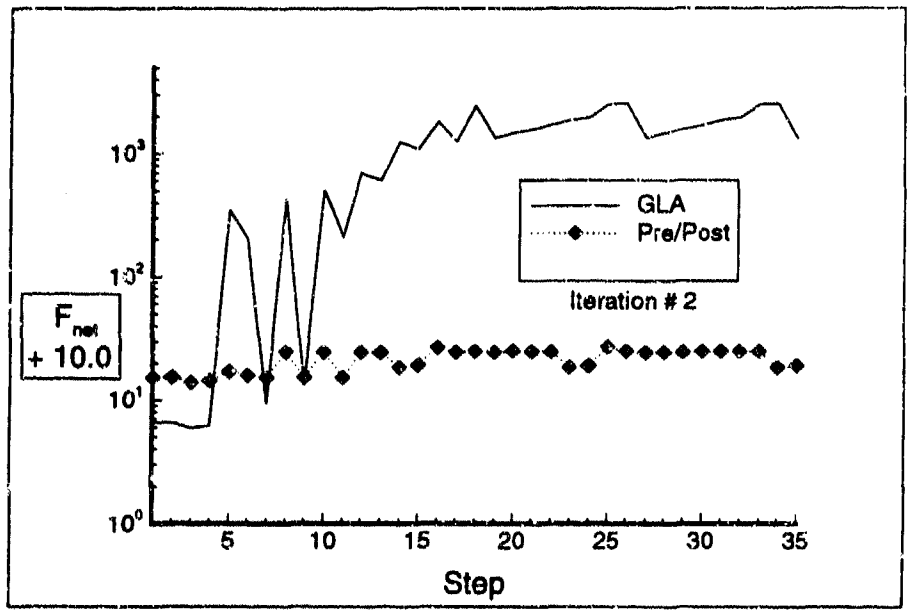

Note: 10.0 is added to F_{net} to allow log plotting of neg values.

Fig. 5.5 Behavior of GLA and approximate methods within one iteration. (Note log scale.)

To illustrate this effect, consider one element of the wall pressure gradient calculation for a GLA which will involve a shock which moves during the calculation. (See Fig. 5.6.) Let X_1 be the design variable of interest. Fig. 5.6a shows the shock impingement point moves from point A to point B as the design variable is perturbed for the derivative calculation. Fig. 5.6b shows the wall pressure distributions for the two shock configurations. Note that the *change* in pressure is much greater in region II than in either of regions I or III. This is manifested in the derivative calculation plotted in Fig. 5.6c, in which, for compactness in the figure, the peak value is actually very much under-represented, since the denominator of the calculation is very small, due to the small perturbation in the design variable. Thus, for calculation of correction factors, or for calculating a search direction, the gradient calculation dictates that the effect of the shock movement is to be dominated by an extreme sensitivity to the design variable in region II (which is fixed in space).

In reality, we know that the spike in region II is an artifact of not recognizing that the shock is in transit. A more reasonable representation of the derivative is that in Fig. 5.6d, in which there is a moving shock location, and separate derivatives upstream and downstream of the shock.

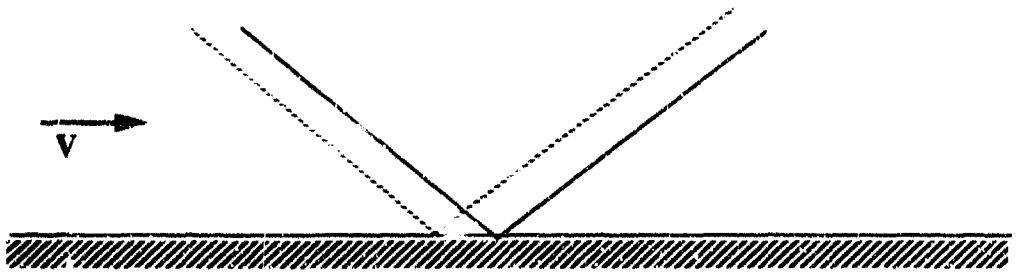

a.) Shock locations for initial and perturbed design variable.

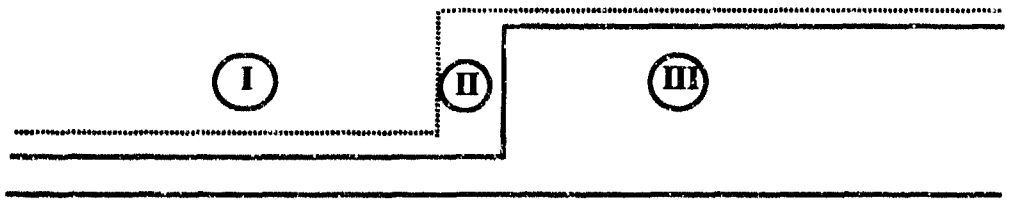

b.) Wall pressures.

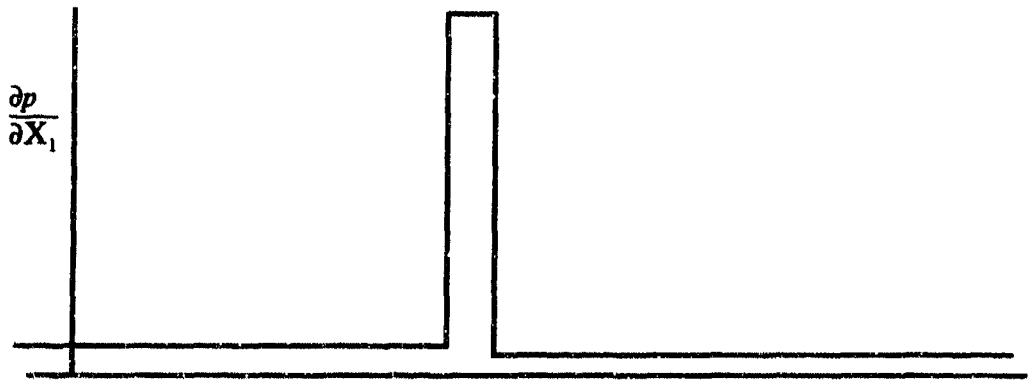

c.) Derivative of pressure wrt design variable.

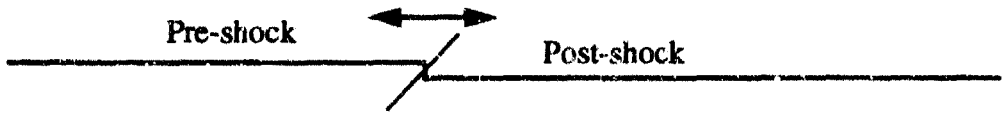

d.) Actual derivative, if properly calculated.

Fig. 5.6 Effect of moving shock impingement point in gradient calculation.

Interestingly, the inability to account for the movement of the shock is somewhat alleviated when using CFD calculations for performing the derivatives. This is because the shock dissipation inherent in the CFD solution "spreads out" the shock, thus giving adjacent points some warning that the shock is approaching. This partially explains why the Taylor series approach is better behaved, if not more accurate, than the GLA. In addition, the Taylor series involves only one set of gradient calculations, namely those based on the CFD. The GLA uses gradients based both on the CFD and on the approximate method, which uses sharp shock discontinuities, such as those in Fig. 5.6. The problem is thus magnified for the GLA.

The obvious solution to this problem is to calculate separate gradient and correction factor calculations for pre- and post-shock locations, and apply them only where appropriate. This requires devising two adjoining non-dimensionalized coordinate systems for each wall surface, with the physical location of the interface to be determined (by the approximate method) once the location of the shock is known. This process is depicted in Fig. 5.7. As the optimization is performed using the GLA, at each step the shock location is first found using the approximate method, and the approximate method wall pressures are then corrected by application of the pre- or post-shock correction factors, as appropriate. Similar calculations must be performed for the inlet plane flow properties, since the intersection of the cowl shock (or its reflection) with the inlet plane also moves.

One limitation of this method is that it requires the approximate method (which is the only one used in the actual optimizations) to be able to predict fairly accurately the shock locations. In the problem at hand, this is not a problem, since the oblique shock theory is very accurate in this regard. For more complicated problems, this may require more attention.

The pre-and post-shock coordinate system technique for calculating gradients and correcting wall pressures was applied to one iteration (40 steps) of an optimization using the GLA. (Note that the inlet plane flow properties were not treated.) The result was a marked decrease in the erratic behavior. See Fig. 5.8. (Note that 10.0 has been added to the values of F_{net} in the plot, to allow the negative values to be plotted on the logarithmic scale.) The maximum value of F_{net} recorded in this iteration was 14.99, compared to 2551 for the same iteration using the original formulation of the GLA. The uncorrected approximate model (which mimics the CFD very well)

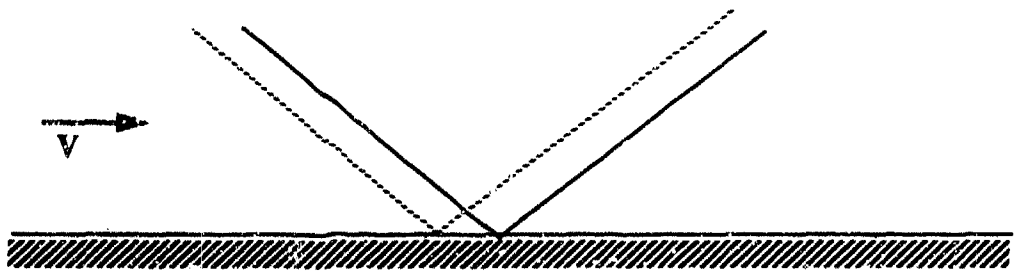

a.) Shock locations for initial and perturbed design variable.

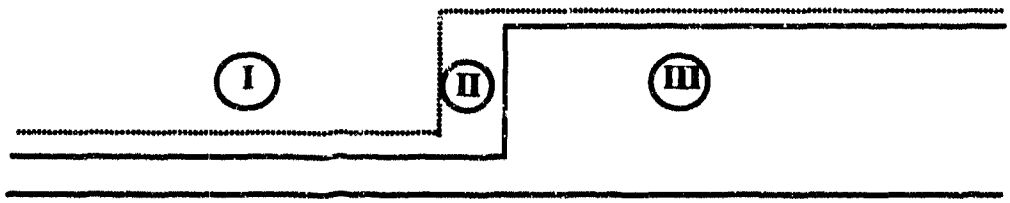

b.) Wall pressures.

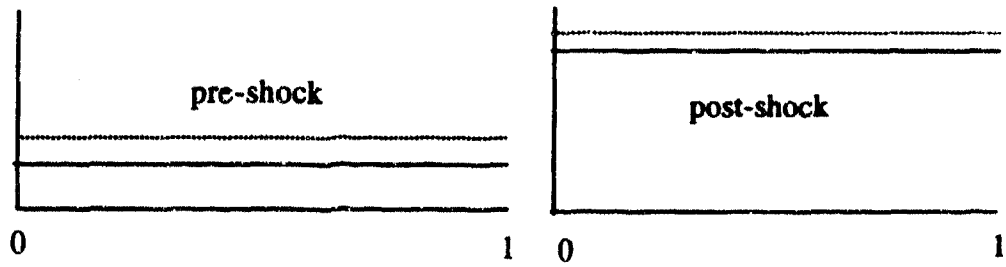

c.) Wall pressures, in non-dimensionalized pre- and post-shock coordinate systems.

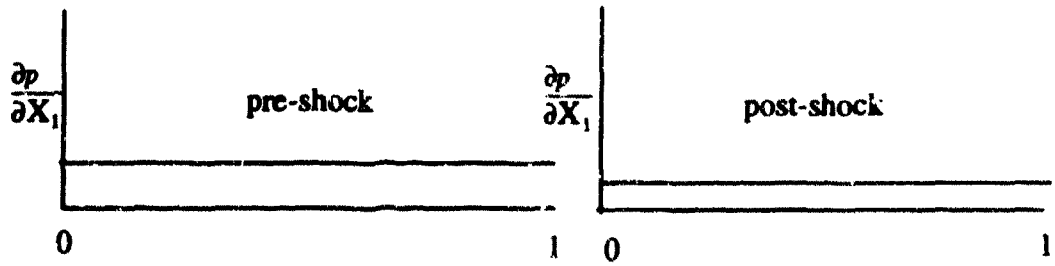

d.) Derivative calculations in non-dimensionalized pre- and post-shock coordinate systems.

Fig. 5.7 Gradient calculation using pre- and post-shock coordinate system.

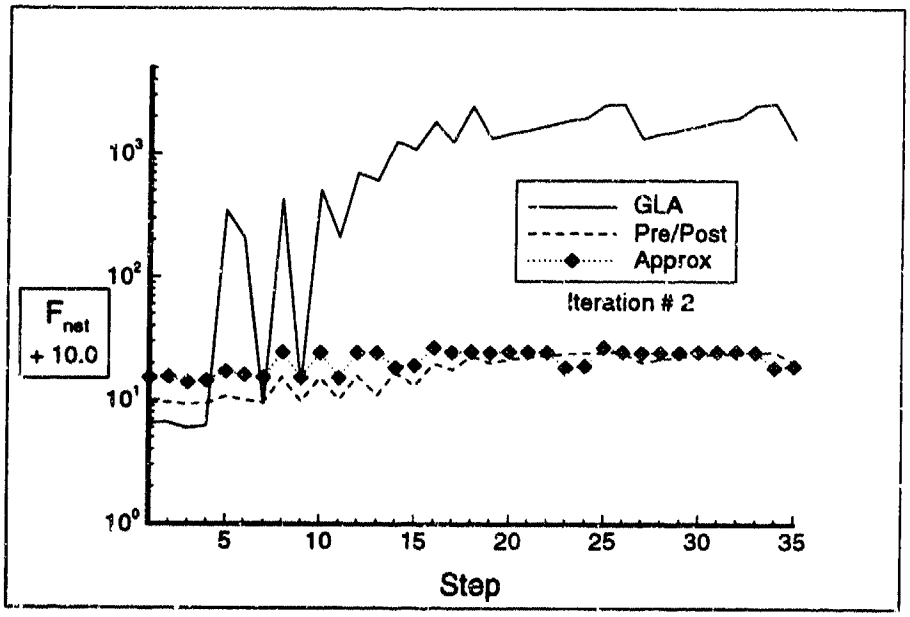

Fig. 5.8 Effect of using pre- and post-shock coordinate systems on one iteration of the GLA in the forebody/inlet region. (Note log scale.)

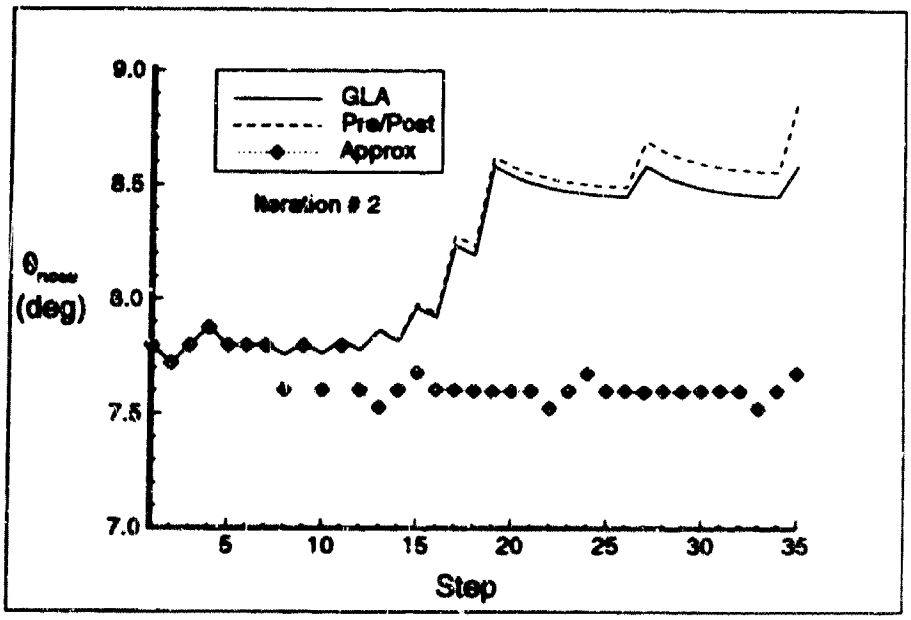

Fig. 5.9 History of nose angle for one GLA iteration, using pre-and post-shock coordinate systems, with comparison to approximate model.

calculated F_{net} to be 14.96 for the optimum design in this iteration of the new GLA test. However, the values of thrust and drag found by the improved GLA were too high (97.4 and 82.4 respectively, versus 55.3 and 40.3 as found by the approximate method). So it is apparent that the new GLA formulation does not entirely solve the problem. The error in thrust may be a result of the lack of a pre- and post-shock system for the inlet plane flow properties. The drag error may also be due in part to the shock dissipation in the CFD solution. Because of this, the approximate method and the CFD do not capture shocks equally crisply, and the result will be that erroneous correction factors will be calculated around shocks. As the wall pressures increase due to increasing shock strength during the optimization, the errors induced by the erroneous correction factors will grow. Indeed, this increasing error was found in the test of the pre- and post-shock coordinate systems.

A history of the nose angle for this iteration is shown in Fig. 5.9. Note that, although the erratic behavior of F_{net} has largely been cured by using the pre- and post-shock coordinate systems, the optimizer treats this model almost exactly the same as it does the original GLA. Thus, the poor selection of an optimum design by the GLA is perhaps more due to the other sources of error mentioned in the previous paragraph than due to the need for a pre-and post-shock coordinate system. Nevertheless, the reduction in erratic behavior afforded by the pre- and post-shock system is an important ingredient in formulating a generally-applicable GLA. This is especially true when active behavior constraints (such as limits on the pressure at the ramp tip) are encountered. In such cases, the wild fluctuations in wall pressure are important in their own right.

Thus, it is apparent that a straightforward application of GLA's to the forebody/inlet region, using the techniques used in structural optimization problems, will not meet with success. More work is needed in this area to unlock whatever potential the GLA method has for the forebody/inlet region. In fact, for the GLA to be applied to point properties in *any* flow regime which has moving, discontinuous phenomena (such as shocks, transition to turbulence or separation), these problems will have to be overcome.

Because of this behavior, a complete GLA optimization, based on point properties, was not performed. However, because the Taylor series did not suffer as badly in this regard, it was included in the set of complete optimizations.

5.5.2 GLA's Applied to Integral Measures

An attempt to circumvent the problems with applying the GLA to point properties was made, by applying it to the integrated properties (thrust, drag, and F_{net}). The central idea here is that the smoothing process inherent in integrating would alleviate the problems with shock motion.

Several optimizations were run. It was found that there was no apparent advantage to applying the GLA to thrust and drag separately, as opposed to applying it directly to F_{net}. It was also found that including derivative information in the GLA caused the optimizer to select a different optimum than the CFD and approximate methods did. However, if the GLA was limited to zeroth-order (i.e. constant scaling factor), excellent agreement with the approximate method (and CFD) was achieved. It is important to note that, when such a simple scaling is applied to the integral measures, this is the same as simply multiplying all the approximate method solutions (within one iteration) by a constant number.

5.5.3 Optimization Results

Complete optimizations were performed using CFD, the uncorrected approximate method, and the Taylor series method. The results of these optimizations are shown in TABLE 5.2. Note that the optimum designs are presented in terms of the design variables of set a.) in Section 5.4, even though the actual design variables were those of set b.) This was done to simplify interpretation of the results.

For the CFD-only case, 25 calls to the CFD solver (excluding those for gradient calculations) were required. The optimized design increased the net thrust by 248% over the initial design. The shock placement configuration for this design is shown in Fig. 5.10. This figure confirms the reasoning of Section 5.4, in which it was postulated that there are influences which should keep the shocks from being grossly misplaced. Indeed, the improvement in shock placement is substantial. The only significant deviation from what was expected based upon the "perfect shock placement" test was that the nose angle decreased instead of increasing.

TABLE 5.2 Results of forebody/inlet optimizations. (All net thrust values are as found by CFD solver.)

	Θ_{nose}	Θ_{ramp}	L_{fb}	L_{ramp}	L_{cowl}	F_{net} *	CFD Calls
	8.000	18.000	35.000	13.000	3.200	5.422	-----
	[illegible]	[illegible]	[illegible]	[illegible]	[illegible]	[illegible]	[illegible]
	7.705	19.998	34.940	12.932	3.393	[illegible]	-----
	7.045	20.063	26.977	8.541	2.794	[illegible]	7
	7.786	20.027	35.149	13.184	3.491	[illegible]	1

* As calculated by the CFD solver.

Note, in TABLE 5.2, that the optimum design found by the uncorrected approximate model is close to that found by using only CFD. The only significant differences in design variables are for Θ_{nose} (5.6% error) and L_{cowl} (6.1% error). And the value of F_{net} is 8.2% lower than that found using only CFD. The approximate model apparently captures all the relevant physics sufficiently well to correctly replicate the general behavior of the CFD model. And the cost of using the approximate model is very much lower than that of the CFD. (25 seconds per function evaluation, versus 9000 seconds.) Although the Taylor series (with 10% move limits) improved upon the initial design, it did not find the same design as the CFD, and the increase in net thrust was modest, at 70%. Although the Taylor series optimization did not exhibit the erratic behavior of the GLA, it also suffers (to a lesser degree) the inability to account for the movement of shock impingement points. (See Section 5.5.1.) The reason that the problem is less severe is that the smearing of the shock, due to the numerical dissipation, conveys the information that the shock is moving into a new region, even before it gets there. In addition, the issue of the disparity in shock-capturing "crispness" between the CFD and the approximate model, which hurt the GLA, is not an issue in the Taylor series approach, since the approximate model is not used there. Nevertheless, the Taylor series optimization did not behave well.

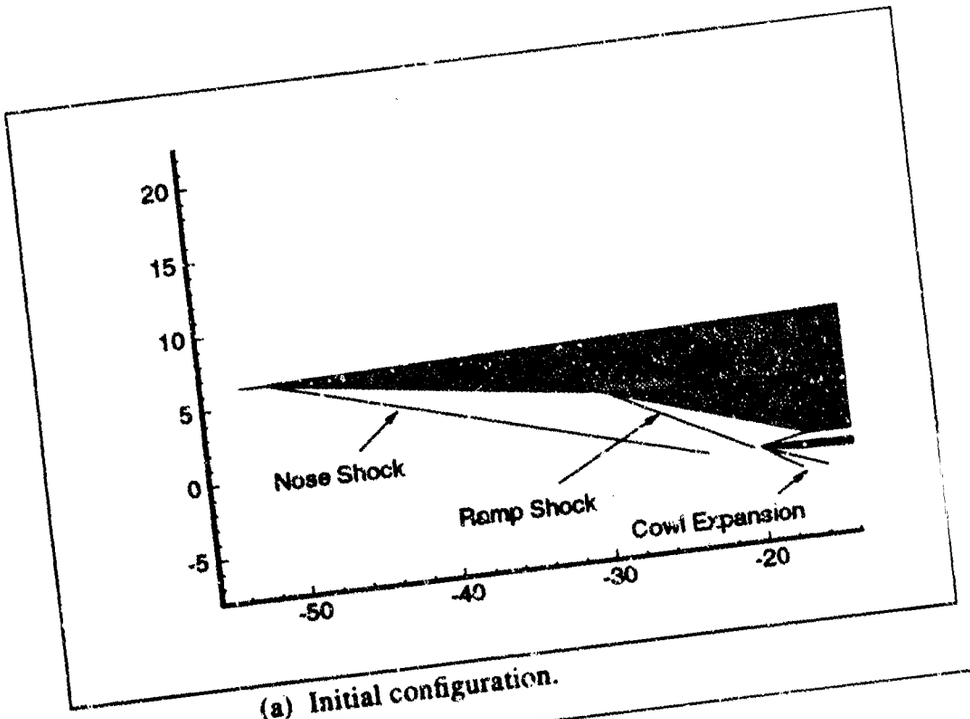

(a) Initial configuration.

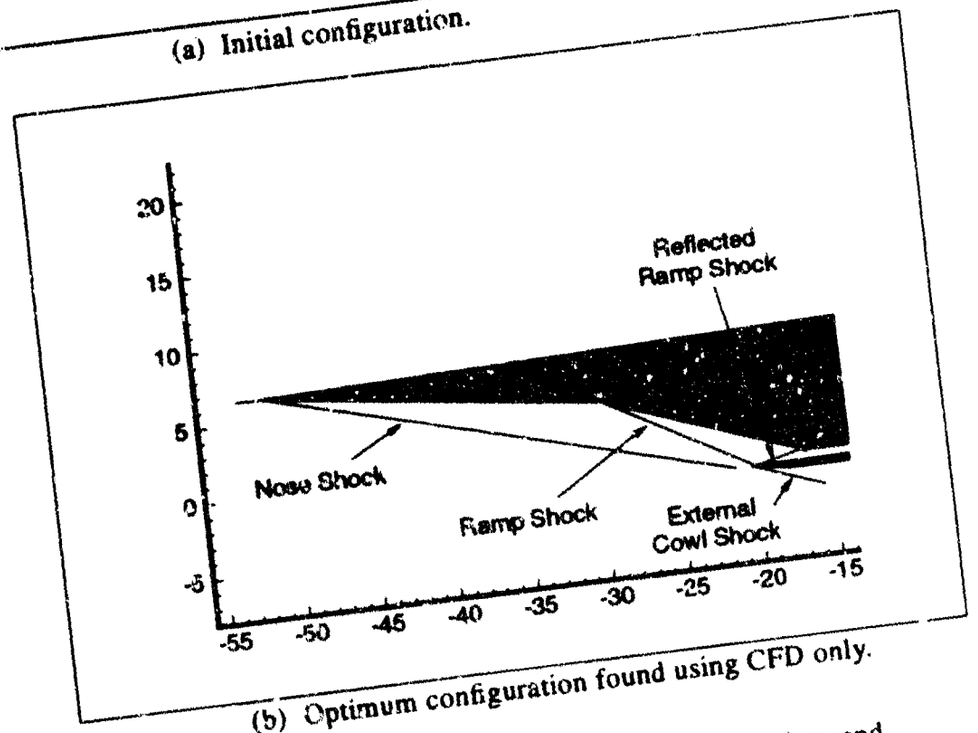

(b) Optimum configuration found using CFD only.

Fig. 5.10 Forebody/inlet initial and optimum designs and shock structures..

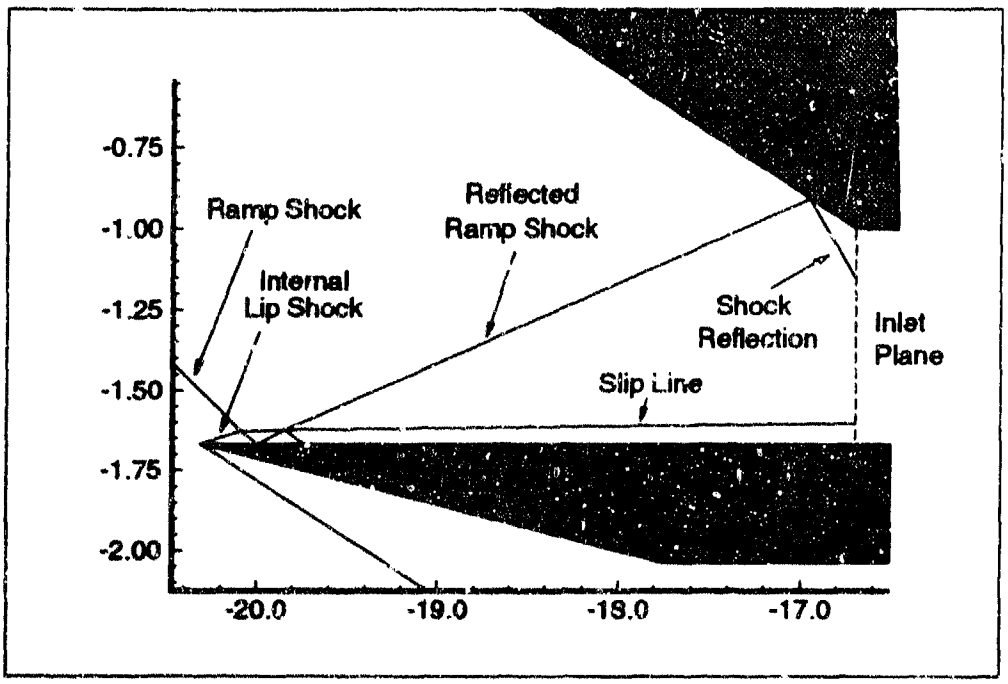

(c) Details of inlet shock system for optimum configuration.

Fig. 5.10 (cont'd) Forebody configurations and shock structures.

As mentioned in Section 5.5.2, a zeroth-order GLA was then applied to F_{net} instead of to the point properties. This technique yielded an optimum design very close to that found by the CFD. It is important to note that when such a simple scaling is applied to the integral measures, this is the same as simply multiplying all the approximate method solutions (within one iteration) by a constant number. It is not surprising, then, that there should be excellent agreement, at least for an unconstrained problem, when the approximate model alone does such a good job. This also allowed the zeroth order integral measure GLA to use very wide move limits (20%), which is a major reason that only 1 iteration was required by this technique. This may seem to belittle the significance of applying a zeroth-order scaling to the integral measures. However, if it there are constraints on any integral measures in the optimization, such scaling of the constraint values would be necessary for proper activation of the constraints. Therefore, there is value in using such an approach to the GLA,

when the approximate model captures the general behavior of the CFD model with high fidelity. The simplicity of implementing this technique is also attractive.

Optimization histories of F_{net}, θ_{nose} and L_{ramp} are shown in Fig. 5.11a-c. The horizontal axes there represent function evaluations, meaning the number of CFD calls for the CFD and Taylor series methods, and the number of approximate model calls for the approximate model method. (Note that the values of F_{net} shown are as calculated by the CFD solver, except for those for the approximate model. This accounts for the apparently much higher F_{net} values for this method.) Fig. 5.11b appears to show that the Taylor series method was better than the approximate model for finding θ_{nose}. However, as can be seen from Fig. 5.11c and TABLE 5.2, the approximate method really does a better job of replicating the behavior of the CFD solver.

It is clear from these results that the GLA and Taylor series method cannot be applied to correcting point properties in the forebody/inlet region with the same ease as was done in the nozzle region. Thus, the application of GLA's to regions where shocks dominate the flow requires a much different treatment than that used in current structural optimization applications.

5.6 Summary

After careful selection of design variables, a successful optimization of the forebody/inlet region was performed using the CFD alone. The approximate method (uncorrected) was found to optimize to a very similar design. The Taylor series and GLA (applied to point properties) did not perform well, due to their inability to account for the movement of shock impingement points. A method of partially alleviating this problem has been proposed and tested in one iteration of a GLA optimization. This method is based upon using non-dimensionalized, pre- and post-shock coordinate systems for gradient and correction factor calculations. This method appears to have promise, but more work is needed in this area. Additional optimizations were performed using the GLA applied to integral measures (thrust, drag, and F_{net}. A zeroth-order application of this method was successful, and holds some promise for constrained optimization problems in which the approximate model replicates well the general behavior of the CFD solver.

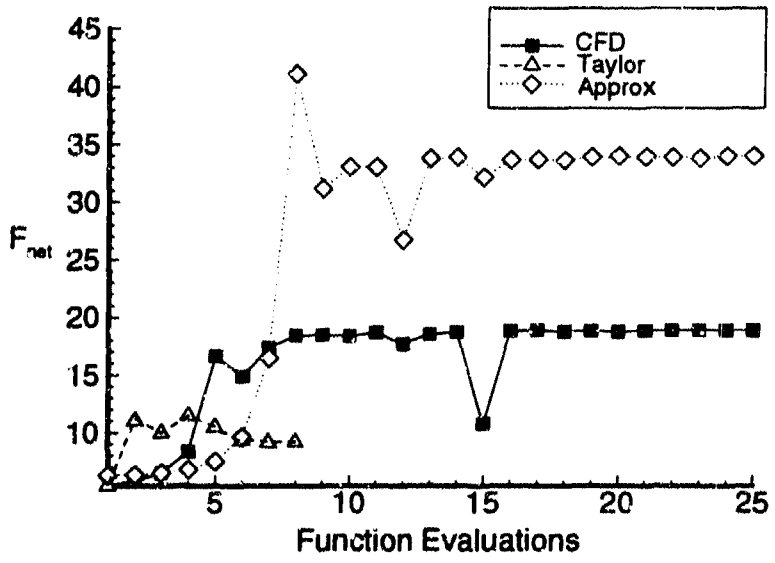

(a) Optimization histories of F_{net}. (Note: F_{net} values shown are from CFD solver, except approximate. method values.)

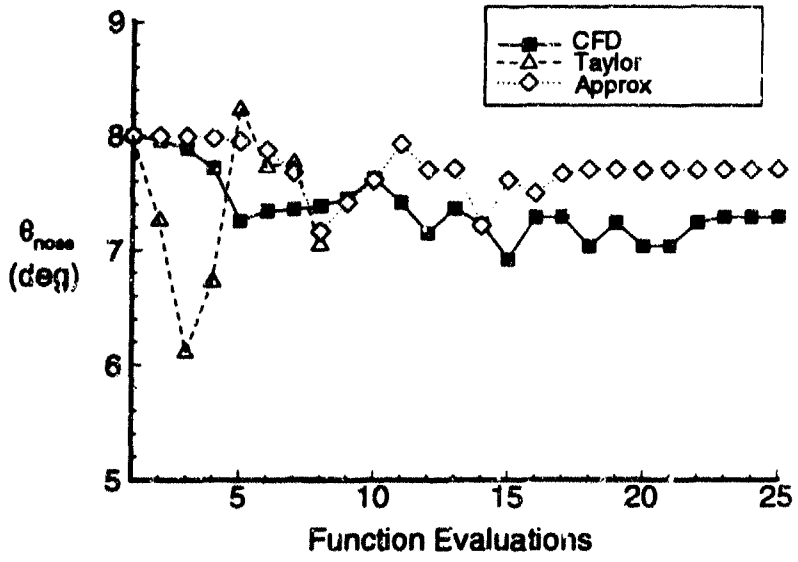

(b) Optimization histories of θ_{nose}.

Fig. 5.11 Optimization histories for forebody/inlet.

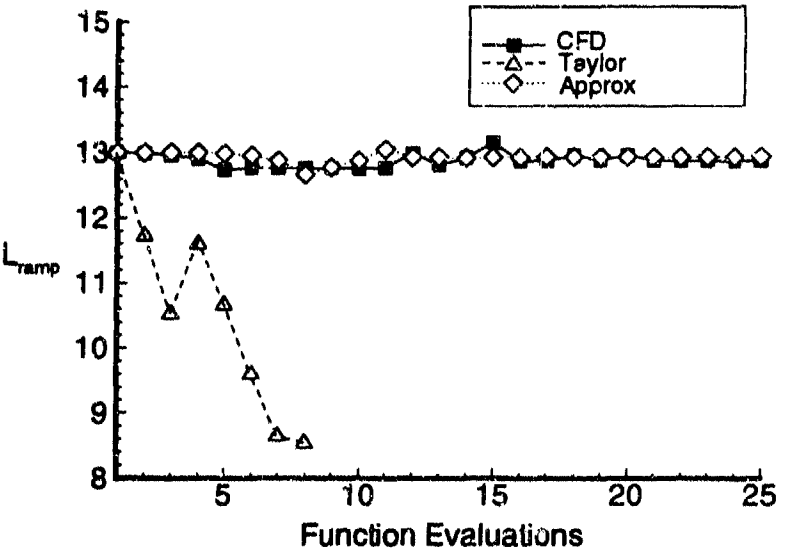

(c) Optimization histories of L_{ramp}.

Fig. 5.11 (cont'd) Optimization histories for forebody/inlet.

Chapter 6

Conclusions

6.1 Constructing Approximation Concepts With CFD

It was found that approximation concepts, as they are currently employed in structural optimization, cannot be employed in aerodynamic optimization problems without modification.

When forming an aerodynamic approximation concept, special attention must be paid to the fact that the number of CFD grid points may change as the grid clustering adapts to changes in the design variables. This means that the GLA or Taylor series correction factors cannot be tied to CFD grid points. This problem had previously been identified (Ref. 3) but had not heretofore been solved.

This research effort found a general solution to this problem, by forming a new "correction point" grid system, which is independent of the size and density of the CFD grid. The correction point grid system consists of a very dense non-dimensionalized 1-D grid for each wall surface of interest, as shown in Fig. 2.2. (A similar philosophy was applied to the inlet plane, for correction of the flow properties there.) Whenever the CFD solver is run, the wall pressures are interpolated into the non-dimensionalized grid for each surface. Similarly, the approximate model results are either interpolated into this grid system or, better yet, are calculated there originally, when this is practical. (A case where this is not practical is for the Method of Characteristics, where the MOC grid is set by the MOC solution, and cannot easily be determined beforehand.)

One special consideration inherent in constructing a GLA or Taylor series model with CFD as the detailed model is that the crispness of shock capturing may be different for the CFD solver and for the approximate method. This can lead to erroneous correction factors in the GLA.

In addition, there are special problems involved in using GLA's in fluid flow regimes in which moving discontinuous phenomena occur (such as shock waves,

transition to turbulence, or separation). Such moving discontinuities, if not properly treated, can cause erratic behavior of the objective function.

Another special consideration when using CFD in optimizations, especially when the gradient calculations are performed by "brute force" finite differences, is that the quality of the CFD solution must be very high. Artificial pressure spikes or excessive numerical dissipation may not only cause errors in the values of the objective function, but may also result in the optimizer calculating poor search directions, with a resultant degradation in the optimization results. This underscores the desirability of using analytical or quasi-analytical means of finding the sensitivity coefficients.

It is important that the "noise level" of the CFD calculations be established by examining the convergence histories of typical solutions. For meaningful optimizations, the differences between successive CFD solutions must be above the noise level. This is most critical during the gradient calculations, since small errors in the CFD solution there may result in very poor search directions being used.

6.2 Choices of Design Variables

It has long been recognized that the selection of design variables can have a dramatic effect on the efficiency of an optimization scheme. In this research it was found, for the forebody/inlet, that the choice of design variables was crucial in determining whether the optimizer selected a *reasonable* optimum design.

Specifically, the most intuitive design variable set (the angles and lengths which control the shock strengths and locations) did not produce good results, because it did not allow for the simultaneous changes in some design parameters which good design practice dictates. Several design variable sets using only lengths were tried, and a satisfactory one was found. As yet, there are no general rules for determining the best design variables.

The sensitivity of this optimization problem to the design variables is, in large part, due to the fact that arbitrary shock locations were allowed. When only perfectly-placed shocks are considered, there are only two design parameters (the nose and ramp angles), and the optimization proceeds smoothly with these selected as the design variables.

The nozzle/afterbody optimizations (which did not have to contend with shock impingements) were found to be insensitive to which of the two candidate sets was used.

6.3 Nozzle/Afterbody Optimizations

Taylor series approximations and two GLA's (one based on the 2-D, steady MOC, and one based on isentropic 1-D flow theory) were successfully applied to the nozzle/afterbody region. All of these methods gave optimum designs which were very close to that found by using the CFD alone, with a 68% reduction in computational cost. The successes in the nozzle/afterbody region highlight the great potential of approximation concepts for aerodynamic design optimization.

6.4 Forebody/Inlet Optimizations

Optimizations were performed on the inlet/forebody of the 2-D scramjet vehicle, in which arbitrary shock configurations were allowed. The objective function was the net thrust. The optimization using CFD alone proceeded without difficulty. The uncorrected approximate method performed well, optimizing to a design very close to that found using the CFD. The GLA (applied to point properties), however, was unsuccessful, owing to an inability to account for the motion of shocks as the design variables were changed. This resulted in poor search direction selection, and in erratic behavior of the objective function during the optimization iterations. The Taylor series method did not encounter the same erratic behavior, but did not optimize to the same design that the CFD and approximate methods did.

To alleviate this problem, the GLA method was then applied to the integral measure (net thrust). Although such a first-order GLA was not successful, a zeroth-order GLA was found to successfully optimize to the same design as the CFD.

To guide future research, the detailed behavior of the point property GLA was observed, and a partial solution to the problems encountered by the GLA and Taylor series was investigated. The basis of this is to replace the non-dimensionalized wall coordinate systems mentioned in Section 6.1 with non-dimensionalized pre- and post-shock coordinate systems, as explained in Section 5.5.1. The gradients and correction factors are calculated in these systems, and the correction factors are applied

there before the pressures are converted back into dimensioned coordinates, once the location of the shock impingement points are known. This method was found to remove the erratic behavior of the GLA. However, there were still problems with the GLA, in that the values of thrust and drag were too high, and the *optimizer* treated the new GLA almost exactly as it did the original one. This may have been due in part to the fact that this type of coordinate system was not also applied to the inlet plane flow conditions, and to the fact that the CFD and approximate method do not capture shocks equally crisply, resulting in erroneous correction factors in the vicinity of shocks.

This concept of using non-dimensionalized pre- and post-discontinuity coordinate systems appears to be a general one for the application of GLA's to any problem involving discontinuous phenomena which shift positions as the design variables are changed. Examples of such phenomena are shocks, transition to turbulence, and separation.

6.5 Recommended Further Research

For the GLA approach to be used in flow fields with shocks or other shifting discontinuities, a method of properly accounting for the motions of these phenomena in the gradient and correction factor calculations is essential. Research in this area should also address the issue of the difference in "crispness" with which the detailed and approximate methods capture such discontinuities. If such techniques can be found, the GLA approach may be made generally applicable in aerodynamic optimization problems.

Research should be performed into finding rules for determining which design variable sets are likely to provide the best results.

The optimizations performed in this work had no active constraints with regard to the flow properties. Only geometric constraints were active. The behavior of the GLA in the presence of active "behavior" constraints must be examined.

Once these issues have been resolved, attempts should be made to apply the GLA concept to more complicated problems, such as optimizing a 2-D scramjet vehicle with chemically-reacting internal and external flows. 3-D vehicle optimizations present a more challenging test of the method, but also one in which the potential payoff of the GLA is great.

References

1 Optimization

1 Anderson, Bernhard H., "Optimization of Supersonic Inlets Using the Method of Characteristics", in "Analytic Methods in Aircraft Aerodynamics", NASA SP-228, 1969.

2 Nickerson, G. R., Dunn, S. S. and Migdal, D., "Optimized Supersonic Exhaust Nozzles for Hypersonic Propulsion", AIAA Paper 88-3161, July 1988.

3 Frank, Paul D., and Shubin, Gregory R., "A Comparison of Optimization-Based Approaches for Solving the Aerodynamic Design Problem", presented at the Third Air Force/NASA Symposium on Recent Advances in Multidisciplinary Analysis and Optimization, San Francisco, Sep. 24-26, 1990.

4 Baysal, Oktay, and Eleshaky, Mohamed E., "Aerodynamic Design Optimization Using Sensitivity Analysis and Computational Fluid Dynamics," *AIAA Journal*, vol. 30, no. 3, Mar. 1992, pp. 718-725.

5 Levine, M., Ide, H. and Hollowell, S., "Multidisciplinary Hypersonic Configuration Optimization", presented at the Third Air Force/NASA Symposium on Recent Advances in Multidisciplinary Analysis and Optimization, San Francisco, Sep. 24-26, 1990.

6 O'Neill, M. K., and Lewis, M. J., "Optimized Scramjet Integration on a Waverider", AIAA Paper 91-1693, June 1991.

7 Barthelemy, Jean-Francois M., and Haftka, Raphael T., "Recent Advances in Approximation Concepts for Optimum Structural Design", NASA TM-104032, Mar. 1991.

8 Haftka, Raphael T., "Combining Global and Local Approximations," *AIAA Journal*, vol. 29, no. 9, Sep. 1991. pp. 1523-1525.

9 Chang, Kwan J., Haftka, Raphale T., Giles, Gary L., and Kao, Pi-Jen: "Sensitivity-Based Scaling for Correlating Structural Response From Different Analytical Models," AIAA Paper 91-0925, Apr. 1991.

10 Hutchison, M., Unger, E., Mason, W., Grossman, B., and Haftka, R., "Variable-Complexity Aerodynamic Optimization of an HSCT Wing Using Structural Wing-Weight Equations," AIAA Paper 92-0212, Jan. 1992.

11 Vanderplaats, Garret N., "Numerical Optimization Techniques for Engineering Design: With Applications," McGraw-Hill, New York, 1984.

12 "DOT Users' Manual," Vanderplaats, Miura & Associates, Inc, Goleta CA, 1990.

13 Elbanna, H. M., and Carlson, L. A., "Determination of Aerodynamic Sensitivity Coefficients Based on the Transonic Small Perturbation Formulation", *Journal of Aircraft*, vol. 27, no. 6, June 1990, pp. 507-515.

14 Sobieszczanski-Sobieski, J., "Sensitivity of Complex, Internally Coupled Systems", *AIAA Journal*, vol. 28, no. 1, Jan. 1990, pp. 153-160.

2 Scramjets

15 Schindel, Leon H., "Design Model of High-Performance Ramjet or Scramjet-Powered Vehicles", *Journal of Spacecraft and Rockets*, vol. 27, no. 6, Nov.--Dec. 1990, pp. 613-617.

16 Van Wie, D. M., White, M. E., and Waltrup, P. J., "Applicaton of Computational Design Techniques in the Development of Scramjet Engines", AIAA Paper 87-1420, June, 1987.

17 Anderson, J. Thomas, "Airframe/Propulsion Integration of Supersonic Cruise Vehicles", AIAA Paper 90-2151, July, 1990.

18 Townend, L. H., Pike, J., Nonweiler, T. R. F., and Parker, E. Ann, "Forebody Design for the Aerospaceplane", AIAA Paper 90-2472, July, 1990.

19 Jachimowski, Casimir J., "An Analytical Study of the Hydorgen-Air Reaction Mechanism With Application to Scramjet Combustion", NASA Technical Paper 2791, 1988.

20 Billig, Frederick S., "Combustion Processes in Supersonic Flow", *Journal of Power and Propulsion*, vol. 4, no. 3, May-June 1988, pp. 209-216.

21 Ferri, Antonio, "Mixing-Controlled Supersonic Combustion", vol. 5 in M. van Dyke, W. G. Vincenti, and J. V. Wehausen (eds.), "Annual Review of Fluid Mechanics", Annual Reviews, Inc., 1973, pp. 301-338.

22 Armangaud, F., Decher, R., Koopman, A., and Lafosse, B., "One-Dimensional Modeling of Hypersonic Flight Propulstion Engines", AIAA Paper 89-2026, July, 1989.

23 Weissman, D., "Representation of Two-Dimensional Hypersonic Inlet Flows for One-Dimensional Scramjet Cycle Analysis", AIAA Paper 90-0527, Jan. 1990.

24 Lewis, M. J., "Propulsion/Airframe Integration for Hypersonic Waveriders", AIAA Paper 92-0304, Jan. 1992.

25 Takashima, N., and Lewis, M. J., "Navier-Stokes Computation of a Viscous Optimized Waverider", AIAA Paper 92-0305, Jan. 1992.

3 CFD

26 Steger, Joseph L., and Warming, R. F., "Flux Vector Splitting of the Inviscid Gasdynamic Equations With Application to Finite Difference Methods", NASA TM-78605, July, 1979.

27 Davis, W. H., "The Role of CFD Applied to High Performance Aircraft", AIAA Paper 90-3071

28 Dash, S. M., Sinha, N., Wolf, D. E. and York, B. J., "Computational Models for the Analysis/Design of Hypersonic Scramjet Components -- Part I: Combustor and Nozzle Models", AIAA Paper 86-1595, June 1986.

4 Aerodynamics/Thermodynamics

29 Shapiro, Ascher H., "The Dynamics and Thermodynamics of Compressible Fluid Flow, Volume I," The Ronald Press Co., New York, 1953.

30 Kerrebrock, Jack L., "Aircraft Engines and Gas Turbines," The MIT Press, Cambridge, Mass., 1980.

31 Liepmann, H.W., and Roshko, A., "Elements of Gasdynamics," Wiley, New York, 1957.

32 Zucrow, Maurice J., and Hoffman, Joe D., "Gas Dynamics, Vol. I", Wiley, New York, 1976.

33 Anderson, John D., "Modern Compressible Flow With Historical Perspective", McGraw-Hill, New York, 1982.

34 Sullins, G. A., and Billig, F. S., "Force Accounting for Airframe Integrated Engines", AIAA Paper 87-1965, July 1987.

35 Bussing, Thomas R. A., and Eberhardt, Scott, "Chemistry Associated With Hypersonic Vehicles", AIAA Paper 87-1292, June 1987.

36 Donovan, A.F., and Lawrence, H.R. (eds), "Aerodynamic Components of Aircraft at High Speeds," vol VII in T. von Karman, et al (eds), "High Speed Aerodynamics and Jet Propulsion," Princeton University Press, Princeton, N.J., 1957.

37 Chushkin, P.I., "Numerical Method of Characteristics for Three-Dimensional Supersonic Flows," in D. Kuchemann (ed.), "Progress in Aeronautical Sciences, Vol 9", pp. 41-119, Pergamon, New York, 1968.

5 Experiments

38 Baysal, Oktay, Engelund, Walter C., Eleshaky, Mohamed E., and Pittman, James L., "Adaptive Computations of Multispecies Mixing Between Scramjet Nozzle Flows and Hypersonic Freestream", AIAA Paper 89-0009, Jan., 1989.

39 Pittman, James L., "A Mach 6 External Nozzle Experiment with Argon-Freon Exhaust Simulation", SAE Technical Paper Series 892315, Sep. 1989.

40 Richardson, Pamela F., Parlette, Edward B., et. al., "Comparison Between Experimental and Numerical Results for a Research Hypersonic Aircraft", *Journal of Aircraft*, vol. 27, no. 4, Apr. 1990, pp. 300-305.

Appendix A

The Method of Feasible Directions

A.1 Introduction

Each scramjet vehicle optimization was performed by combining the well-proven optimization software package "Design Optimization Tools", or DOT (See Ref. 12.), with one or more 2-D flow solvers (or "analysis programs"). DOT uses the "Modified Method of Feasible Directions" to solve constrained nonlinear optimization problems. In this case, DOT was instructed to find the vehicle design which maximized net thrust (Thrust - Drag), and which also met certain constraints on vehicle dimensions and flow properties at critical points on the vehicle. The flow solvers provided DOT with the values of net thrust and of the flow properties considered in the constraints.

This chapter describes the salient features of the Method of Feasible Directions.

A.2 Optimization Method

The general optimization problem can be formulated as follows. Let the objective function (in this problem, the net thrust) be F(X), where X is the vector of design variables (e.g. nose angle, inlet compression ramp angle, etc.). The elements of $\mathbf{X}$ are X_1, X_2, etc. Let g be the vector of inequality constraints (e.g. pressure at the end of the nozzle wall must be greater than some value, to prevent reverse flow in the nozzle). Define h as the vector of equality constraints. Furthermore, let the elements of X be limited to certain ranges of values (side constraints). Following the terminology in Ref. 11, we now write the problem statement as:

Maximize	$F(\mathbf{X})$		Objective function
Subject to:	$g_j(\mathbf{X}) \le 0$	$j = 1,m$	Inequality constraints
	$h_k(\mathbf{X}) = 0$	$k = 1,l$	Equality constraints
	$X_i^l \le X_i \le X_i^u$	$i = 1,n$	Side constraints

where

$$\mathbf{X} = \begin{Bmatrix} X_1 \\ X_2 \\ \vdots \\ X_n \end{Bmatrix}$$ Design variables

The vector **X** defines a design space. Each point in the design space has associated with it a value of the objective function. The constraints can be thought of as boundaries within the space. Fig. A.1 portrays such a problem which has only two design variables. (This figure is based on Fig. 1.6 of Ref. 11.) The basic concept of the Method of Feasible Directions is that, as we search the design space for an optimum, we search in directions which both improve the value of the objective function, and do not violate any constraints. At point A in Fig. A.1 the constraint is active. If we try to search in the direction of $\nabla g(X)$, we will only increase the violation of the constraint. The only way to guarantee that the constraint will not be violated (at least for a small step) is to limit the search to directions which lie on the opposite side of a line normal to $\nabla g(X)$. All such directions are defined as being "feasible" directions. Similarly, the only way to guarantee, for a small step, that moving in a given search direction will result in an increase in the objective function, is to require that direction to lie in the half-plane which is bounded by the normal to $\nabla F(X)$, and which includes the direction $\nabla F(X)$. All such directions are "usable" directions. In short, we should search in a direction which is to some degree "along" $\nabla F(X)$ and "opposite to" $\nabla g(X)$. Or, we seek a direction which is both "usable" and "feasible". The usable-feasible sector at point A in Fig. A.1 contains all the usable-feasible directions emanating from that point. Note, however, that as we move in such a direction, we may soon find ourselves in violation of the constraint. The usability and feasibility of a direction is guaranteed only in the immediate vicinity of the originating point.

At point B, there is no usable-feasible direction, so this point is the optimum design for this simple example. The optimality criterion in this case is that $\nabla F(X)$ and $\nabla g(X)$ are in exactly opposite directions.

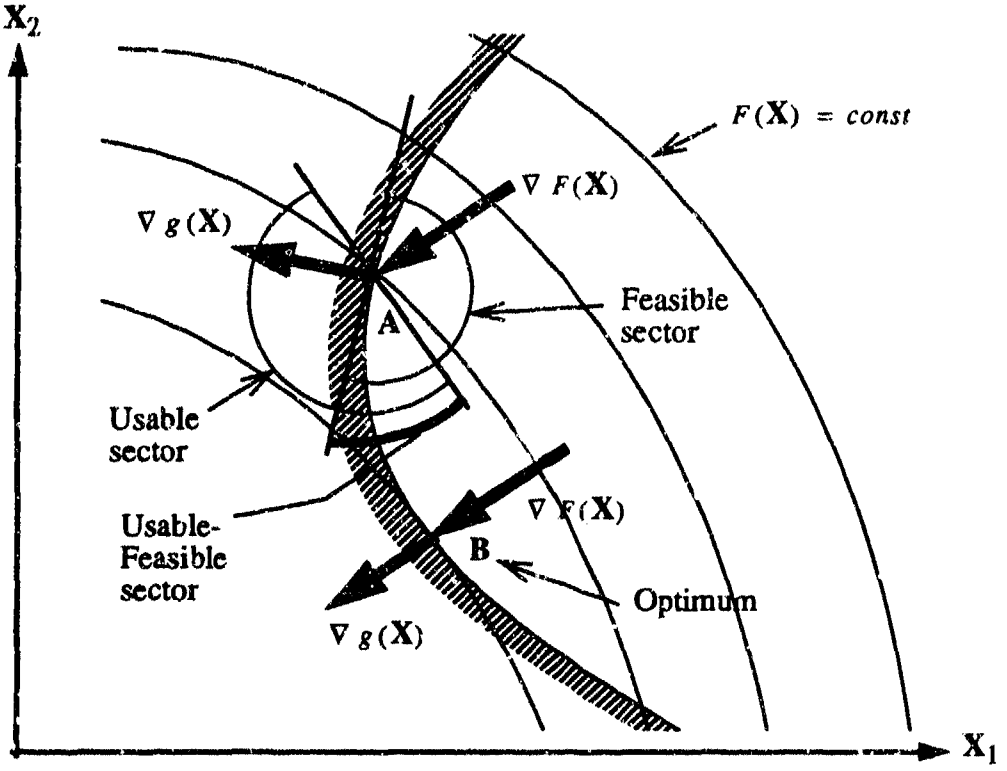

Fig. A.1 Example of two-variable design space with inequality constraint.

To determine the optimality criteria for a more general design problem, we again consider the gradients of the objective function and constraints, as shown in Fig. A.2a. Point **X*** is the constrained optimal point in this space. That point is nestled in the "valley" formed by the inequality constraints. This can be expressed mathematically by noting that, for such a configuration, the gradients of the two constraints straddle $\nabla F(X)$. Thus we could construct a linear combination of $\nabla \mathbf{g}_1(X)$ and $\nabla \mathbf{g}_2(X)$ which will be exactly equal to $\nabla F(X)$. This way of denoting that the optimal point is at the

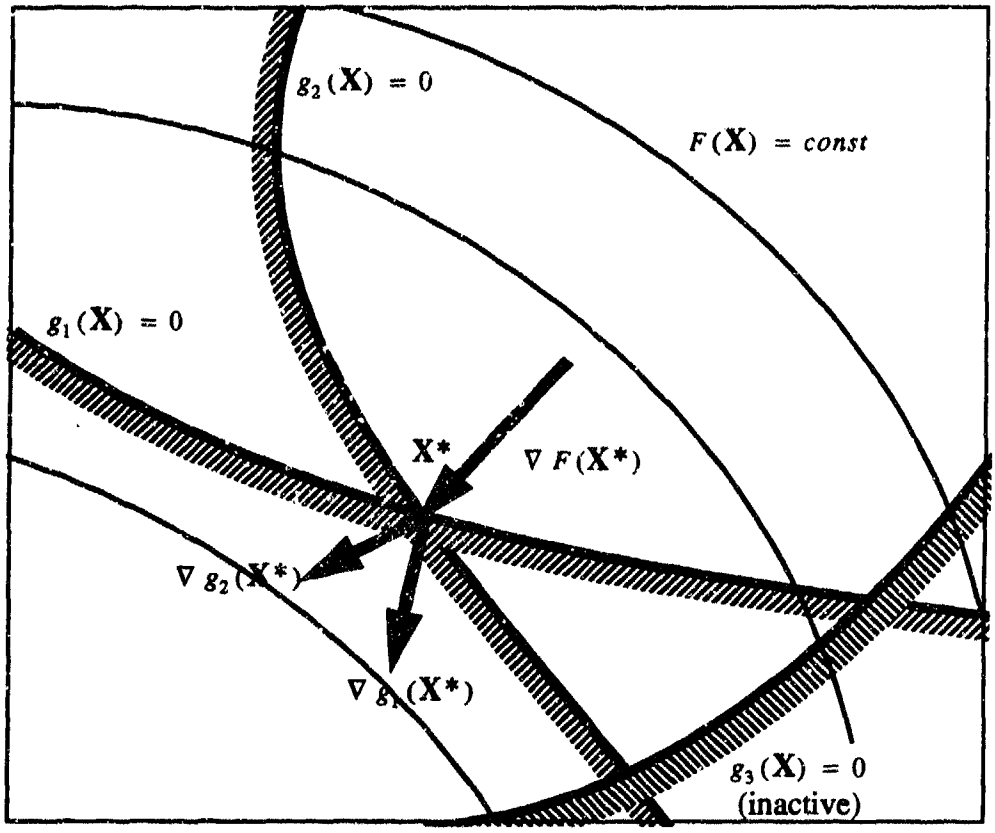

(a) Objective function and constraint geometry.

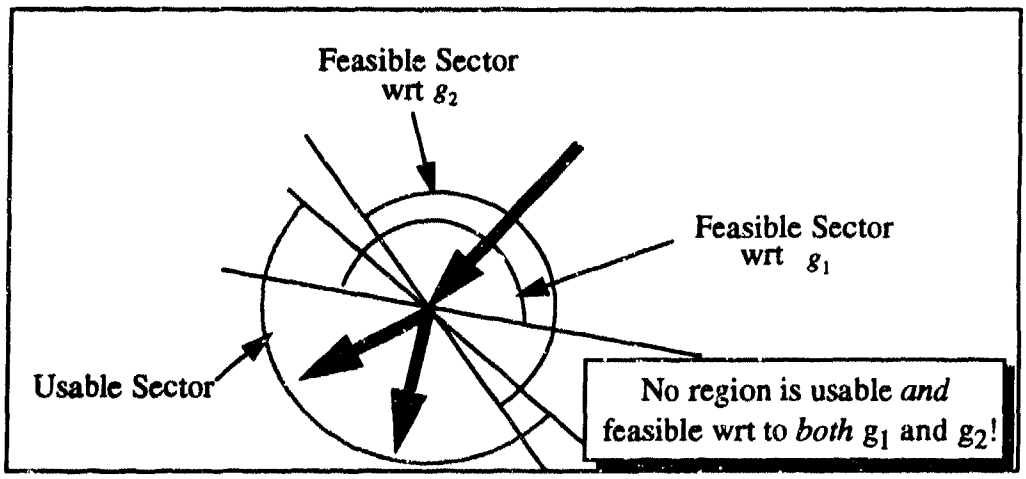

(b) Usable and Feasible Directions at optimal point.

Fig. A.2 Illustration of Kuhn-Tucker optimality conditions for a two-design variable problem with two active constraints.

bottom of the valley is embodied in the well-known Kuhn-Tucker necessary conditions for optimality.

1. $\mathbf{X}^*$ is feasible. (A.1)

2. $\lambda_j g_j(X) = 0 \quad j = 1,m \quad \lambda_j \leq 0$ (A.2)

3. $\nabla F(X^*) + \sum_{j=1}^{m} \lambda_j (\nabla g_j)(X^*) + \sum_{k=1}^{l} \lambda_{k+m} \nabla h_k(X^*) = 0$ (A.3)

$\lambda_j \leq 0$

λ_{k+m} unrestricted in sign.

Equations (A.1) and (A.2) simply require that the design be feasible and satisfy all inequality constraints. Eq. (A.3) requires that some linear combination of the gradients of the active constraints be equal to $\nabla F(X)$. As shown in Fig. A.2b, this implies that there is no usable-feasible search direction at this point. Note that both inequality and equality constraints are considered in Eq. (A.3). Note also that if no constraints are active, then Eq. (A.3) says that the optimal design occurs where $\nabla F(X) = 0$. This is analogous to the familiar "zero slope" condition for the extremum (maximum, minimum or inflection point) of a function of a single variable.

The Kuhn-Tucker conditions can only guarantee that a local extremum has been reached. They could just as easily indicate a local minimum or saddle point as they would a local maximum. The search technique used will help avoid settling on the wrong type of extremum. A further difficulty is that there may well be other local optima which yield higher values of F(X). For problems which are highly non-linear, it is usually necessary to choose an initial design in the neighborhood of the global optimum to guarantee that the global optimum will be reached. However, even if the global best is not found, this method will usually produce a design which is better than the initial design. For many engineering applications, this may be sufficient justification for using such techniques.

The first step in implementing the Method of Feasible Directions with DOT is to select an initial design, $\mathbf{X}^0$. Then DOT calculates an initial search direction, which is in the direction of $\nabla F(X)$, unless the initial design is infeasible. In that case, DOT first seeks to relieve the constraint violation, while improving the value of F(X), if this

is possible. All evaluations of $F(\mathbf{X})$, $\nabla F(\mathbf{X})$, and $\nabla g(\mathbf{X})$ are provided by a separate "analysis program" (in this research, the flow solver program). If the analysis program does not provide the gradients directly, then they are calculated by repeated evaluations of $F(\mathbf{X})$ and $g(\mathbf{X})$, wherein the elements of $\mathbf{X}$ are perturbed about the initial design, $\mathbf{X}^0$. This finite-difference method of finding the elements of $\nabla F(X)$ (which are commonly referred to as the "sensitivity coefficients" of $F(\mathbf{X})$) can be extremely costly in computer resources. Much work has been done in recent years on determining aerodynamic sensitivity coefficients analytically or by approximate numerical techniques, to avoid having to use finite differencing. (See Ref's. 4, 13, and 14, for example.) However, the present work used finite differences exclusively.

A "one-dimensional search" is performed along the search direction, until the optimal constrained value of $\nabla F(\mathbf{X})$ for this direction is found. Then a new search direction is calculated. This direction is not in the direction of $\nabla F(\mathbf{X})$, but is rather in a direction determined by the Conjugate Direction Method or the Variable Metric Method. (See Ref. 11.) Such methods achieve much faster convergence than using the gradient direction. As the search approaches a constraint, "push-off factors" are used in the constraint calculations to force the search back into the feasible region, before the constraint is actually violated. A new one-dimensional search is performed, and the process continues until no further improvement can be made in the objective function without violating any constraint. The resulting design is then considered to be optimal.

The major limitations of this type of optimization scheme are: that it requires that the objective function and constraint functions be continuous; and that it will only guarantee a local optimum will be found. Since many engineering problems do not have continuous objective and constraint functions, the first limitation would appear to severely limit the usefulness of the method. But is has been found in practice that some degree of discontinuity can be tolerated. The problem of determining if the optimal solution is actually a global optimum can be somewhat alleviated by running the optimization several times starting at different initial designs. This may be quite expensive, particularly if there is a large number of design variables.

A.3 Summary

The optimization technique used in this research employs the Modified Method of Feasible Directions, as embodied in the optimization package DOT. This scheme requires function and constraint evaluations and their gradients (with respect to the design variables), which are provided by one or more analysis programs. The gradients were found using the "brute force" finite-difference method. The optimization method establishes a search direction in the usable-feasible sector (if one exists) and then performs a 1-dimensional search in this direction. When the optimal point in this direction is found, a new search direction is determined and a new 1-dimensional search is conducted. The process is repeated until convergence is reached. The Kuhn-Tucker necessary conditions for optimality are used. These conditions can only guarantee that a local optimum is reached.

Vita

Peter D. McQuade

B. S., Aeronautics and Astronautics, Massachusetts Institute of Technology, June, 1977.

M. S., Aeronautics and Astronautics, Massachusetts Institute of Technology, January, 1982.

Ph.D., Aeronautics and Astronautics, University of Washington, August, 1992.